UNIVERSIDADE FEDERAL DE SANTA CATARINA
CAMPUS JOINVILLE
PROGRAMA DE PÓS-GRADUAÇÃO EM ENGENHARIA E CIÊNCIAS MECÂNICAS

Igor Silva Flôres Siqueira

Analysis of the thermal integration between a Solid Oxide Full Cell and an ethanol reformer through a heat exchanger network

Joinville
2024

Igor Silva Flôres Siqueira

Analysis of the thermal integration between a Solid Oxide Full Cell and an ethanol reformer through a heat exchanger network

Dissertation of Graduate Program in Mechanical Engineering and Sciences of Centro Tecnológico de Joinville of Universidade Federal de Santa Catarina to obtain the title of Master in Engineering and Mechanical Sciences.
Advisor: Prof. Rafael de Camargo Catapan, Dr.Eng.
Co-Advisor: Prof. Bruno Francisco Oechsler, Dr.Eng.

Joinville
2024

Ficha de identificação da obra elaborada pelo autor,
através do Programa de Geração Automática da Biblioteca Universitária da UFSC.

Siqueira, Igor Silva Flôres
Analysis of the thermal integration between a Solid Oxide Full Cell and an ethanol reformer through a heat exchanger network / Igor Silva Flôres Siqueira ; orientador, Rafael de Camargo Catapan, coorientador, Bruno Francisco Oechsler, 2024.
98 p.

Dissertação (mestrado) - Universidade Federal de Santa Catarina, Campus Joinville, Programa de Pós-Graduação em Engenharia e Ciências Mecânicas, Joinville, 2024.

Inclui referências.

1. Engenharia e Ciências Mecânicas. 2. Célula de combustível. 3. SOFC. 4. Efficiência. I. Catapan, Rafael de Camargo . II. Oechsler, Bruno Francisco. III. Universidade Federal de Santa Catarina. Programa de Pós-Graduação em Engenharia e Ciências Mecânicas. IV. Título.

Igor Silva Flôres Siqueira

Analysis of the thermal integration between a Solid Oxide Full Cell and an ethanol reformer through a heat exchanger network

The present Master level work was evaluated and approved by the jury composed by the following members:

Prof. Pedro Curto-Risso
Universidad de la República - Uruguay, Dr. Ing.

Prof. Sergio Gómez González, Dr. Eng.
Universidade Federal de Santa Catarina

Profa. Talita Sauter Possamai, Dr. Eng.
Universidade Federal de Santa Catarina

We certified that this is the original and final version of the concluding work, which was judged appropriate to obtain the title of master of engineering and mechanical sciences.

Documento assinado digitalmente
Diego Santos Greff
Data: 26/01/2024 14:09:38-0300
CPF: ***.266.630-**
Verifique as assinaturas em https://v.ufsc.br

Coordination of the Postgraduate Program

Documento assinado digitalmente
Rafael de Camargo Catapan
Data: 26/01/2024 13:33:16-0300
CPF: ***.036.159-**
Verifique as assinaturas em https://v.ufsc.br

Prof. Rafael de Camargo Catapan, Dr.Eng.
Advisor

Joinville, 2024.

This work is dedicated to everyone who came before me,
who made my existence possible.

ACKNOWLEDGEMENTS

To my Mother and my brother Kauê, for their understanding during absences, and also for their support during the period I was enrolled in the program.

To my friend Fernando Petters for the help in the start of the master program, and the contributions during my master thesis, revisions and suggestions.

To my former collegues and great supporters of my enrollment in postgraduate studies, Pablo Rodeiro and Márcio Demétrio.

To my advisor Prof. Rafael Catapan and my co-Advisor Prof. Bruno Oechsler, for guiding the work and all the knowledge passed on to me.

UFSC for the opportunity to attend a quality postgraduate course at no cost.

To the POSECM Professors who shared a lot of knowledge and teachings with me in recent years.

To the members of the evaluation panel, for their commitment and dedication in evaluating this work.

“What we know is a drop, what we don’t know is an ocean.”
(NEWTON, Isaac)

RESUMO

Este trabalho investiga a eficiência energética de um sistema SOFC (Solid Oxide Fuel Cell) integrado a um reformador de etanol, usando um modelo 0D para simular a célula SOFC, enquanto o reformador foi simulado por modelos de equilíbrio termodinâmico. Um modelo de célula SOFC, obtido a partir da revisão da literatura, foi implementado em linguagem Python, e posteriormente conectado aos modelos de reformador, misturador adiabático, trocadores de calor, formando a base para os resultados apresentados. Foram realizadas simulações em regime permanente para investigar os efeitos da variação de temperatura dentro da faixa de 600℃ a 900℃, assim como para razões oxigênio/etanol na faixa de 0% a 100%. As variáveis de saída investigadas foram a eficiência e a potência elétrica da célula SOFC, considerando a potência nominal da SOFC como 5 kW. Como resultado, observou-se que para razões de oxigênio/etanol superiores a 40%, o reformador opera de maneira exotérmica (com taxa de calor de aproximadamente 1kW), favorecendo a integração de calor.No entanto, o rendimento em hidrogênio diminuiu com o aumento da razão oxigênio/etanol, resultando na redução da potência elétrica (2,5-2,0 kW), eficiência da célula. (55-35%) e taxa de calor liberada pela reação eletroquímica (-6 a -3kW). Por outro lado, o aumento da temperatura possibilitou maiores rendimentos em hidrogênio, resultando no aumento da potência elétrica (2,0-3,0 kW), eficiência da célula (42-62%), taxa de calor liberada pela célula (-5 a -7 kW), mas também ocasionando um aumento na demanda de calor para o reformador (-0.04 a 0.7 kW). A simulação do sistema sem integração de calor apresentou eficiência global de 44% com a SOFC operando com 5kW de potência nominal, e as seguintes condições de operação: vazão de alimentação igual a 0,377 g/s, razão vapor/etanol igual a 3,0, razão ar/etanol igual a 0,5 e temperaturas da SOFC e do reformador iguais a 610 e 600℃, respectivamente. Além disso, avaliou-se a recirculação dos gases quentes de saída da SOFC (gás e ar residual do anodo e catodo) como estratégia de integração de calor. A rede de trocadores de calor foi sintetizada a partir da análise pynch, permitindo a recuperação de 842 W de calor. A eficiência global do sistema integrado foi 61.24%, um aumento de 16.84% em relação ao sistema sem integração. Cabe também mencionar que nenhuma fonte de calor externa à SOFC foi usada na rede, visto que é também possível recuperar calor da SOFC.

Palavras-chave: Efficiência, Etanol, SOFC, Reformador, Integração de calor, Análise Pinch.

RESUMO EXPANDIDO

INTRODUÇÃO

O aumento da demanda por produção de energia e a preocupação ambiental impulsionam pesquisas em eficiência de sistemas. Atualmente, a maioria dos veículos é alimentada por combustíveis fósseis, resultando em emissões de gases de efeito estufa. A busca por métodos mais eficientes de geração de energia, especialmente para veículos, está em crescimento. Nesse sentido, a Célula a Combustível de Óxido Sólido (SOFC) surge como uma alternativa promissora, substituindo fontes tradicionais e sendo aplicados em veículos elétricos híbridos. Apesar do hidrogênio ser um combustível eficiente, sua alta pressão necessária para armazenamento pode ser trazer desafios na sua utilização. A solução proposta envolve o uso de um reformador integrado à SOFC, permitindo o uso de gás natural, etanol e outros hidrocarbonetos mais manejáveis. No contexto brasileiro, a acessibilidade ao etanol é uma vantagem, impulsionada pela ampla rede de postos de combustivel com álcool disponível. A Nissan apresentou um veículo elétrico com SOFC integrado a um reformador, alimentado por etanol, oferecendo uma solução versátil e acessível. A operação da SOFC com reformadores integrados oferece benefícios, mas a necessidade de calor no processo de reforma é uma consideração importante, entretanto a integração térmica, utilizando calor residual do sistema, pode aumentar a eficiência. O processo de reforma autotérmica é uma alternativa que demanda menos calor. A literatura destaca o potencial da integração de calor, principalmente no contexto de reforma a vapor, mas o processo autotérmico merece investigação. A compreensão dos trade-offs de parâmetros é crucial para otimizar a eficiência, especialmente em sistemas que utilizam etanol.

OBJETIVOS

O objetivo deste trabalho é investigar a eficiência energética de um sistema SOFC integrado a um reformador de etanol avaliando também a integração térmica na célula a combustível empregando modelagem de alto nível. Além disso, o potencial de integração térmica será investigado através da recuperação de calor através da reação exotérmica dentro da célula a combustível para fornecer a energia necessária para a reação de reforma endotérmica.

METODOLOGIA

A investigação da eficiência do sistema se da por meio da implementação de códigos para representar a integração de uma Célula de Combustível de Óxido Sólido (SOFC) com um reformador e outros componentes, como trocadores de calor, com

foco na avaliação da eficiência do sistema. O reformador opera em condições autotérmicas, usando o calor liberado pela oxidação parcial para suprir a demanda de calor da reforma a vapor. A operação autotérmica do reformador, permite a recuperação de calor dependendo das condições de entrada de etanol, água e ar. O reformador é considerado em equilíbrio acoplado à SOFC, e a capacidade térmica é calculada seguindo o princípio da conservação de energia. O equilíbrio químico é utilizado para estimar a composição dos gases de reforma, através da aplicação da bibilioteca cantera. Trocadores de calor e evaporadores são descritos por modelos lumped que consideram a transferência de calor entre correntes quente e fria, além de um misturador adiabático é usado para combinar etanol e água. Um caso de referência é estabelecido com condições de operação específicas para atingir a potência nominal de 5kW baseado nos dados obtidos da literatura. O sistema é implementado em duas etapas: sem recirculação e com recirculação na etapa seguinte, de modo a permitir a investigação dos impacto da recirculação na eficiencia do sistema proposto, em combinação com estudos de sensibilidade para os parametros de entrada do modelo aplicado.

RESULTADOS E DISCUSSÃO

Os resultados obtidos através da utilização dos modelos de SOFC e reformador foram validados com dados experimentais, ajustando parâmetros para melhor concordância com base na literatura disponível. As simulações realizadas apresentam concordancia com dados experimentais para a tensão da SOFC e taxa de transferência de calor do reformador. A influência da temperatura e da relação oxigênio/etanol nas taxas de transferência de calor foi analisada, onde os resultados indicaram que o aumento da quantidade de oxigênio na reforma do etanol pode melhorar a eficiência do sistema integrado com SOFC ao reduzir a carga térmica do sistema combinado. O estudo investigou o impacto das variações de parametros de entrada no desempenho do sistema. Foram realizadas simulações para avaliar as vazões mássicas de etanol e água no reformador visando atingir uma potência de 5 kW na SOFC. Variáveis como a relação oxigênio/etanol, razão água/etanol, temperatura do reformador e SOFC, e vazão mássica de etanol também foram consideradas. Observou-se que o aumento da proporção ar/Etanol pode resultar em uma diminuição na tensão da SOFC devido a perdas por concentração. O efeito da temperatura também foi analisado, destacando a influência nas taxas de produção de hidrogênio, potência elétrica e eficiência do sistema para temperaturas abaixo de 700 °C. A temperatura afetou as taxas de transferência de calor do reformador e da SOFC, indicando a necessidade de estratégias combinadas em temperatura e relação oxigênio/etanol para otimizar as taxas de reação. Os resultados sugerem a importância da temperatura e das condições de entrada na eficiência global do sistema integrado SOFC-reformador de etanol. A análise também destacou o efeito da temperatura na eficiência do sistema e na potência elétrica, ev-

idenciando a importância do controle dessas variáveis para otimizar o desempenho do sistema integrado SOFC-reformador de etanol. Foram analisados os efeitos das variações de temperatura (600 a 900℃) na SOFC, observando que temperaturas até cerca de 700 ℃ favorecem a produção de hidrogênio, enquanto temperaturas superiores podem reduzir essa produção devido a mudanças nos rendimentos de dióxido de carbono, monóxido de carbono e água. Uma análise comparativa foi conduzida para examinar os efeitos da razão ar/etanol nos rendimentos de hidrogênio e transferência de calor no reformador. Os resultados destacam a influência significativa dessa razão, indicando que um aumento superior a 40% leva à diminuição nos rendimentos de hidrogênio e afeta a transferência de calor no reformador devido ao favorecimento da reação exotérmica de oxidação. Por fim, é proposto um sistema sem integração com objetivo de mensurar o impacto da integração, alcançando uma potência nominal de 5 kW e uma eficiência de 44,4% para uma vazão de 0.377g/s. A aplicação de uma análise de pinch é realizada de modo a propor uma rede de troca de calor, visando recuperar calor dos fluxos de saída da SOFC. Essa abordagem proporciona um benefício adicional de 16.84%, resultando em uma eficiência total de 61,2%.

CONSIDERAÇÕES FINAIS

Uma revisão da literatura foi realizada com o objetivo de compreender possíveis diagramas e cenários para eficiência energética em sistemas integrados de SOFC (Células a Combustível de Óxido Sólido). A análise identificou os três principais tipos de reformadores integrados na literatura, expondo suas vantagens e desvantagens. Uma tabela foi elaborada com os principais parâmetros de referência relacionados ao uso de etanol em sistemas integrados de SOFC, abrangendo eficiências elétricas, térmicas e globais.Para estudar a melhoria da eficiência do sistema, optou-se por representar um modelo de SOFC integrado com um reformador em estado de equilíbrio para simular o conjunto SOFC e reformador. Modelos para representar os trocadores de calor e evaporadores foram implementados como parte da integração térmica. O estudo examinou os efeitos de variações de temperatura de 600 a 900 ℃ na SOFC. Os resultados indicam que um aumento de temperatura até cerca de 700 ℃ favorece a produção de hidrogênio, mas temperaturas superiores a 700 ℃ reduzem essa produção devido à diminuição do rendimento de dióxido de carbono e ao aumento nos rendimentos de monóxido de carbono e água. A influência da temperatura na produção de hidrogênio tem um efeito favorável a eficiência elétrica, mas o aumento de temperatura também aumenta as taxas de calor necessárias pelo reformador o que impacta negativamente o sistema. Um estudo comparativo foi conduzido para examinar os efeitos da razão ar/etanol nos rendimentos de hidrogênio e transferência de calor no reformador. A análise revelou que um aumento na razão oxigênio/etanol leva a uma diminuição nos rendimentos de hidrogênio e influencia a transferência de calor no reformador, pro-

movendo reações de oxidação exotérmicas. Considerando os resultados das variações de temperatura e da razão ar/etanol, foi sugerido um sistema sem integração térmica a fim de entender a influência dessa integração. O sistema proposto alcançou uma potência nominal de 5 kW conforme o objetivo do projeto, a uma temperatura de 883 K, resultando em uma eficiência de 44,4%. Utilizando a análise pinch foi proposto uma possível rede de troca de calor, capaz de recuperar 842 W de calor dos fluxos de saída da SOFC, representando um benefício de 16,8% na eficiência total, atingindo 61,2%. O sistema proposto demonstrou que a recuperação de calor dos fluxos quentes da SOFC tem um alto impacto na eficiência do sistema, e existem soluções viáveis para alcançar os objetivos do projeto. Apesar de o processo de reforma a vapor permitir rendimentos de hidrogênio mais altos, soluções com processo de reforma auto-térmica também são viáveis, proporcionando benefícios na integração térmica. O trabalho propôs um sistema com integração térmica, sem o uso do pós-combustor, focando na utilização do calor disponível da SOFC operando a 883 K, oferecendo vantagens adicionais em termos de custo de implementação e redução da necessidade de materiais de resistência térmica.

Palavras-chave: Efficiência, Etanol, SOFC, Reformador, Integração de calor, Análise Pinch.

ABSTRACT

This work investigates the energy efficiency of an SOFC system integrated into an ethanol reformer, using a 0D model to simulate the SOFC cell, while the reformer was simulated by thermodynamic equilibrium models. A SOFC cell model, obtained from the literature review, was implemented in the Python language and subsequently connected to reformer, adiabatic mixer and heat exchanger models, forming the basis for the presented results. Steady-state simulations were conducted to investigate the effects of temperature variation within the range of 600℃ to 900℃, as well as for oxygen/ethanol ratios in the range of 0% to 100%. The investigated output variables were the efficiency and electrical power of the SOFC cell, considering the nominal power of the SOFC as 5 kW. As a result, it was observed that for oxygen/ethanol ratios above 40%, the reformer operates exothermically (with a heat rate of approximately 1 kW), favoring heat integration. However, the hydrogen yield decreased with the increase in the oxygen/ethanol ratio, resulting in a reduction in electrical power (from 2.5 kW to 2.0 kW), cell efficiency (from 55% to 35%), and heat release rate from the electrochemical reaction (from -6 kW to -3 kW). Conversely, the increase in temperature allowed for higher hydrogen yields, resulting in an increase in electrical power (from 2.0 kW to 3.0 kW), cell efficiency (from 42% to 62%), heat release rate from the cell (-5 kW to -7 kW), but also causing an increase in the heat demand for the reformer (-0.04 a 0.7 kW). The simulation of the system without heat integration showed an overall efficiency of 44%, with the SOFC operating at a nominal power of 5 kW, under the following operating conditions: feed flow rate of 0.377 g/s, steam/ethanol ratio of 3.0, air/ethanol ratio of 0.5, and temperatures of the SOFC and reformer equal to 610℃ and 600℃, respectively. Additionally, the recirculation of the hot gases exiting the SOFC (residual gas from the anode and cathode) was evaluated as a heat integration strategy. The heat exchanger network (HEN) was synthesized through pinch analysis, allowing for the recovery of 842 W of heat. The overall efficiency of the integrated system was 61.24%, representing an increase of 16.84% compared to the system without integration. It is also worth mentioning that no external heat source to the SOFC was used in the network, as it is also possible to recover heat from the SOFC.

Keywords: Efficiency, Ethanol, SOFC, Reformer, Heat integration, Pynch analysis.

LIST OF FIGURES

Figure 1 – Scheme of partial pressures - three-phase boundary. 30
Figure 2 – SOFC schematic. 35
Figure 3 – Example of direct internal reformer using methane fuel. 37
Figure 4 – Example of indirect internal reformer using methane fuel. 38
Figure 5 – Example of external reformer using methane fuel. 39
Figure 6 – Simplified SOFC system with heat and power integration. 40
Figure 7 – Indirect integration of a SOFC and a gas turbine. 40
Figure 8 – Heat integration for SOFC systems with an adiabatic reformer. . . . 41
Figure 9 – Schematic diagram of the SOFC, illustrating the mass inflow and outflow for both the anode and cathode. 47
Figure 10 – Schematic of a reformer 48
Figure 11 – Schematic of the heat exchangers. 50
Figure 12 – Schematic of the evaporator 51
Figure 13 – Schematic of the mixer. 52
Figure 14 – Schematic of SOFC System 54
Figure 15 – Example of temperature-interval diagram (TID). 57
Figure 16 – Schematic of code flowchart including the user inputs. 59
Figure 17 – Comparison between simulated and experimental results of cell voltage at 873 and 1073 K 62
Figure 18 – Effect of temperature on the H_2, CO, CO_2 and CH_4 yields from the reformer. 65
Figure 19 – Effect of temperature in power and efficiency 66
Figure 20 – Effect of temperature in heat transfer rates of reformer and SOFC. . 67
Figure 21 – Effect of temperature in reformer heat rate and SOFC electrical power 67
Figure 22 – Effect of oxygen/ethanol ratio in yields 68
Figure 23 – Heat demand for SOFC and Reformer 69
Figure 24 – Effect of oxygen/ethanol ratio in power and efficiency 69
Figure 25 – Temperature-interval diagram for system 72
Figure 26 – Flowsheet of heat exchanger network for 1st temperature interval . . 73
Figure 27 – Flowsheet of heat exchanger network for 2nd temperature interval . 74
Figure 28 – Flowsheet of heat exchanger network for 3rd temperature interval . 75
Figure 29 – Flowsheet of heat exchanger network for the 4th temperature interval 76
Figure 30 – Flowsheet of heat exchangers for 5th temperature interval 77
Figure 31 – HX Diagram 80
Figure 32 – Keyword:SOFC - Papers per Year, Countries and Journals 92
Figure 33 – Keyword:SOFC + Modeling - Papers per Year, Countries and Journals 93

LIST OF TABLES

Table 1 – SOFC integrated with Reformer system models 45
Table 2 – Operation conditions of the benchmark case, without heat recovering. 55
Table 3 – Example of required inputs for a preliminary heat exchanger network (HEN) synthesis. 56
Table 4 – SOFC Model Parameters 61
Table 5 – SOFC and reformer parameters at nominal conditions 62
Table 6 – Comparison between experimental and simulated results of heat transfer rates in ethanol reforming under different conditions of steam/ethanol ratio, oxygen/ethanol rate and temperature 64
Table 7 – SOFC parameters for system without heat integration 70
Table 8 – Inlet variables for heat integration using pinch analysis 71
Table 9 – Residuals and heat rates for hot and cold streams in each interval-temperature 72
Table 10 – Detailed list of heat exchangers used in the heat exchanger network . 78

LIST OF ABBREVIATIONS AND ACRONYMS

DIR	Direct Internal Reformer
ER-SOFC	External reformer
GT	Gas Turbine
PEM	Polymer-Electrolyte Membrane
SOFC	Solid Oxide Fuel Cell
TPB	Three Boundary Phase
VCS	Villars-Cruise-Smith algorithm

LIST OF SYMBOLS

ΔH	Standard heat of reaction (kJ mol^{-1})
ΔG	Gibbs free energy (Jmol)
n	Number of electrons transferred (-)
F	Faraday constant (C mol^{-1})
E	Open Circuit Voltage (V)
V	Operating cell voltage (V)
i	Current (A)
v_{fuel}	Rate of fuel supplied (mols/s)
$\eta_{el,sys}$	Electric Efficiency (-)
P_{SOFC}	Electrical power output (W)
m_{fuel}	Fuel mass flow (kg/s)
LHV_{fuel}	Low heat value of fuel (kJ/mol)
$\eta_{the,sys}$	Thermal Efficiency (-)
Q_{heat}	Heat recovery in system (W)
j	Current density (A m^{-2})
$\dot{z}$	Amount of hydrogen consumed by the electrochemical reaction (mol s^{-1})
A_c	Fuel cell active area (m^2)
U_f	Fuel utilization factor (-)
$\dot{n}_{CH4}$	Molar flow (kmols/s)
$\dot{n}_{H2}$	Mass flow (kmols/s)
$\dot{n}_{CO}$	Mass flow (kmols/s)
E_{OCV}	Open-circuit voltage (V)
R	Gas constant (kJ $mol^{-1} K^{-1}$)
T	Temperature (K)
$P_{H_2O,f}$	Partial pressures of Water at TPB (bar)
$P_{H_2,f}$	Partial pressures of Hydrogen at Fuel inlet (bar)
$P_{O_{2,a}}$	Partial pressures of Oxygen at air inlet (bar)
η_{act}	Activation Overpotential (V)
η_{ohm}	Ohmic Overpotential (V)
η_{conc}	Concentration Overportential (V)
R_{ohm}	Total internal resistance (Ωm^2)
τ_{anode}	Thickness of anode (μm)
$\tau_{electrolyte}$	Thickness of electrolyte ((μm)
$\tau_{cathode}$	Thickness of cathode (μm)
σ_{anode}	Electronic conductivity of anode ($\Omega^{-1} m^{-1}$)
$\sigma_{cathode}$	Electronic conductivity of anode ($\Omega^{-1} m^{-1}$)
$\sigma_{electrolyte}$	Electronic conductivity of electrolyte($\Omega^{-1} m^{-1}$)

$\eta_{conc,a}$	Concentration Overportential at anode (V)
$\eta_{conc,c}$	Concentration Oveportential at cathode (V)
$P_{H_2O,TPB}$	Partial pressures of Water at TPB (bar)
$P_{H_2,TPB}$	Partial pressures of Hydrogen at TPB (bar)
$P_{O_2,TPB}$	Partial pressures of Oxygen at TPB (bar)
P_i	Partial pressures of component i (bar)
$D_{eff,anode}$	Effective gaseous diffusivity through anode ($m^2 s^{-1}$)
$D_{eff,cathode}$	Effective oxygen diffusivity through cathode ($m^2 s^{-1}$)
P	Operating pressure of SOFC (bar)
α	Transfer coefficient (-)
$\eta_{act,cathode}$	Activation Overpotential at cathode (V)
$\eta_{act,anode}$	Activation Overpotential at anode (V)
$j_{0,anode}$	Exchange current density at anode (A m^{-2})
$j_{0,cathode}$	Exchange current density at cathode (A m^{-2})
E_{anode}	Activation energy of anode (kJ mol^{-1})
$E_{cathode}$	Activation energy of cathode (kJ mol^{-1})
k_{anode}	Pre-exponential factor of the anode (Am^{-2})
$k_{cathode}$	Pre-exponential factor of the cathode (Am^{-2})
MW_{H2}	molar mass (g/mols)
$\dot{m}^j$	Mass flow (kg/s)
h^j	Specific enthalpy (kJ/kg)
$G^o_{f_i}$	Formation Gibbs free energy of the chemical species (Jmol)
$\dot{n}_i$	Molar flow rate of chemical species i on outlet (mols/s)
$a_{i,k}$	Total number of atoms (-)
$\dot{n}_{io}$	Molar flow rate of chemical species i on outlet (mols/s)
$\dot{m}$	mass flowrate (kg/s)
cp	Heat capacity (J/kg.K)
ΔT	Temperature (K)
cp_{Water}	Heat Capacity water (J/kg.K)
T_{in}	Temperature (K)
$T_{Water,Sat}$	Mass flow (kg/s)
$P2_w$	Water reference pressure (kPa)
$P1_w$	Water reference pressure (kPa)
ΔH_{Vap}	Mass flow (kg/s)
$\dot{m}_{Outlet}$	Outlet mass flow (kg/s)
$\dot{m}_{Ethanol}$	Ethanol mass flow (kg/s)
$\dot{m}_{Water}$	Water mass flow (kg/s)
T_{out}	Temperature (K)
Q	Thermal energy (kW)

U	Mass flow (kg/s)
R_{k-1}	Heat load (W)
$Q_{i,k}$	Heat load (W)
$Q_{j,k}$	Heat load (W)

CONTENTS

1 INTRODUCTION 21
1.1 OBJECTIVE 24
1.1.1 Main objective 24
1.1.2 Specific objectives 24
1.2 ORGANIZATION 24
2 FUNDAMENTALS 25
2.1 MASS CONSERVATION 25
2.2 ENERGY CONSERVATION 25
2.3 EFFICIENCIES 25
2.3.1 Overall efficiency of the SOFC 25
2.3.1.1 Thermal efficiency 25
2.3.1.2 Electrical efficiency 26
2.3.1.3 Fuel efficiency 26
2.3.2 Integrated system efficiencies 27
2.4 SOFC MODEL 27
2.4.1 Cell voltage and current density 27
2.4.2 Losses in the cell voltage 28
3 THEORETICAL FRAMEWORK 32
3.1 FUEL REFORMING 32
3.2 SOLID OXIDE FUEL CELL (SOFC) 34
3.3 INTEGRATION BETWEEN SOFC AND REFORMER 36
3.3.1 Direct internal reformer 36
3.3.2 Indirect Internal Reformer 37
3.3.3 External reformer 38
3.4 HEAT INTEGRATION 39
3.5 SYSTEM EFFICIENCIES USING ETHANOL 41
4 METHODOLOGY 46
4.1 UNIT OPERATIONS 46
4.1.1 SOFC 46
4.1.2 Reformer 48
4.1.3 Heat exchangers 49
4.1.4 Evaporator 50
4.1.5 Mixer 51
4.2 STRATEGIES FOR HEAT INTEGRATION 52
4.3 PINCH ANALYSIS 55
4.4 MODEL IMPLEMENTATION 58
5 RESULTS AND DISCUSSIONS 60

5.1 VALIDATION OF THE SOFC MODEL 60
5.1.1 Model parameters and inlet variables for validation 60
5.1.2 Ethanol reforming 63
5.2 SENSITIVITY ANALYSIS 64
5.2.1 Temperature effect 65
5.2.2 Air/Ethanol effect 68
5.3 RESULTS OF MODEL WITHOUT HEAT INTEGRATION 70
5.4 PINCH ANALYSIS 70
5.4.1 First Interval 73
5.4.2 Second Interval 73
5.4.3 Third Interval 75
5.4.4 Fourth Interval 75
5.4.5 Fifth Interval 76
5.4.6 Heat exchanger network (HEN) 76
6 CONCLUSIONS 81
6.1 SUGGESTION FOR FUTURE WORK 82
REFERENCES 83
APPENDIX A – PAPERS RESEARCH 91
APPENDIX B – EQUATION (22) AND EQUATION (23) 94
B.1 DEMONSTRATION OF EQUATION (22): 94
B.2 DEMONSTRATION OF EQUATION (23): 95

1 INTRODUCTION

The increase in demand for energy production and the concern with the environmental impact caused by the traditional sources of energy has become a driver for research in system efficiencies, to improve as much as possible the use of generated energy to minimize these effects on the environment (KACZMARCZYK; GURGUL, 2021; ALHAZMI et al., 2021).

Nowadays, most vehicles around the world are feed by fossil fuel, which results in greenhouse gas emissions in the atmosphere. The growing concern with the environment has been reflected into new definition of standards for pollutant emission, become challenging the development of internal combustion engine, with some countries setting a target of no longer sell combustion vehicles after 2050. Thus, the search for more efficient methods of energy generation for vehicles is a growing field (MA et al., 2021; KELES et al., 2008).

In this context, solid oxide fuel cell (SOFC) systems at high temperature has become a promising alternative for power generation, replacing traditional sources such as thermoelectric, as well as in new hybrid electric vehicles (BADUR et al., 2018; ZHAO; BURKE, 2009). The SOFC is a device where the chemical energy is converted to electricity by the consumption of hydrogen as a fuel. However, hydrogen is a fuel that requires high pressure to be stored which can consume space and requires extra safety features for a vehicular application. A solution to mitigate this problem is the application of a reformer integrated with a fuel cell, which allows the system to be filled with natural gas, ethanol, and another hydrocarbon which are easier to handle (O'HAYRE et al., 2016).

The advantage of using fuel cell in Brazil is the accessibility to proper infrastructures for the use of ethanol, with the vast number of gas stations around the country. The success of ethanol use can be attributed to the Proalcool program (National Ethanol Program (BIODIESELBR, 2006), developed by the government in the 70s to encourage the production and use of ethanol as fuel to reduce the dependence on petroleum, which had high prices during that period. From 1975 to 1976, which is the start of the program, Brazil produced around 600 million litres. In comparison, the production in 2015-2016 was about 28 billion litres (BIODIESELBR, 2006; FAPESP, 2016).

More recently, Nissan presented an electric vehicle coupled to a SOFC integrated with a reformer to be used as a range extender and ran tests in Brazil and Japan (MA et al., 2021). The reformer was connected to a tank filled with ethanol, which allowed the car to be filled almost everywhere as ethanol is highly available in the country. According to Nissan, the vehicle can run 600 km with thirty liters of ethanol, running a battery of 24 kWh (NISSAN, 2016). This requirement reinforces the necessity to study the energetic efficiency of the system, allowing for reduction to a better-defined size

of components according to the module necessity, which can result in cost and size reduction.

The operation of SOFC with integrated reformers offers numerous benefits, including the ability to utilize a wide variety of fuels (O'HAYRE et al., 2016; SRISIRIWAT, N.; WUTTHITHANYAWAT, 2013). Nonetheless, the reformer may require heat in accordance with the reforming process; the steam reforming process, an endothermic reaction, is the most prevalent. Consequently, a specific quantity of heat is necessary, which can be supplied by the heat retrieved from the system via heat integration (TIPPAWAN; ARPORNWICHANOP, 2014a). Thus, system efficiency is increased as reformer heating energy is decreased. As a consequence, the system enhances efficiency by producing the same quantity of hydrogen with less fuel by generating more electricity from the same amount of fuel (O'HAYRE et al., 2016; KUPECKI, 2018).

In a system without heat integration, the supply of this energy must be sourced from an external entity. Therefore, heat integration presents a significant potential to enhance system efficiency by utilizing waste heat that would otherwise be released into the environment to provide heating for the reformer or any necessary utilities (O'HAYRE et al., 2016; KUPECKI, 2018).

While a significant portion of the existing literature primarily emphasizes the potential of heat integration in the context of the steam reforming process, which is characterized by its endothermic reactions, the autothermal reforming process offers an alternate approach that requires less heat input to the system. Furthermore, within a specific range, this process can exhibit exothermic behavior (TIPPAWAN; ARPORNWICHANOP, 2014a).

Hence, there exists a significant area that warrants investigation in the examination of efficiencies pertaining to heat integration inside fuel cell systems integrated with reformers operating under varying parameter sets. This exploration is crucial for comprehending the parameter trade-offs that align with the desired target, as their impact in the heat integration specially for systems using ethanol.

In the last 20 years, the number of papers related to the SOFC term has been increasing substantially, achieving more than 27,000 articles. These works mainly involve anode material development, experimental methods, and simulation models to predict the behavior and the key features of energy production. The modeling topic has been explored primarily in the United States, China, Germany, and Italy with an average of 165 papers per year (Appendix A). The fuel cell models will take an important position in the next 20 years, especially because they allow to predict the behavior of these systems in different conditions, helping to understand the effect of parameters in the cell performance results. The SOFC literature is vast and several types of models have been developed, from 0D (lumped) to 3D models tested in a steady state or transient conditions, utilizing different strategies, such as theoretical, semi-empirical, or empirical

models (YANG et al., 2020; CHEDDIE; MUNROE, 2007; WANG et al., 2011).

The literature provide multiple studies, in which the system diagrams are compared reforming characteristics (positions in relation to SOFC, reforming process), use of different materials, fuels, and reuse of SOFC outlet gas with afterburner and re circulation (KUPECKI, 2018; O'HAYRE et al., 2016; CHOUDHURY; CHANDRA; ARORA, 2013). The SOFC system within the range of 600-1000℃ has as reported efficiency within the range 25.0% to 62.0%, which can depend of the application, fuel and the defined characteristics select (KUPECKI, 2018). The SOFC heat integration systems has a efficiency reported of 40.0% to 51.0% for ethanol fuel (ARTEAGA-PEREZ et al., 2009; SAEBEA et al., 2013). As a comparison the efficiency of a combustion motor is in the range of 30% for ethanol (AMBRÓS et al., 2015). Therefore, the investigation of efficiencies holds value in offering an alternative resolution to address the energy requirements in vehicular applications through the utilization of a sustainable fuel source.

Despite the existence of numerous publications, an optimized architecture for heat integration has yet to be developed. Various configurations of heat exchangers, along with diagrammatic representations, including afterburners and the incorporation of gas turbines, can be found in the existing literature. The literature presents various configurations for integrating gas turbines and reformers (CHOUDHURY; CHANDRA; ARORA, 2013; WANG et al., 2011), which are potential options to be investigated due to their strong connection with system power and implementation.

From a quantitative standpoint, the models can be implemented with varying levels of granularity, contingent upon the specific objectives of the investigation. The existing body of literature includes various studies that center on the analysis of three-dimensional heat transfer phenomena for the purpose of identifying hot spots through the utilization of computational fluid dynamics (CFD) (ALHAZMI et al., 2021). Additionally, there are works that employ simplified representations of the model, ranging from zero-dimensional to two-dimensional approaches (MA et al., 2021; KIM, M. S.; KIM, D. K., 2020; BIANCHI et al., 2020). Several studies have conducted a literature review, categorizing various aspects and conducting comparisons among different works. These studies have also provided a comprehensive overview of the limitations associated with each type of model implementation (BAO et al., 2018; WANG et al., 2011; BHATTACHARYYA; RENGASWAMY, 2009). The authors of this study assert that the limitations are associated with the extent of detail that must be captured within the system. The models employed in this study utilize lumped, one-dimensional (1D), and two-dimensional (2D) methodologies, which involve certain simplifications. However, these approaches offer the advantage of low computational time, making them well-suited for real-time applications. Furthermore, they strike a favorable balance between accuracy and computational efficiency. The aim of this study is to comprehensively analyze the primary factors influencing the system efficiencies from a global standpoint.

To achieve this, the chosen methodology involved the utilization of lumped models. This approach offers the benefit of rapid simulation time and the potential for seamless integration with other platforms.

1.1 OBJECTIVE

1.1.1 Main objective

The objective of this work is to investigate the energetic efficiency of an SOFC system integrated with an ethanol reformer also evaluating thermal integration in the fuel cell employing high level modeling. Furthermore, the potential for thermal integration will be investigated by recovering heat through the exothermic reaction within the fuel cell to supply the energy needed for the endothermic reforming reaction.

1.1.2 Specific objectives

Considering the development of the work and the general objective presented, the following specific objectives stand out:

- Review the literature related to the models to integrate reformer with SOFC;
- Implement a flow sheet model to simulate the operation of a solid oxide fuel cell (SOFC) in Python using the Cantera library;
- Investigation of the efficiency of an SOFC integrated with an ethanol reformer in an open circuit configuration with no heat integration, verifying the results with literature data used as reference;
- Apply the Pynch analysis to propose a preliminary heat exchanger network from heat integration of hot streams of SOFC cell and heat recovered of SOFC and reformer;
- Analyse the best condition for the input variables to improve the thermal efficiency of the system.

1.2 ORGANIZATION

In Chapter 2, the literature regarding to the topics of SOFC and reformer integration were reviewed. Thus, in the Chapter 3 is provide the details of methodology, presenting the steps of code implementation as the strategy to represent the SOFC cell integrated with the reformer, as the details of components models implemented and diagrams used for this study. Chapter 4 presents the results of the investigation for sensibility analysis, as the results of the pynch analysis, and the comparison of integrated heat system to the system without integration. Lastly, Chapter 5 presents the conclusions for the analysis, and suggestions for future works.

2 FUNDAMENTALS

2.1 MASS CONSERVATION

The principle of mass conservation applied to a control volume states that the liquid rate o which the mass enter the volume is equal to its variation in the system. At steady state the following equation represents the steady-state mass conservation in a control volume (ÇENGEL; GHAJAR, 2009), where m_{in}, m_{out} represent the mass flow in (kg/s).

$$\sum \dot{m}_{in} - \sum \dot{m}_{out} = 0 \tag{1}$$

2.2 ENERGY CONSERVATION

The first law of thermodynamics states that energy can not be created or destroyed throughout a process. As a result, every amount of energy must be considered during a process. The first law of thermodynamics written for a control volume, at steady state is presented by equation (2) (ÇENGEL; GHAJAR, 2009).

$$\dot{Q} - \dot{W} = \sum \dot{m}_{in} h_{in} - \sum \dot{m}_{out} h_{out} \tag{2}$$

where m_{in}, m_{out} (kg/s) represent the mass flow, h_{in} and h_{out} (kJ/kg) represent the specific enthalpy, $\dot{Q}$ (W) is the heat and $\dot{W}$ is the work (W), assuming variation in potential and kinetic energy are zero.

2.3 EFFICIENCIES

2.3.1 Overall efficiency of the SOFC

The overall efficiency of the SOFC is presented in the equation (3), also called real efficiency of a fuel cell in the literature. This efficiency is the product of thermal efficiency ($\eta_{thermal}$), electrical efficiency ($\eta_{eletrical}$), and fuel efficiency (η_{fuel}) (O'HAYRE et al., 2016; REVANKAR; MAJUMDAR, 2016).

$$\eta_{overall} = \eta_{thermal} \eta_{eletrical} \eta_{fuel} \tag{3}$$

2.3.1.1 Thermal efficiency

The thermodynamic efficiency of a fuel cell is the ratio between the available electrical energy and useful energy of the fuel (REVANKAR; MAJUMDAR, 2016). The useful energy of a fuel is expressed by the enthalpy of the reaction ΔH (O'HAYRE et al.,

2016). The maximum amount of energy for a chemical reaction that can be converted into electrical energy is limited by the Gibbs free energy ΔG (REVANKAR; MAJUMDAR, 2016; O'HAYRE et al., 2016). Thus, thermodynamic efficiency of the SOFC is defined as presented in equation (4).

$$\eta_{thermal,max} = \frac{\Delta G}{\Delta H} \tag{4}$$

However, this efficiency can be presented in a more practical format relating the electrical work produced with the enthalpy of the reaction, given by equation (5) (REVANKAR; MAJUMDAR, 2016).

$$\eta_{thermal} = \frac{nFE}{\Delta H} \tag{5}$$

where n is the number of electrons transferred per molecule during the electrochemical reaction, F is the Faraday constant, and E is the open-circuit voltage.

2.3.1.2 Electrical efficiency

The electrical efficiency is the ratio between the work available in the fuel cell, and the reversible work, considering the major losses: activation, ohmic and concentration loss (REVANKAR; MAJUMDAR, 2016; O'HAYRE et al., 2016). This efficiency is defined by equation (6). An important aspect of the electrical efficiency is the dependence of current: the voltage in the cell will decrease with the increase of current load, leading to a low electrical efficiency. Therefore, a fuel cell is more efficient with low current (REVANKAR; MAJUMDAR, 2016).

$$\eta_{electrical} = \frac{E}{V} \tag{6}$$

where E is open-circuit voltage and V the operating cell voltage.

2.3.1.3 Fuel efficiency

This efficiency considers that not all the fuel available will generate electrical energy, and some part of the fuel can pass by the cell without reacts during the process (O'HAYRE et al., 2016). Fuel efficiency is the ratio between the fuel available in the system and the fuel used to generate the reaction, given by equation (7).

$$\eta_{fuel} = \frac{\frac{i}{nF}}{v_{fuel}} \tag{7}$$

where i is the current generated, n is the number of electrons transferred per molecule during the electrochemical reaction, F is the Faraday constant (C/mol) and v_{fuel} is the molar flow rate of hydrogen supplied (mol/s).

2.3.2 Integrated system efficiencies

In addition to the efficiency calculated for the SOFC itself, the efficiencies (electrical, thermal, and overall) of the integrated system, including reformer and heat recovered, can also be calculated. These relations were used to evaluate the operating point of the system in multiple cases in the literature (ZHOU et al., 2022; MA et al., 2021; SAEBEA; PATCHARAVORACHOT; ARPORNWICHANOP, 2012).

The system electric efficiency ($\eta_{el,sys}$) is given by equation (8), as the relation of electric power produced by the SOFC to the enthalpy of reaction (ZHOU et al., 2022).

$$\eta_{electrical,system} = \frac{P_{SOFC}}{m_{fuel} LHV_{fuel}} \tag{8}$$

where P_{SOFC} is electric power of SOFC, m_{fuel} is fuel mass flow rate and LHV_{fuel} is lower heating value for the fuel.

Similarly, the thermal efficiency ($\eta_{the,sys}$) is given by equation (9) (ZHOU et al., 2022).

$$\eta_{thermal,system} = \frac{Q_{heat}}{m_{fuel} LHV_{fuel}} \tag{9}$$

where Q_{heat} is the thermal energy recovered from the SOFC.

Overall efficiency for the type ER-SOFC is the direct sum of the electrical and thermal efficiency, given by equation (11) (ZHOU et al., 2022).

$$\eta_{overall,system} = \eta_{electrical,system} + \eta_{thermal,system} \tag{10}$$

2.4 SOFC MODEL

2.4.1 Cell voltage and current density

The model to represent the SOFC is based on the work of (SAEBEA; PATCHARAVORACHOT; ARPORNWICHANOP, 2012). The current density (j) is computed through a correlation which depends on hydrogen consumption in the electrochemical reaction and area, as presented in Equation (11): (SAEBEA; PATCHARAVORACHOT; ARPORNWICHANOP, 2012)

$$j = \frac{2F\dot{z}}{A_c} \tag{11}$$

in which $\dot{z}$ ($mols^{-1}$) is the amount of hydrogen consumed in the reaction, and A_c (m^2) the active area of fuel cell. The hydrogen consumption rates $\dot{z}$ in electrochemical reaction depends on fuel utilization factor U_f and the inlet molar flow rates of components

$\dot{n}_{CH4}$, $\dot{n}_{H2}$ and $\dot{n}_{CO}$ (kmol/s). This correlation is expressed by equation (12). However, as the process occurs in high temperature it is possible to occur the water gas shift reaction and steam reforming reacting of methane in the SOFC (SAEBEA; PATCHARAVORACHOT; ARPORNWICHANOP, 2012). Thus, including the CH_4 and CO is a way to take those reaction into account without the need for a more complex modeling.

$$U_f = \frac{\dot{z}}{4\dot{n}_{CH4} + \dot{n}_{H2} + \dot{n}_{CO}} \tag{12}$$

The open circuit voltage E_{OCV}, also called as reversible cell voltage, for an SOFC is given by the Nerst Equation, which relates the cell voltage with species concentration (O'HAYRE et al., 2016).

$$E_{OCV} = E^0 - \frac{RT}{2F} ln\left(\frac{P_{H_2O,f}}{P_{H_2,f} P_{O_2,a}^{0.5}}\right) \tag{13}$$

where E_{OCV} is the open circuit voltage (V), the R is the constant of the gas (J/mol·K), T is temperature (K), and $P_{H_2O,f}$, $P_{H_2,f}$ and $P_{O_{2,a}}$ are the partial pressure of water, hydrogen, oxygen (bar), respectively. E^0 is the open circuit voltage at standard pressure, presented in the equation (14):

$$E^0 = 1.253 - 2.4516 \times 10^{-4} T \tag{14}$$

However, in a actual condition, the voltage (V) is lower than the open circuit voltage E_{OCV}, due to of the irreversible losses in the system. This voltage is given by equation (15), which takes into account the activation loss (η_{act}), ohmic loss (η_{ohm}) and concentration loss (η_{conc}) (SAEBEA; PATCHARAVORACHOT; ARPORNWICHANOP, 2012), which will be explained in details in the next section.

$$V = E_{OCV} - \eta_{act} - \eta_{conc} - \eta_{ohm} \tag{15}$$

2.4.2 Losses in the cell voltage

The ohmic loss, η_{ohm} (V), occurs due to the conduction resistance of materials to the flow of electrons through the cell components. This loss has linear dependence with the current density and voltage drop, as presented in equation (16) (SAEBEA; PATCHARAVORACHOT; ARPORNWICHANOP, 2012).

$$\eta_{ohm} = jR_{ohm} \tag{16}$$

where R_{ohm} (Ωm^2) is the internal resistance represented by equation (17) (SAEBEA; PATCHARAVORACHOT; ARPORNWICHANOP, 2012).

$$R_{ohm} = \frac{\tau_{anode}}{\sigma_{anode}} + \frac{\tau_{electrolyte}}{\sigma_{electrolyte}} + \frac{\tau_{cathode}}{\sigma_{cathode}} \tag{17}$$

where τ_{anode}, $\tau_{electrolyte}$ and $\tau_{cathode}$ are the thickness (μm) of the anode, electrolyte and cathode layer, respectively. σ_{anode} and $\sigma_{cathode}$ are the electric conductivity ($\Omega^{-1} m^{-1}$), for the anode and cathode, respectively, while $\sigma_{electrolyte}$ is the ionic conductivity of the electrolyte.

The concentration loss, η_{conc} (V), emerges from the transport limitations within the porous structure of the electrolyte due to the resistance to the mass transport. It is expressed as the sum of losses in the anode, $\eta_{conc,a}$ (V), and in cathode, $\eta_{conc,c}$ (V), shown in the equation (18), (19) and (20) (SAEBEA; PATCHARAVORACHOT; ARPORNWICHANOP, 2012).

$$\eta_{conc} = \eta_{conc,a} + \eta_{conc,c} \tag{18}$$

$$\eta_{conc,a} = \frac{RT}{2F} ln \left(\frac{P_{H_2O,TPB} P_{H_2,f}}{P_{H_2O,f} P_{H_2,TPB}} \right) \tag{19}$$

$$\eta_{conc,c} = \frac{RT}{2F} ln \left(\frac{P_{O_{2,a}}}{P_{O_{2,TPB}}} \right) \tag{20}$$

where $P_{H_2O,TPB}$ and $P_{H_2,TPB}$ are the partial pressure of water and hydrogen, respectively, at three-phase boundary (TPB), as explained below. $P_{H_2,f}$ and $P_{H_2O,f}$ are the partial pressures of the species in the anode and cathode, which describes the transport rates of the species in the electrodes (CHAN; KHOR; XIA, 2001).

Figure 1 presents a scheme of the partial pressures in the three-phase boundary mentioned above in order to elucidate the mechanism of chemical species diffusion in the fuel cell. The hydrogen partial pressure $P_{H_2,f}$ is present in the left side of anode together with the $P_{H_2O,f}$. Next section is the region called three-phase boundary, in which is possible to observe the last point for H_2 pressure mentioned as $P_{H_2,TPB}$, and $P_{H_2O,TPB}$. The same consideration can be made for the cathode side for $P_{O_{2,a}}$, and $P_{O_2,TPB}$.

The partial pressures for hydrogen and oxygen, P_i, required to calculate the concentration loss are determined using a Fick law (SAEBEA; PATCHARAVORACHOT; ARPORNWICHANOP, 2012; ARPORNWICHANOP et al., 2009). Equation (23) is calculated based in the isothermal gas species transport equation for a mixture of 2 gases, considering a dominant contribution of binary diffusion to the transport through electrode in a steady state condition (KIM, J.-W. et al., 1999), representing the partial pressure of oxygen in the cathode. The authors presented in details the steps to ob-

Figure 1 – Scheme of partial pressures - three-phase boundary.

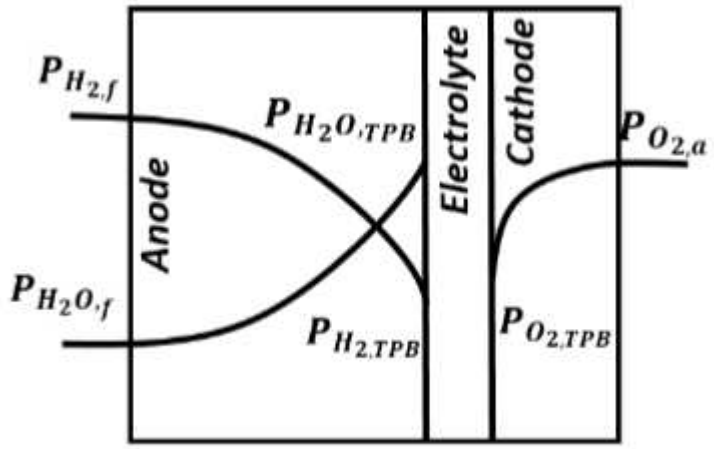

Source: Adapted from (AGUIAR; ADJIMAN; BRANDON, 2004)

taining by theoretical analysis the equations (21), (22) and (23), which represents the partial pressures of hydrogen, water and oxygen at three-phase boundary (TPB).

$$P_{H_2,TPB} = P_{H2,f} - \frac{RT\tau_{anode}}{2FD_{eff,anode}}j \tag{21}$$

$$P_{H_2O,TPB} = P_{H_2O,f} + \frac{RT\tau_{anode}}{2FD_{eff,anode}}j \tag{22}$$

$$P_{O_2,TPB} = P - (P - P_{O_{2,a}})exp\left(\frac{RT\tau_{cathode}}{2FD_{eff,cathode}P}j\right) \tag{23}$$

where $D_{eff,anode}$ (m^2s^{-1}) is the effective gas diffusivity through the anode, and $D_{eff,cathode}$ (m^2s^{-1}) is the effective gas diffusivity through the cathode, both considering gas mixture of H_2 and H_2O for the anode and O_2 and N_2 in cathode (SAEBEA; PATCHARAVORACHOT; ARPORNWICHANOP, 2012), $P_{H_2,f}$ (bar) and $P_{H_2O,f}$ (bar) are the partial pressure of hydrogen and water in the anode inlet (indicate with subscribe f) presented in Figure 1. Similarly, $P_{H_2,TPB}$ (bar), $P_{O_2,TPB}$ (bar) and $P_{H_2O,TPB}$ (bar) are the partial pressure in the three-phase boundary (TPB) for hydrogen, oxygen and water, respectively. P is the pressure in the SOFC (bar), and $P_{O_{2,a}}$ the partial pressure in the air channel (bar).

The last irreversible loss to be calculated in the system is the activation loss, which is caused by the slow electrochemical reaction at the electrode surface. The activation losses from the anode and cathode, can be calculated using the Bulter-Volmer equation, as shown in equations (24) and (25) (SAEBEA; PATCHARAVORACHOT; ARPORNWICHANOP, 2012).

$$j = j_{0,anode}\left[\frac{P_{H_2,TPB}}{P_{H_2,f}} exp\left(\frac{\alpha nF}{RT}\eta_{act,anode}\right) - \frac{P_{H_2O,TPB}}{P_{H_2O,f}} exp\left(-\frac{(1-\alpha)nF}{RT}\eta_{act,anode}\right)\right] \tag{24}$$

$$j = j_{0,cathode}\left[exp\left(\frac{\alpha nF}{RT}\eta_{act,cathode}\right) - exp\left(-\frac{(1-\alpha)nF}{RT}\eta_{act,cathode}\right)\right] \tag{25}$$

where α is the transfer coefficient, n is the number of electrons transferred. $\eta_{act,cathode}$ (V) and $\eta_{act,anode}$ (V) are the activation overpotentials.

As α is 0.5 and n is 2, the equation (24) and (25) can be rewrite as equation (26) and (27) (THANOMJIT et al., 2015). The steps to obtain the equations (26) and (27) are described in the appendix B.

$$n_{act,anode} = \frac{RT}{0.5nF}\log\frac{\left[\sqrt{4(\frac{P_{H_2,TPB}}{P_{H_2,f}})(\frac{P_{H2O,TPB}}{P_{H2O,f}}) + (\frac{j}{j_{0\,anode}})^2} + (\frac{j}{j_{0\,anode}})\right]}{(\frac{P_{H_2,TPB}}{P_{H_2,f}})} \tag{26}$$

$$n_{act,cathode} = \frac{RT}{F} ln\left[\frac{j}{2j_{0\,cathode}} + \sqrt{\left(\frac{j}{2j_{0\,cathode}}\right)^2 + 1}\right] \tag{27}$$

where $j_{0,anode}$ (Am^{-2}) and $j_{0,cathode}$ (Am^{-2}) are the exchange current density at anode and cathode, respectively, as presented in equations (28) and (29).

$$j_{0,anode} = \frac{RT}{nF} k_{anode} exp\left(-\frac{E_{anode}}{RT}\right) \tag{28}$$

$$j_{0,cathode} = \frac{RT}{nF} k_{cathode} exp\left(-\frac{E_{cathode}}{RT}\right) \tag{29}$$

where E_{anode} and $E_{cathode}$ are the activation energies ($kJmol^{-1}$) of electrochemical reactions in anode and cathode, respectively, and k_{anode} (Am^{-2}) and $k_{cathode}$ (Am^{-2}) are pre-exponential factors of the anode and cathode, respectively.

3 THEORETICAL FRAMEWORK

This chapter presents a literature review of topics relevant to this research, starting with the options of integration of SOFC (Solid Oxide Fuel Cell) with the reformer options and the energy cogeneration through the heat recovery. Furthermore, this chapter outlines the efficiencies and presents a reference table containing simulation results for integrated SOFC-reformer models.

3.1 FUEL REFORMING

An integrated SOFC-reformer system is composed by a fuel reformer, which converts fuel to a hydrogen rich gas, followed by a fuel cell, which converts hydrogen and oxygen into water with electric energy generation. In these systems, the required hydrogen supply for the SOFC is achieved through the cogeneration of fuel using a reformer. Reforming reactions decomposes a fuel in presence of water steam, CO_2 or oxygen into a gas mixture comprised by CO, CO_2 and H_2, supplying the hydrogen to the fuel cell (KUPECKI, 2018).

Inside the fuel reformer, ethanol, for example, can be converted to a hydrogen rich gas through different catalytic routes such as steam reforming, dry ethanol reforming, partial oxidation and autothermal reforming (MA et al., 2021).

Steam reforming is an endothermic process, which combines ethanol and water steam at high temperatures (TIPPAWAN; ARPORNWICHANOP, 2014a). This process is the most used reforming method because it provides a high hydrogen yield with high selectivity for side reactions. The steam reforming reaction is given by the following chemical reaction R1 (TIPPAWAN; ARPORNWICHANOP, 2014a):

$$C_2H_5OH + 3\,H_2O \rightleftharpoons 2\,CO_2 + 6\,H_2 \quad \Delta H = +347\,\mathrm{kJmol}^{-1} \qquad \text{(R1)}$$

The partial oxidation is an exothermic process wherein ethanol reacts with oxygen, forming hydrogen, carbon dioxide and other components. The advantages of this reforming process is its fast start-up, since this system does not require an external heat source to takes place. However, the stoichiometric hydrogen yield is lower than that from steam reforming. This reaction is shown in reaction R2 (TIPPAWAN; ARPORNWICHANOP, 2014a):

$$C_2H_5OH + \tfrac{3}{2}O_2 \rightleftharpoons 2\,CO_2 + 3\,H_2 \quad \Delta H = -620.3\mathrm{kJmol}^{-1} \qquad \text{(R2)}$$

The autothermal reforming is a combination of steam reforming and partial oxidation in a single process represented by R3. This method is almost thermoneutral for ethanol reforming, depending on the amounts of oxygen and water steam fed into reformer (TIPPAWAN; ARPORNWICHANOP, 2014a).

$$C_2H_5OH + xO_2 + (3–2\,x)H_2O \rightleftharpoons (6–2\,x)H_2 + 2\,CO_2 \quad \text{(R3)}$$

In particular, the performance of reforming reactions depends mainly on catalysts employed in the process. Depending on catalyst, side reactions occur in ethanol reforming. Water-gas shift reaction is the most important, and desirable, side reaction in reforming systems, as presented in R4. Typically, reforming reaction are performed with excess of water steam to promote the conversion of CO into H_2 and CO_2. Therefore, this reaction increase the H_2 yield, when it is shifted towards the exothermic direct reaction (SAEBEA; PATCHARAVORACHOT; ARPORNWICHANOP, 2012; TIPPAWAN; ARPORNWICHANOP, 2014a).

$$CO + H_2O \rightleftharpoons CO_2 + H_2 \quad \text{(R4)}$$

An important aspect of the reforming process is catalysts, which prevent the formation of coke and allow high ethanol conversion and selectivity regarding the side reactions. The Bourdoard reaction (R5) is the main reactions that lead to the formation of carbon and coke (SAEBEA; PATCHARAVORACHOT; ARPORNWICHANOP, 2012).

$$2\,CO \rightleftharpoons CO_2 + C \quad \text{(R5)}$$

In general, the catalysts used in reforming reactions can be classified in 3 groups: noble metal based, non-noble metal based and bi-metallic catalysts (BARUAH et al., 2015; BRITO et al., 2020). To provide a brief overview of the main catalysis material the groups are detail with most common materials:

- Noble metal based: Rhodium, palladium, platinum, ruthenium. These catalysts are very efficient for autothermal ethanol reforming, despite the high cost associated to its production (BRITO et al., 2020; BARUAH et al., 2015);
- Non-noble metals based: Nickel and cobalt. These catalysts have good stability and selectivity, improving the resistance of catalysts regarding the deactivation by coke formation (BRITO et al., 2020; BARUAH et al., 2015);
- Bi-metallic catalysts: Nickel palladium and silver (BRITO et al., 2020; BARUAH et al., 2015).

To maximize the hydrogen yields, the proper selection of reaction conditions is crucial, particularly the temperature, the ratio of oxygen to ethanol, and the ratio of water to ethanol. Reforming conditions may vary depending on the specific type of process and the catalyst materials employed. From the published works, one can see the typical reforming conditions, in which the temperature range is between 300 ℃ to 700 ℃, an oxygen/ethanol ratio predominantly around 0.5. The water/ethanol ratio around 3, with some experiment testing up to 13. In particular, the steam is fed in excess to favor the water-gas shift reaction, allowing high yield of hydrogen, as well

as decrease the coke formation rates. It is well known in literature that coke formation is not thermodynamically spontaneous in high water to ethanol ratios (TIPPAWAN; ARPORNWICHANOP, 2014b; BARUAH et al., 2015).

3.2 SOLID OXIDE FUEL CELL (SOFC)

Fuel cells are electrochemical devices that convert chemical energy into electrical energy, and include different types. These systems are similar to a battery that generates energy based on an electrochemical reaction but with the difference that it can work indefinitely as long as fuel is injected into the system.

As shown in Figure 2, the SOFC cell is comprised by three main components: anode, electrolyte, and cathode. The cathode of an SOFC is typically comprised of porous materials coated with a catalyst, often synthesized from perovskite materials. Oxygen molecules (O_2) from the air are supplied to the cathode, where they are reduced with electrons from the anode to form oxygen ions (O_2–), as presented in Reaction R6. (KUPECKI, 2018; REVANKAR; MAJUMDAR, 2016).

$$0.5\,O_2 + 2\,e \rightleftharpoons O^{2-} \quad \text{(R6)}$$

The anode is also comprised of porous materials, and it is also typically coated with a catalyst, such as nickel. Hydrogen rich gas from reformer is supplied to the anode, where it undergoes a catalytic reaction, releasing electrons and hydrogen ions (H^+) through Reaction R7 (KUPECKI, 2018; REVANKAR; MAJUMDAR, 2016; O'HAYRE et al., 2016).

$$H_2 \rightleftharpoons 2\,{H_2}^{++}e \quad \text{(R7)}$$

At the electrolyte interface, either oxygen ions (O_2–) from the cathode diffuse through the solid oxide electrolyte to the anode, or hydrogen ions (H^+) from the anode migrate to the cathode, depending on the nature of the electrolyte. Diffusion process of ions generates an electric current by allowing electrons to flow through an external circuit, producing electrical power. The hydrogen ions reacts with oxygen ions producing water as presented by Reaction R8 (KUPECKI, 2018; REVANKAR; MAJUMDAR, 2016; O'HAYRE et al., 2016).

$$H_2 + 0.5\,O_2 \rightleftharpoons H_2O \quad \text{(R8)}$$

The functioning of the cell is associated with different irreversibilities. The main forms of potential losses include: activation, ohmic and concentration. Activation loss can be described as the decrease of electrochemical charge transfer reaction. As the cell has to overcome irreversibilities, part of the energy is lost in the process (O'HAYRE et al., 2016; SRISIRIWAT, N.; WUTTHITHANYAWAT, 2013). Ohmic loss is related to the

Figure 2 – SOFC schematic.

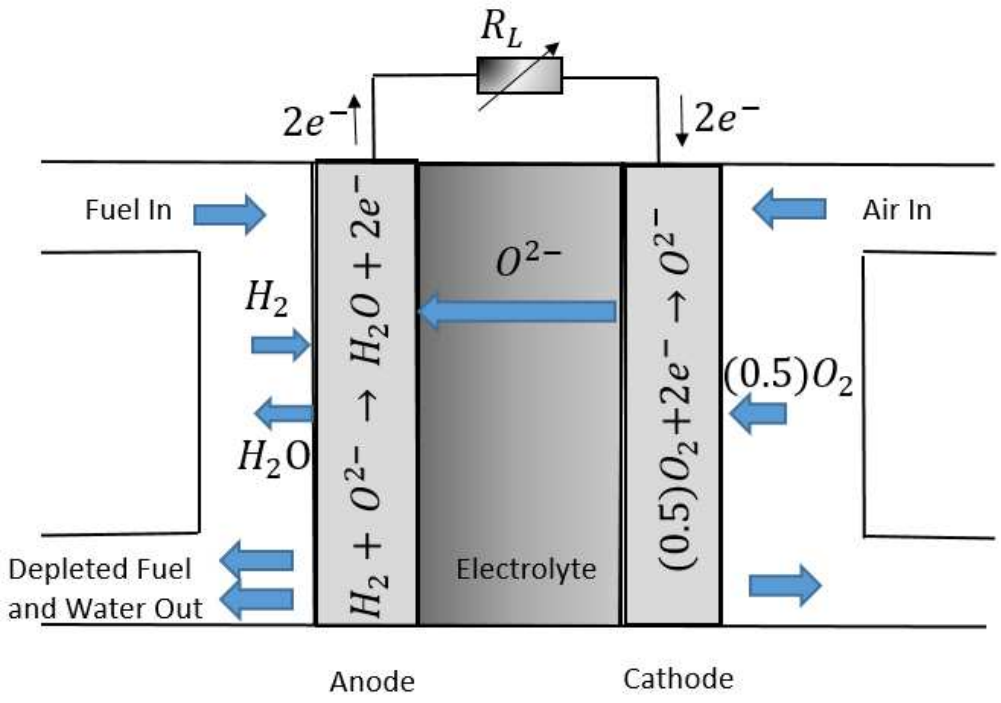

Source:(CHEN, X.; PAN; CHEN, J., 2010).

ionic resistance of the material and can be minimized using high temperatures. However, the cell operation at high temperatures reduces the life of the cell and requires for more expensive materials. Concentration loss arises from transport limitations within the porous electrode structure. If the electrochemical process is controlled by diffusion transfer rates, there is a decrease in the partial pressure of oxygen at the anode and oxygen at the cathode, increasing polarization until the voltage becomes zero (O'HAYRE et al., 2016; SRISIRIWAT, N.; WUTTHITHANYAWAT, 2013).

The SOFC operates between 600 ℃ and 1000 ℃, achieving an electrical efficiency of around 50%, potentially reaching 90% for integrated applications (O'HAYRE et al., 2016). It has multiple advantages such as the wide range of fuel flexibility, waste of heat for co-generation, and relative high power density. However, the operation in high temperatures brings challenges with sealing and materials compatibility (O'HAYRE et al., 2016; SRISIRIWAT, N.; WUTTHITHANYAWAT, 2013). A operation temperature up to 700 ℃ can significantly reduce operational challenges while maintaining the majority of benefits (O'HAYRE et al., 2016).

The residual energy that remains unconverted into electricity within a fuel cell system manifests as heat, resulting from the exothermic reaction inherent to fuel cells (REVANKAR; MAJUMDAR, 2016; O'HAYRE et al., 2016). The stack and exhaust gas contain heat that can be recovered as a heat source for the system, which has a significant impact on the efficiency of the cells (O'HAYRE et al., 2016).

In order to recover heat from a SOFC, a refrigerant fluid must be chosen. The

choice of refrigerant fluid is determined by the capacity and dimensions of the fuel cell. As a rule, high power systems employ liquid refrigerants as opposed to gaseous ones, primarily due to the former's superior thermal capacity, which renders it more compatible with high heating capacity cells. In the context of high-capacity automotive applications, deionized water or a water-glycol mixture is frequently employed (O'HAYRE et al., 2016).

As mentioned in the section on fuel reforming, SOFC can operate with different hydrocarbon fuels using an appropriate reforming process. The integration of the reformer with the SOFC is an important aspect with advantages and disadvantages that need to be considered, as will be discussed in the next section.

3.3 INTEGRATION BETWEEN SOFC AND REFORMER

In the next sub-sections, three types of reformers are going to be introduced along with their advantages and disadvantages.

The integration of SOFC with reformer if divide in three main configurations:

- Direct internal reformer (DIR);
- Indirect internal reformer (IIR);
- External reformer (ER).

3.3.1 Direct internal reformer

The direct internal reformer (DIR) is characterized by feeding fuel (such as methane, for example) and steam directly into the anode surface of the SOFC. As the anode is comprised by a porous material coated by nickel catalyst, the simultaneous methane reforming reaction and electrochemical oxidation of hydrogen produced by reforming reaction can occur (BARUAH et al., 2015). The high temperature, and the exothermic reaction facilitates the endothermic fuel reforming process, as presented in Figure 3 (KUPECKI, 2018). This characteristic results in high efficiency and high conversion, because the heat generated by exothermic eletrochemical reaction in the anode can be used to supply the heat of endothermic reforming reaction. Moreover, this system takes advantage of the high temperatures of the SOFC, which is compatible with the high temperatures of the fuel reformer (O'HAYRE et al., 2016).

The advantages of this configuration type include its simplicity, low cost, and the fact that it is generally considered the most efficient design. The position of the reformer with the cell reduces the cooling requirements and air flow passing in the cathode. It increases the system efficiency by eliminating the need to transfer heat to an external reformer (KUPECKI, 2018). In comparison with Indirect Internal Reformer (IIR), this method has the possibility to reuse the steam generated from eletrochemical reaction as part of the steam required for reforming reaction. (FAHEEM et al., 2022).

Figure 3 – Example of direct internal reformer using methane fuel.

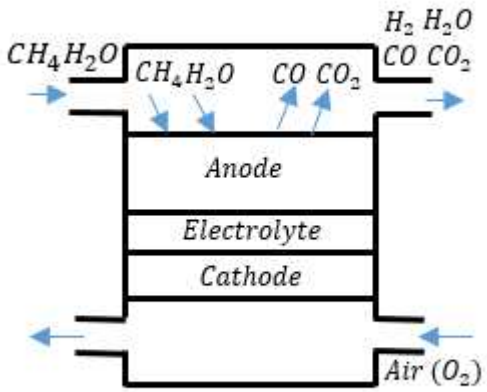

Source:(CHOUDHURY; CHANDRA; ARORA, 2013)

However, the limitation of this configuration is related to the possibility of carbon formation in the anode, and for some specific conditions of reforming reactions, the high temperature variation can lead to mechanical stresses on the SOFC, reducing its lifetime (FAHEEM et al., 2022; KUPECKI, 2018).

3.3.2 Indirect Internal Reformer

The indirect internal reformer (IIR) is a configuration where the reformer is located close to the anode of the SOFC. In this configuration the conversion of fuel into hydrogen occurs inside the reformer. This position gives leverage to the system as it provides heat transfer between the reformer and the fuel cell. This configuration is illustrated in Figure 4. Heat transfer between the components is expected to provide heat to the auto thermal operation (CHOUDHURY; CHANDRA; ARORA, 2013; LAOSIRIPOJANA et al., 2009; FAHEEM et al., 2022).

In this configuration, the catalysts for reforming and electrochemical reactions can be optimized individually, (LAOSIRIPOJANA et al., 2009; FAHEEM et al., 2022). However, one problem mentioned in the literature is the difficulty to control the reforming reaction, resulting in a fuel conversion before reaching anode (KUPECKI, 2018). In IIR system, the reforming reaction should ideally take place close to the anode but not inside it. This allows the generated hydrogen to be utilized for electricity generation. However, if the reforming reaction rate is high, for instance, in the anode vicinity, some of the hydrogen can be used for undesirable reactions, leading to energy losses.

Moreover, early fuel conversion can result in the formation of carbonaceous compounds, such as carbon or coke. These compounds can deposit on the anode and other components, causing performance degradation, blockages, and potentially

Figure 4 – Example of indirect internal reformer using methane fuel.

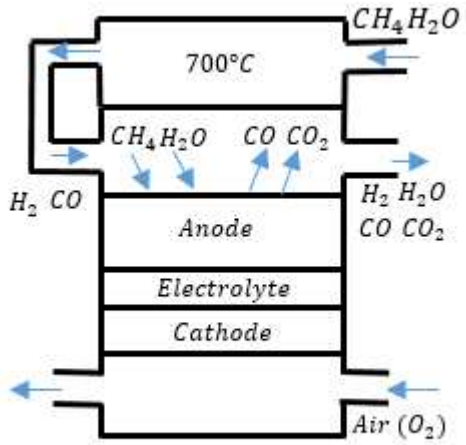

Source:(CHOUDHURY; CHANDRA; ARORA, 2013)

damaging the fuel cell (KUPECKI, 2018). The difference between the reaction rates in the reformer and the fuel cell can create a mismatch between the heat requirements, creating local temperature gradients that can result in mechanical failure due to thermal stresses (KUPECKI, 2018; LAOSIRIPOJANA et al., 2009).

As this configuration is small, and requires less weight, it is more suitable for mobile applications (PAZ FIUZA et al., 2012). This configuration is considered the simplest, most cost-effective, and with efficient design (KUPECKI, 2018).

3.3.3 External reformer

The main characteristic of the external reformer (ER), as the name suggests, is related with its position which is not directly integrated with the SOFC as presented in Figure 5. The fuel is processed inside the reformer which then turns into a rich hydrogen gas by reforming reactions (KUPECKI, 2018). In an external reformer configuration, there is no heat transfer between the fuel reformer and the fuel cell, which demands its own heat exchange arrangement (KUPECKI, 2018).

One of the advantages of this configuration type is the flexibility of the fuel processor, which is not limited to the fuel cell stack design. This is the safest model, and sometimes the only option to use liquid fuel. Another advantage is that as the reforming reactions do not happen in the anode directly, the deactivation of the electrode due to carbon formation is not a problem. On the other hand, this configuration is the most complex and inconvenient for fuel processing, due to a low efficiency and less cost-benefit in comparison with other configurations available (KUPECKI, 2018). Despite the complexity, a vehicular prototype using an external reformer running with ethanol and with a convectional SOFC was presented by Nissan (KUPECKI, 2018; MA et al., 2021).

Figure 5 – Example of external reformer using methane fuel.

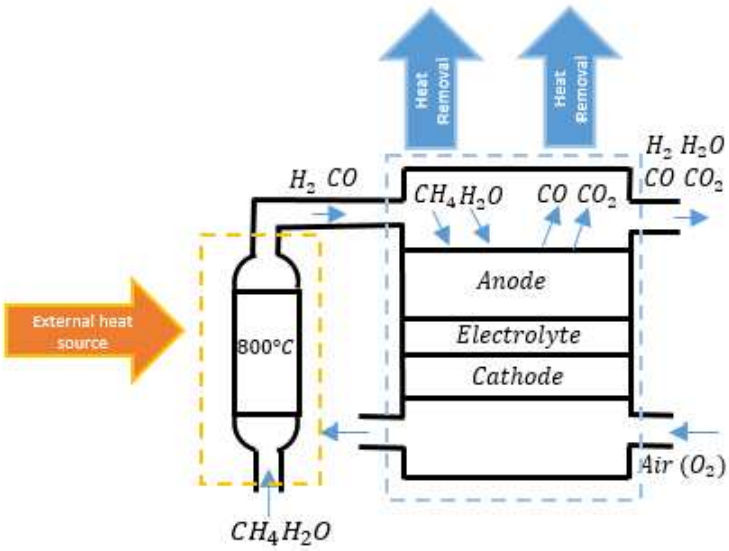

Source:Adapted from (CHOUDHURY; CHANDRA; ARORA, 2013)

Each configuration of the system has its own vantages and disadvantages which can be better for certain applications depending on multiple variables. In the current work, only the external reformer configuration will be evaluated because of the opportunity to reuse the released heat by the reformer (when operates in autothermal condition) and by fuel cell as a source to improve efficiency.

3.4 HEAT INTEGRATION

A SOFC system is composed generally by a fuel cell and a fuel reformer, which converts fuel in a hydrogen rich gas. Due to the concentration loss, the voltage drops with time, leading to SOFC operates with around 80% to 95% of the available fuel. Therefore, a residual amount of fuel is purged through the exhaust of the system. This residual fuel can be reused with an afterburner and the heat released by the exothermic combustion reaction can be used to supply the heat to the endothermic reforming reactions. Moreover, the hot combustion gases can be used to preheat the fuel and air in the reformer and SOFC cell inlets, respectively. The heat integration allows an improvement in the thermal efficiency of the SOFC system.

Figure 6 presents a basic example of a cogeneration system for SOFC. The air stream (blue line) passes through preheater 1, where it is heated and flows to the cathode. Preheater 1 and preheater 2 are heated by the exhaust gas from the afterburner, which combusts the remaining fuel from the reaction. The fuel (red line) is heated before it goes to the reformer, improving the reformer process.

Another option mentioned in literature is the combination of SOFC with gas

Figure 6 – Simplified SOFC system with heat and power integration.

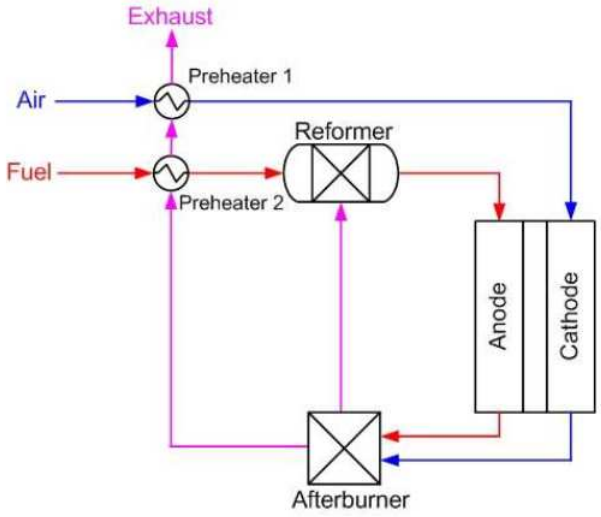

Source:(LAOSIRIPOJANA et al., 2009)

turbine GT to generate additional energy (LAOSIRIPOJANA et al., 2009). The gas turbine can be connected directly or indirectly to the system. In the first scenario, the exhaust gas of the afterburner is sent to a heat exchanger, which compresses the gas previous heated. Therefore, the heat exchanger works in a very high temperature and pressure, requiring a specific material to support these conditions (LAOSIRIPOJANA et al., 2009).

In the second scenario (as can be seen in Figure 7), the air is compressed and sent directly to cathode. The remaining fuel in the outlet of fuel cell is combusted in the afterburner, where the exhaust is directed to another compressor. In this solution, the SOFC operates in a very high pressure. It is reported that the turbine system can improve the efficiency up to 70% (LAOSIRIPOJANA et al., 2009).

Figure 7 – Indirect integration of a SOFC and a gas turbine.

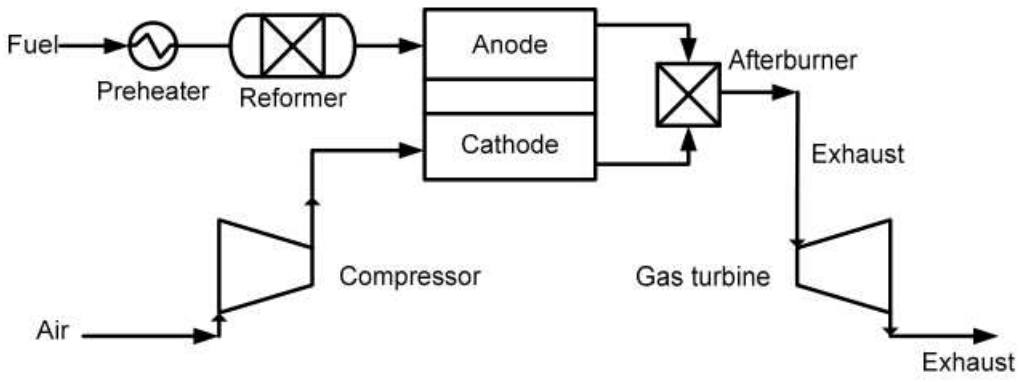

Source:(LAOSIRIPOJANA et al., 2009)

Besides the position of the reformer in the system, its operation conditions are

also important and affect the process architeture, since the reformer can operate endo or exotermically, depending of the reformer process. Looking at the importance of this definition, some works proposed system without afterburner when the reformer is operating at adiabatic condition, using the SOFC exhaust gas to do heat integration (SRISIRIWAT, A., 2008; WUTTHITHANYAWAT; SRISIRIWAT, N., 2014), as present in Figure 8.

Figure 8 – Heat integration for SOFC systems with an adiabatic reformer.

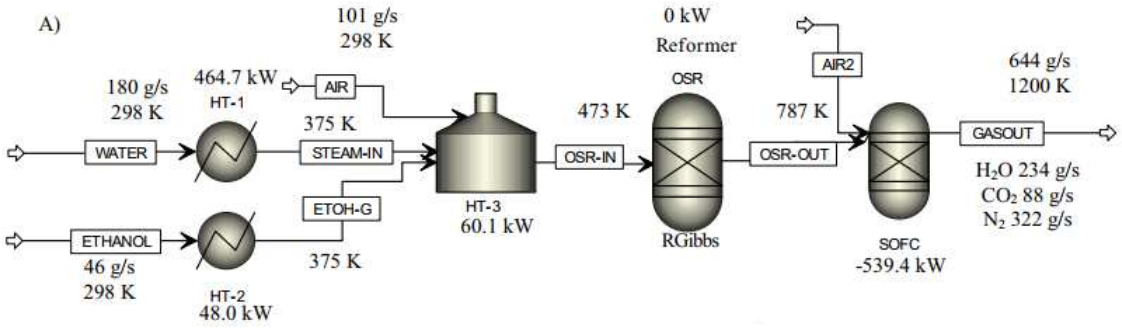

Source:(SRISIRIWAT, A., 2008)

A further line of study is the comparison between the reformer process (autothermal, steam reforming, and partial oxidation) aiming the maximum hydrogen yields, and minimizing the carbon formation (TIPPAWAN; ARPORNWICHANOP, 2014b; HONG et al., 2011). Despite the fact that efficiency for steam reforming present values 10% higher, the heat required by the reformer significantly reduces with the autothermal and partial oxidation process, and the reformer can operates releasing heat (exothermic condition), depending on ratios between reactants (TIPPAWAN; ARPORNWICHANOP, 2014b).

3.5 SYSTEM EFFICIENCIES USING ETHANOL

In 1999, a numerical analysis was performed to study the efficiency of a SOFC system running integrated reformer with ethanol, comparing steam reforming with partial oxidation in the temperature range between 800-1200K.The findings of the study revealed that steam reforming exhibited a significantly better electrical efficiency of 83.6%, which was approximately 4% greater than that seen for partial oxidation (TSIAKARAS, P. et al., 1999).

Another study with a similar concept was carried out comparing the electrical efficiency of a integrated system running steam reforming of methanol and ethanol fuels (DOUVARTZIDES; TSIAKARAS, 2001). The results indicated that the electrical efficiency between the two fuels is very close, 83.9% to 93.8% for methanol and 86% to 96% for ethanol, for the temperature variation range (800 to 1200 K). Furthermore,

these authors states that both fuels can be considered with similar values of efficiencies for SOFC (DOUVARTZIDES; TSIAKARAS, 2001).

A similar study using a SOFC cell with a direct internal reformer (DIR) with ethanol was carried out in order to understand the steam to carbon ratio (S/C) range where carbon formation is unfavorable (ASSABUMRUNGRAT et al., 2004). The results indicated the increasing the water-to-ethanol ratio enhanced the formation of carbon dioxide, preventing carbon formation by the Bourdard reaction. However, the results indicate that carbon deposition can occur not only by the Bourdard reaction but also by the thermal cracking of hydrocarbons, which can result in carbon deposition on the electrode surface. In addition, this work highlights the risk of polymeric coke, which can result in damage to fuel cells. The carbon formation is a known disadvantage of the direct internal reformer; however, coke formation can be reduced by increasing the ratio water/ethanol preventing carbon formation by raise of CO decomposition in Bourdoard reaction (ASSABUMRUNGRAT et al., 2004).

A bioethanol processing system for a power of 200 kW using SOFC cell was simulated in order to study the pseudo-homogeneous reformer model (ARTEAGA et al., 2008). This model is used to study design parameters and condition operations. The water content in the reaction mixture has a significant effect on the production of hydrogen in the reforming process and on the energetic capacity of the reformed gas on SOFC. To determine the efficiency of the water to ethanol ratio, an efficiency indicator ηRe is proposed, defined as the ratio between the hydrogen amount obtained and the maximum molar flow obtained under equilibrium conditions. Lastly, these authors observed an increase of ηRe efficiency when the water to ethanol ratio was increased within the range of 3-6. The cell uses around 85% - 95% of the energy available in the synthesized gas (ARTEAGA et al., 2008).

An integrated SOFC cell system sized for a power of 150 kW with reformer was presented, and analyzed with three different fuels in order to study the design and process parameters (SAEBEA et al., 2013). The electrical and thermal efficiencies are presented for the three fuels, where ethanol has resulted in 51% electrical efficiency, against 49% for glycerol and 32% for bio-gas. Particularly, this outcome is due to the superior performance of ethanol steam reforming in terms of hydrogen production at an operation temperature of 1073 K compared to other fuels, favoring thermal and electrical efficiency (SAEBEA et al., 2013).

Another study was conducted to understand which reforming route is suitable for integration with SOFC, testing three different routes: steam reforming, partial oxidation and autothermic reforming (TIPPAWAN; ARPORNWICHANOP, 2014a). Energy and exergy analysis were performed to verify the best configuration. The reported electrical efficiencies were 67% for steam reforming, 56% for both partial oxidation and autothermal reforming. As expected, results indicated a higher energy demand in the steam

reforming of ethanol while partial oxidation were less energy demanding. When looking at the whole process, including reformer, evaporator and heat exchangers, partial oxidation appears to occur under neutral conditions (TIPPAWAN; ARPORNWICHANOP, 2014a).

The studies mentioned above presented process parameters and configurations, such as integration with the reformer, cell temperature, power, and fuel utilization, which can be used as references for this work. These parameters are introduced in Table 1, together with information from other studies that carry out analyses using ethanol and methane as fuel. Detailed information were not present in the Table 1 to focus in the main parameters of the SOFC, although it is worth mentioning that this table was build considering models with 0D, 1D and 2D approach. The models from Paulus et al. (2021), Jian et al. (2006), and Dokmaingam et al. (2017) were build up in transient conditions while the other are in stationary conditions.

As conclusion of the data collected, one can see that:

- The fuel utilization parameter varies in the range of 0.7 to 0.9, which is the ratio between rates of fuel consumed and fuel available. This range is defined probably with the objective to provide fuel in excess in the system and avoid the interruption in the hydrogen supply.
- The direct internal reformer appeared 5 times in the published works (PALUS; PIANKO-OPRYCH, 2021; TANIM; BAYLESS; TREMBLY, 2014; TIPPAWAN; ARPORNWICHANOP, 2014a; OLIVA et al., 2013; BRAUN et al., 2003). The external reformer also appeared 5 times: (ARTEAGA et al., 2008; SRISIRIWAT, N.; WUTTHITHANYAWAT, 2013; SAEBEA; PATCHARAVORACHOT; ARPORNWICHANOP, 2012; SAEBEA et al., 2013; TIPPAWAN; IM-ORB; ARPORNWICHANOP, 2017) and it is usually emplyed under higher SOFC powers.
- Most papers do not highlight all the efficiencies. The electrical efficiency appears to be the commonly used parameter in the studies, as the presented in the table. For some papers, the thermal efficiency is also available and used as comparison to understand the effects of components.
- The electrical system efficiency had an average value of about 50%, although for one case it was at 44%. Thermal efficiency was around of 40%. It was observed a case with results close to 90% for a theoretical efficiency, considering the energy conservation (DOUVARTZIDES; TSIAKARAS, 2001).
- The temperature range of a SOFC using ethanol as a fuel, is generally close to 900 K positioned in the group of high-temperature SOFC. The number of reported papers in steady-state are higher than in dynamic conditions, wherein some models were found to be applicable in the process control

studies.

- For variation of the water to ethanol ratio, there is a negative influence in the efficiency when the ratio increase, in which 3:1 appearing to be the most observed ratio with a good impact. Similarly, research on the change of the air to ethanol ratio point that increases in the ratio can lead to reduction of efficiency (TIPPAWAN; ARPORNWICHANOP, 2014a).

The analysis of the data in the table driven the choose for the external reformer, which benefits from flexibility in the development of technology. Take in consideration the objective of the current work to improve the efficiency of a system by the reuse of heat release of fuel cell, the external reformer is the configuration which allow this study. Furthermore, it is a concept which allow a vehicle application.

Table 1 – SOFC integrated with Reformer system models

Reference	Reformer	Fuel	Software	SOFC temperature [K]	Power [kW]	Fuel utilization	Oxygen and ethanol ratio	Water and ethanol ratio	Efficiency reported
(SAEBEA et al., 2013)	External	Ethanol	Matlab	1173	150.0	0.70	N/A	1.5	51.00%[a]42.00%[b]
(ARTEAGA et al., 2008)	N/A	Ethanol	Stastica 6.0	873	200.0	0.85	N/A	3-6	40.50%[c]
(TIPPAWAN; ARPORNWICHANOP, 2014a)	DIR-SOFC	Ethanol	Aspen Plus	1073	N/A	0.70	0-3	0-10	43.50%[c]58.30%[a]
(SRISIRIWAT, N.; WUTTHITHANYAWAT, 2013)	External	Ethanol	N/A	1200	663.0	0.90	N/A	2-10	N/A
(DOKMAINGAM; AREESINPITAK; LAOSIRIPOJANA, 2017)	N/A	Ethanol	Comsol	1173	N/A	0.80	0	1.5-4	N/A
(SAEBEA; PATCHARAVORACHOT; ARPORNWICHANOP, 2012)	External	Ethanol	Matlab	1073	2.1	0.70	N/A	1.5	46.16%[a]35.00%[c]
(HONG et al., 2011)	N/A	Ethanol	GCTool	913	1.0	0.70	N/A	2.5	46.16%[a]30.78%[c]74.39%[b]
(CHEN, B. et al., 2019)	N/A	Ethanol	Comsol	913	N/A	0.90	N/A	6	N/A
(OLIVA et al., 2013)	DIR-SOFC	Ethanol	N/A	1073	1.0	0.90	N/A	3.2-3	69.35%[b]
(PALUS; PIANKO-OPRYCH, 2021)	DIR-SOFC	Ethanol	Aspen Dynamic	835	2.5	0.75	0	1.6	44.00%[a]
(BRAUN et al., 2003)	DIR-SOFC	Gasoline	Matlab	1093	5.5	0.85	N/A	1.5	N/A
(TANIM; BAYLESS; TREMBLY, 2014)	DIR-SOFC	JP-8 (Aviation Fuel)	Aspen Plus	1123	5.0	0.85	0.15	0.1-1	N/A%[a]
(NI, 2013)	N/A	Methane	Fortran	1073	N/A	0.60	N/A	1	N/A
(SRISIRIWAT, N.; WUTTHITHANYAWAT, 2013)	External	Ethanol	Aspen Dynamic	700	505.2-593	0.83	2.2	3.9	40.9%[a]
(ARTEAGA-PEREZ et al., 2009)	External	Ethanol	Aspen Dynamic	700	700	0.7-0.9	N/A	3-6	40.0%[a]

Note (1): The fuel utilization is the correlation between the amount of hydrogen consumed inside the fuel cell reactions to the inlet component in the cell. The relation and details are available in the chapter 3.

Note (2): On the column efficiency reported, the sub notes represent: (a) the Electrical efficiency - equation (6), (b) Overall efficiency - (3) and (c) the Thermodynamic efficiency - equation (5). N/A - Not available.

4 METHODOLOGY

The objective of this chapter is to present the steps of code implementation to represent the SOFC integrated with the reformer and other components, such as heat exchangers, focusing on the evaluation of the system efficiency. The chapter initiates with a discussion about the user input variables and details each system component starting by the SOFC. Finally, the heat integration through pinch analysis is presented as a strategy to minimize the hot utilities consumption in heat exchangers. Process model is lumped and stationary with multiple inlet variables.

4.1 UNIT OPERATIONS

4.1.1 SOFC

The electrical power output, P_{SOFC} (kW), is the current flowing from the fuel cell times the actual voltage, as calculated by equation (30):

$$P_{SOFC} = A_c j V \tag{30}$$

where A_c (m2) is active area of fuel cell, j (Am^{-2}) the current density and V represents the operating cell voltage.

The heat rate released by SOFC ($\dot{Q}_{SOFC}$) is calculated by the conservation of energy in the cell, considering a steady state condition, which takes in consideration the consumption of hydrogen, water and oxygen during the electrochemical reaction, represented by the equation (31). Figure 9 illustrates a schematic representation of the corresponding mass flow rates of streams (in and out) in both the anode and cathode.

$$\dot{Q}_{SOFC} = \sum_{i}^{NC,anode} (\dot{m}_i^{in} h_i^{in} - \dot{m}_i^{out} h_i^{out}) + \sum_{i}^{NC,cathode} (\dot{m}_i^{in} h_i^{in} - \dot{m}_i^{out} h_i^{out}) - P_{SOFC} \tag{31}$$

where $\dot{m}_i^{in}$ (kg/s) represents the mass flowrate of ith chemical species at the input stream and $\dot{m}_i^{out}$ represents the mass flow rate at outlet stream, and h_i^{out} (kJ/kg), h_i^{in} (kJ/kg), represents the corresponding specific enthalpy at the inlet and outlet, and P_{SOFC} is SOFC power.

The main reaction in the SOFC is the reaction R8, in which as result generates water. The rate of hydrogen consumed in this reaction is represented by $\dot{z}$ in the water-gas shift reaction R4 and the Bourdoard reaction R5.

Figure 9 is a schematic diagram of the SOFC, illustrating the mass inflow and outflow for both the anode and cathode (kg/s). In order to calculate the total heat produced by the SOFC in the equation (31), it is necessary to calculate the mass flowrate

Figure 9 – Schematic diagram of the SOFC, illustrating the mass inflow and outflow for both the anode and cathode.

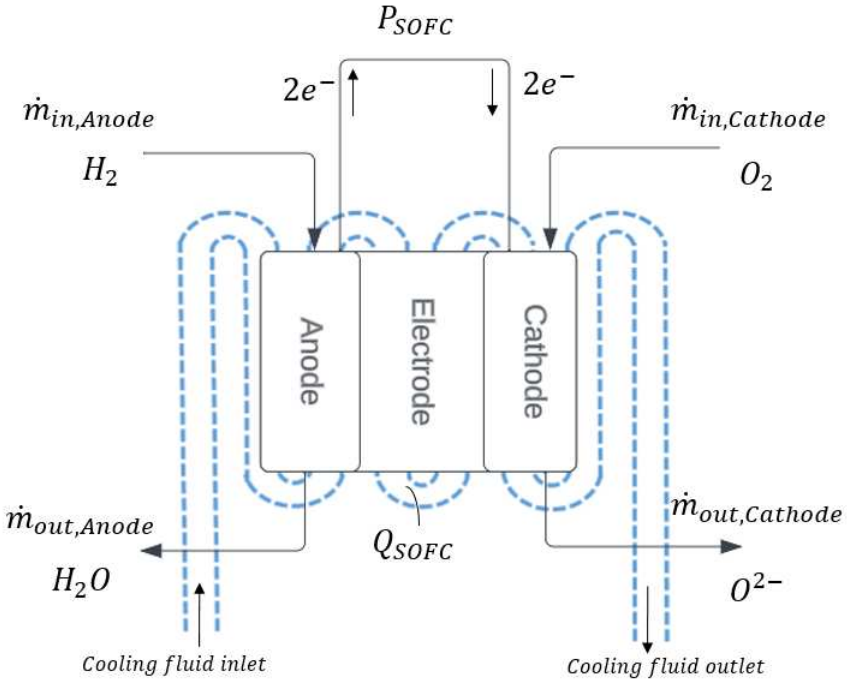

Source:(Author,2022)

at the outlet for hydrogen, water, and oxygen. These flowrates can be determined using equations (34), (35), and (36), which establish a relationship between the mass flowrate at the input of each component and the consumption of hydrogen during the reaction. The mass flow rate can be convert to molar flow rate, as presented in the equation (32), in which $m^{in}_{H2,anode}$ is the mass flow rate (kg/s), n^{in}_{H2} represent the molar flowrate for the hydrogen in inlet (mols/s) and MW_{H2} is the molar mass in (g/mols).

$$\dot{m}^{in}_{H2,anode} = \dot{n}^{in}_{H2,anode} * MWH2 \tag{32}$$

$$X = \frac{\dot{n}^{in}_{H2,anode} - \dot{n}^{out}_{H2,anode}}{\dot{n}^{in}_{H2,anode}} \tag{33}$$

in which, X represents the hydrogen conversion fraction in SOFC, n^{in}_{H2} represent the molar flowrate for the hydrogen in inlet (mols/s), and n^{out}_{H2} molar flowrate at outlet (mol/s). Thus, the global molar balances for the chemical species (H_2 and O_2) considering stoichiometric reactions in SOFC are represented by equations(34) and (35), which allow the computation of molar flowrates for the components in outlet of SOFC. Considering the mass balance expressed by equation (1), the mass flow rate of H_2O can be calculated by equation (36).

$$\dot{n}^{out}_{H2,anode} = \dot{n}^{in}_{H2,anode} - \dot{n}^{in}_{H2,anode}X \tag{34}$$

$$\dot{n}^{out}_{O2,cathode} = \dot{n}^{in}_{O2,cathode} - 0.5\dot{n}^{in}_{H2,anode}X \tag{35}$$

$$\dot{n}^{out}_{H2O,anode} = 1.5\dot{n}^{in}_{H2,anode}X \tag{36}$$

in which, $n^{in}_{O2,cathode}$ represent the molar flowrate for the oxygen in inlet (mol/s), and $n^{out}_{O2,cathode}$ molar flowrate of oxygen at outlet (mol/s), $n^{in}_{H2O,anode}$ represent the molar flowrate for the water in inlet (mol/s);

4.1.2 Reformer

This work considered that the reformer is operating under autothermal conditions. Therefore, the heat released by partial oxidation can be used to supply the heat demand of endothermic steam reforming reactions. Another assumption adopted is the isothermal operation for reformer. In this case, depending on operation condition regarding to inlet flowrates of ethanol, water and air, heat can be recovered from reformer using a heat exchanger. Figure10 presents a scheme of the corresponding mass flowrates for reformer representation.

Figure 10 – Schematic of a reformer

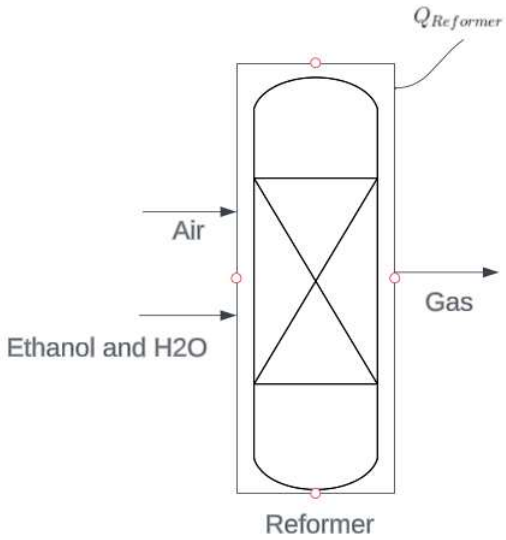

Source:(Author,2023)

The mass balances in reformer were computed as presented in equation (1), assuming that the reformer is in the equilibrium state coupled to the SOFC in the implementation of integrated system. The calculation of the heat capacity of the reformer

was performed using the conservation of energy principle, as presented in equation (37).

$$Q_{reformer} = \sum_{i=1}^{NC} \dot{m}^{Air} h^{Air} + \sum_{i=1}^{NC} \dot{m}^{Ethanol} h^{Ethanol} + \sum_{i=1}^{NC} \dot{m}^{H2O} h^{H2O} - \sum_{i=1}^{NC} \dot{m}^{Gas} h^{Gas} \tag{37}$$

which, $\dot{m}^j$ (kg/s) is the mass flowrate (kg/s) of ith component, specific enthalpy is represented by h^j (kJ/kg), and NC is the component number.

As chemical equilibrium was assumed to estimate the composition of the reforming gases, is possible to use a function of the library Cantera to calculate the equilibrium state. The function used is "Equilibrate" to minimize the total Gibbs free energy of the mixture. The minimization of Gibbs free energy of a single phase system is given by the equation (38) (OECHSLER et al., 2017; SMITH et al., 2000).

$$\dot{G}(\dot{n}_i, P, T) = \sum_{i=1}^{NC} \dot{n}_i \Delta G^o_{f_i} + RT \sum_{i=1}^{NC} (\dot{n}_i P) - RT \sum_{i=1}^{NC} \dot{n}_i \ln \left(\sum_{i=1}^{NC} \dot{n}_i \right) \tag{38}$$

where, $G^o_{f_i}$ is formation Gibbs free energy of the chemical species, $\dot{n}_i$ is molar flow rate of ith chemical species in inlet, and NC is the component number.

Thus, the objective is to find a molar flow set that minimizes equation (38) with defined temperature and pressure, taking into account the mass balance constraints. It is convenient to formulate the mass balance constraints in terms of elementary balances. If $a_{i,k}$ defines the total number of atoms of the kth element present in each chemical species i, while $\dot{n}_i$ and $\dot{n}_{io}$ represent the molar flow rate of chemical species i in the inlet and outlet streams, respectively. Therefore, the mass balance for each element k can be written as: (OECHSLER et al., 2017; SMITH et al., 2000)

$$\sum_{i=1}^{NC} a_{i,k} (\dot{n}_{io} - \dot{n}_i) = 0 \tag{39}$$

Therefore, the minimization of the total Gibbs free energy is calculated using the function using the Villars-Cruise-Smith (VCS) algorithm, as described in the reference documentation (CANTERA, 2022; SMITH et al., 2000).

4.1.3 Heat exchangers

The heat exchangers were described using a lumped model, which consider the effect of heat transfer between hot and cold stream. Figure 11, shows how the model is represented in diagram with one inlet for water stream and a outlet for the steam. The heat balance is given by Equation (40).

Figure 11 – Schematic of the heat exchangers.

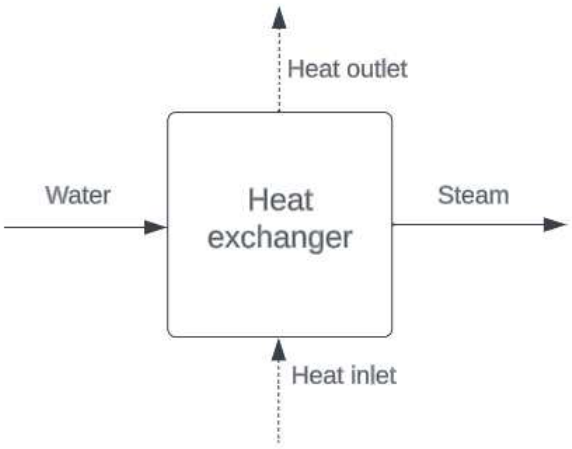

Source:(Author,2022)

$$\dot{m}_{heat} c_{p\,heat} \Delta T_{heat} - \dot{m} c_p \Delta T = 0 \tag{40}$$

where $\dot{m}$ represent the mass flowrate of cold stream (kg/s), cp represent the fluid specific heat (J/kg.K), ΔT is difference of inlet and outlet temperatures for cold stream. The m_{heat} represents the mass flowrate (kg/s) for hot stream, cp_{heat} represents the fluid specific heat (J/kg.K), ΔT is difference of temperature for hot streams and $\dot{Q}_{HX}$ the heat transfer rate between the hot and cold stream.

4.1.4 Evaporator

Conservation of energy was also applied in the evaporator to compute the heat transfer rate involved in this process. Figure 12 presents an scheme of the evaporator model. Heat transfer rate was computed considering the heating to increase the temperature from 25 ℃ until saturation condition (as presented in equation (40)), and the heat rate required for the phase change to saturated steam.

$$\dot{Q}_{Evap,1} = \dot{m} c_{p\,Water} (T_{in} - T_{Water,Sat}) \tag{41}$$

where, $\dot{m}$ represent the mass flowrate (kg/s), cp_{Water} represents the specific heat of water (J/Kg.K), T_{in} is the water inlet temperature (K) and $T_{Water,Sat}$ is the saturation temperature for water (K) at 1 (bar) of pressure.

Clapeyron equation, as presented in Equation (42), was used to calculate the vaporization enthalpy specific for the water:

$$\Delta H_{Vap} = \frac{log(\frac{P2_w}{P1_w}) R}{\frac{1}{T2_w} - \frac{1}{T1_w}} \tag{42}$$

Figure 12 – Schematic of the evaporator

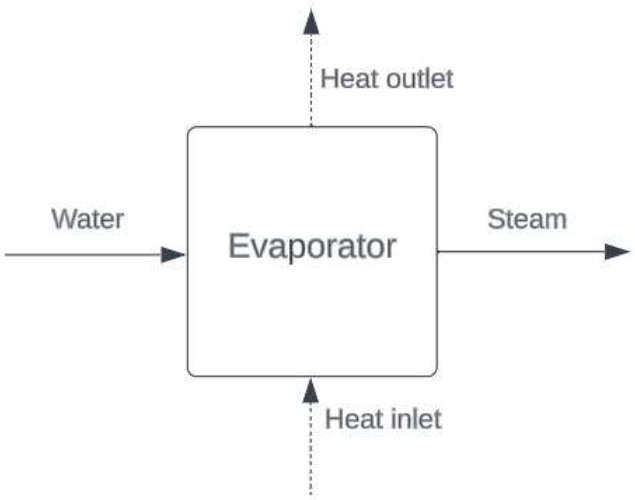

Source:(Author,2022)

where R is the universal gas constant, $P2_w$ and $P1_w$ represents the water pressures (kPa) in saturation temperatures, $T1_W$ and $T2_W$. The first point of reference has values for $P1_W$ of 70.1 (kPa), and $T1_W$ of 363.15 K, and for second point $P2_W$ is 101.325 (kPa) and 373.15 K.

The specific latent heat for phase change was calculated as equation (43), where ΔH_{Vap} represents the vaporization enthalpy computed in equation (42).

$$\dot{Q}_{Evap,2} = \dot{m}\Delta H_{Vap} \tag{43}$$

Therefore, total heat transfer rate is computed as shown in Equation (44):

$$\dot{Q}_{Evap,1} - \dot{Q}_{Evap,2} = 0 \tag{44}$$

4.1.5 Mixer

A mixer was employed to mixture ethanol at 25 ℃ and superheated steam. Figure 13 shows the inlet of water and ethanol that were mixed and join in the reformer through the outlet. The mixer is adiabatic, and the heat exchange between the ethanol and water occurs by the direct contact between these two streams. As one can see, in Figure 14, the ethanol is feed in system at ambient temperature which requires the water to be at a high temperature to heat and vaporize the ethanol stream.

The conservation of mass and energy, as presented in the equations (1) and (2), in the mixer were performed considering the inlet temperature for superheated steam at 590 ℃. This temperature was chosen to allow the temperature difference required to use an integration heat exchanger with the available hot streams at SOFC outlet (610 ℃). The mass balance in the mixer is given by Equation (45):

Figure 13 – Schematic of the mixer.

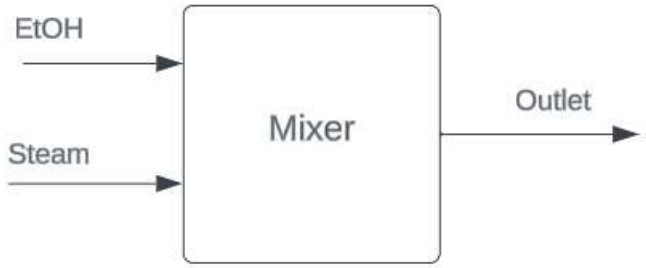

Source:(Author,2022)

$$\dot{m}_{Outlet} = \dot{m}_{Ethanol} + \dot{m}_{Water} \tag{45}$$

where $\dot{m}_{Outlet}$ represent the sum of $\dot{m}_{Ethanol}$ and $\dot{m}_{Water}$ (kg/s).

The conservation of energy in the mixer was performed by a adiabatic mixer to compute the outlet temperature of ethanol/water mixture, as presented in equation (1). The mass flow is represent by $\dot{m}^j$ in kg/s and enthalpy is represent by h^j, where the index j represents the inlet/outlet streams.

$$\dot{m}_{EtOH} h_{EtOH} + \dot{m}_{H2O} h_{H2O} = \dot{m}_{Outlet} h_{Outlet} \tag{46}$$

Since mass flow rate of ethanol and water in inlet are equals to outlet, the equation can be rearrange as equation (47), one can see that:

$$\dot{m}_{H2O}(h^{out}_{H2O} - h^{in}_{H2O}) = \dot{m}_{EtOH}(h^{out}_{EtOH} - h^{in}_{EtOH}) \tag{47}$$

The enthalpy change between the inlet and outlet can be computed by the following equation:

$$(h^{in}_{H2O} - h^{out}_{H2O}) = cp(T_{in} - T_{out}) \tag{48}$$

where, T_{in}, and T_{out} are temperatures (K) for inlet and outlet, and cp is the specific heat for steam in (J/kg.K) which is estimated based in the cantera function at the T_{out}.

4.2 STRATEGIES FOR HEAT INTEGRATION

The system was implemented and tested with two configurations, with and without heat integration, in order to evaluate the effect of heat recovery from SOFC in the improvement of electric efficiency. In this section, the input variables utilized to each

configuration are presented, followed by a description of the analyzes performed in each configuration.

The scheme, presented in Figure 14, is a representation of the proposed setup to evaluate the reformer performance. This scheme was used to evaluate the integration between ethanol reformer and SOFC. The process starts with the water tank (TQ1), which is connected by the stream (1) to the evaporator (E01). Once the water reaches the evaporator (E01), the temperature increases from 25℃ until 100℃, followed by complete evaporation of water, producing saturated steam. In sequence, the stream (02), is fed to the heat exchanger (HX01), which has the function of increasing the temperature until 590℃. Next, the stream (03) is mixed with stream (4) inside the mixer (M01). In this step, the heat from superheated steam (4) is used to heating and evaporate the ethanol stream. In mixer outlet, stream (5) is comprised by a mixture of water and ethanol steam at an intermediary temperature (computed through the heat balance). Then, stream (5) is heated in heat exchanger (HX02) until the desired temperature at reformer inlet (600℃). Next, the water/ethanol mixture, named as stream (6), is fed to reformer (RE01), along with stream (9), comprised by air coming from the air tank (TQ3). The reformed gas, named as stream (11), (RE01) is input in heat exchanger (HX03), which fed the SOFC (FC01), in the cathode side, while the anode is fed with air from (TQ03) by stream (10).

Figure 14 – Schematic of SOFC System

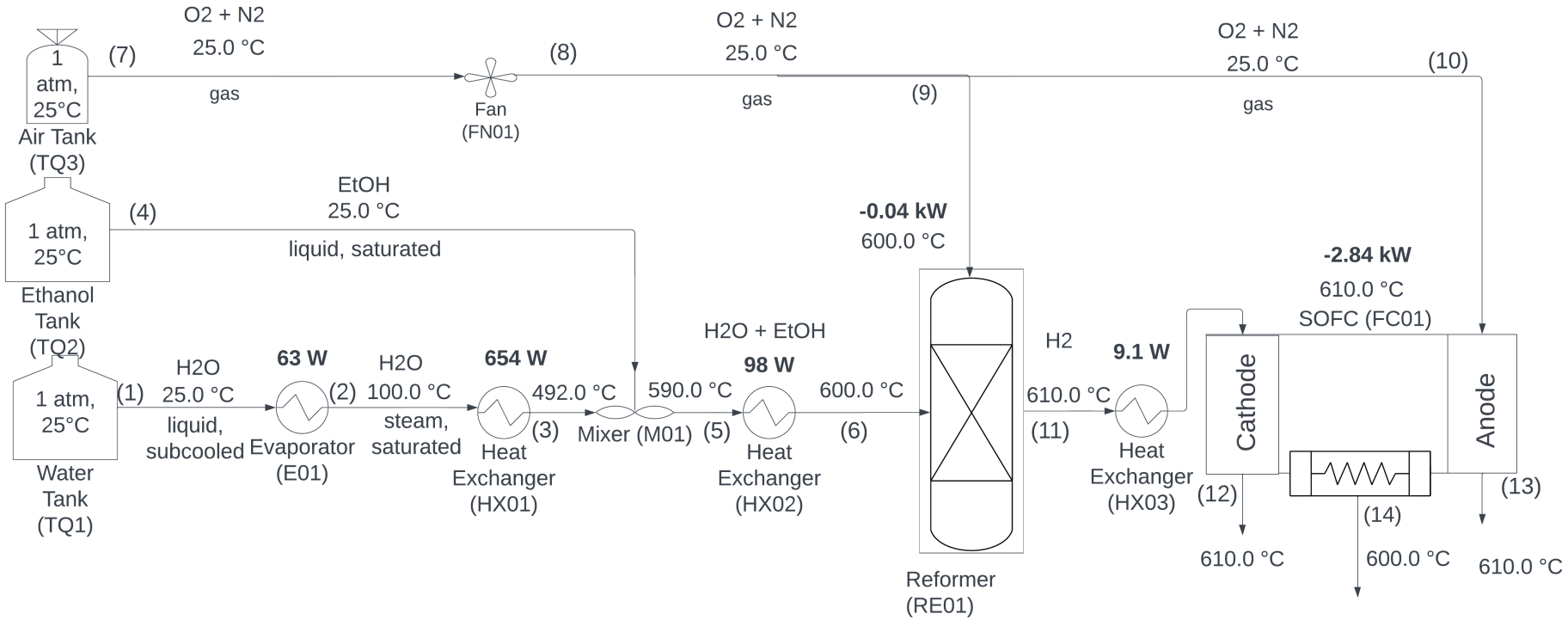

A benchmark case for integrated system was created by definition of a list of operation conditions. The operation conditions used in process flowsheet are presented in the Table 2. The system was implement in two steps, firstly without the recirculation and then with recirculation in the next step. The evaluation of SOFC system with recirculation, requires the heat integration, as will be discussed in the next section.

Table 2 – Operation conditions of the benchmark case, without heat recovering.

Component	Component	Inlet variable	Value	Unit
(RE01)	Reformer	Temperature	700	℃
(FC01)	SOFC	Temperature	710	℃
(FC01)	SOFC	Ambient Temperature	25	℃
(FC01)	SOFC	Fuel utilization	0.7	-
(FC01)	SOFC	Oxygen/Ethanol Ratio	0.5	-
(FC01)	SOFC	Water/Ethanol Ratio	3:1	-
(FC01)	SOFC	Pressure	1	bar
(E01)	Evaporator	Temperature inlet	25	℃
(E01)	Evaporator	Temperature outlet	100	℃
(HX01)	Heat Exchanger	Temperature inlet	492	℃
(HX01)	Heat Exchanger	Temperature outlet	587	℃
(HX02)	Heat Exchanger	Temperature inlet	492	℃
(HX02)	Heat Exchanger	Temperature outlet	600	℃
(HX03)	Heat Exchanger	Temperature inlet	600	℃
(HX03)	Heat Exchanger	Temperature outlet	610	℃

Source:(Author,2022)

4.3 PINCH ANALYSIS

Heat integration consists of using the heat from available hot and cold streams with simultaneous cooling of the hot streams, without consumption of utilities. This approach aims to reduce the use of utilities in the system, and consequently cost

of utilities in the heat exchange network (HEN). (ASSABUMRUNGRAT et al., 2016; PERLINGEIRO, 2005).

The number of possible solutions is a combination of the available hot and cold streams (PERLINGEIRO, 2005). Heat integration requires the identification of the heat demand and offer, named as cold and hot streams, respectively, as well as the available heat sources. These information can be organized in a table which must contain the inlet and outlet temperature, as well as the heat capacity for all streams to provide a visualization of the full system, as presented schematically in the Table 3.

Table 3 – Example of required inputs for a preliminary heat exchanger network (HEN) synthesis.

Stream	Wcp (kW/℃)	$T_{in}(C)$	$T_{out}(C)$
Q1	10	180	90
Q2	2	250	140
F1	5	60	150
F2	7	100	220

Source:(PERLINGEIRO, 2005)

The first column of the system displays the streams. In this particular example, Q1 and Q2 represent the hot stream of the system, whereas F1 and F2 represent the cold streams. The second column displays the Wcp (kW/℃), denoting the heat capacity of each stream, while the final columns provide the inlet and output temperatures, respectively.

Once the data collection is completed, a set of restrictions is required to solve the heat integration problem. A heat exchange between two stream is only thermodynamically possible for a case with one hot stream and a cold stream. Otherwise, the second law of thermodynamics will not be satisfied. For the example in Table 3, streams Q1 and Q2 can not be selected in the streams pairing for the synthesis of heat exchanger network, otherwise the the stream Q1 will be heated by Q2, which may result in the utilization of utilities increasing the cost operation (PERLINGEIRO, 2005). Each stream can have a demand or an offer heat, which is the amount of heat required to reach the desired outlet temperature. Using an energy balance, the heat exchange rate can be computed (PERLINGEIRO, 2005). Lastly, it is important to define a minimal difference of temperature between the hot and cold streams at inlet and outlet of heat exchanger. As one can see in the equation (49), the area of the heat exchangers depends on heat rate between the hot and cold streams, Q (W), the global heat transfer coefficient U (W/K), and the logarithmic mean temperature difference ΔT (K), as presented in the equation (50). For a condition where ΔT tends to zero, the area becomes infinite.

This condition occurs if the inlet temperature and outlet temperature for cold or hot side be equals in equation (50). A standard value to minimum temperature difference between the hot and cold streams at the inlet and outlet of the heat exchanger is 10 ℃ (PERLINGEIRO, 2005).

$$Q = UA\Delta T_{ml} \tag{49}$$

$$\Delta T_{ml} = \frac{(TEQ - TSF) - (TSQ - TEF)}{ln\frac{(TEQ-TSF)}{(TSQ-TEF)}} \tag{50}$$

where TEQ is the inlet hot temperature (K), TSF is outlet cold temperature, TSQ is the outlet hot temperature, and TEF is the inlet for cold stream.

Temperature-interval diagram (TID) is a graphic tool to visualize the streams of system, observing the intervals of temperature required regarding to defined minimal temperature difference. Figure 15 presents the temperature-interval diagram for the set of data presented in Table 3.

Figure 15 – Example of temperature-interval diagram (TID).

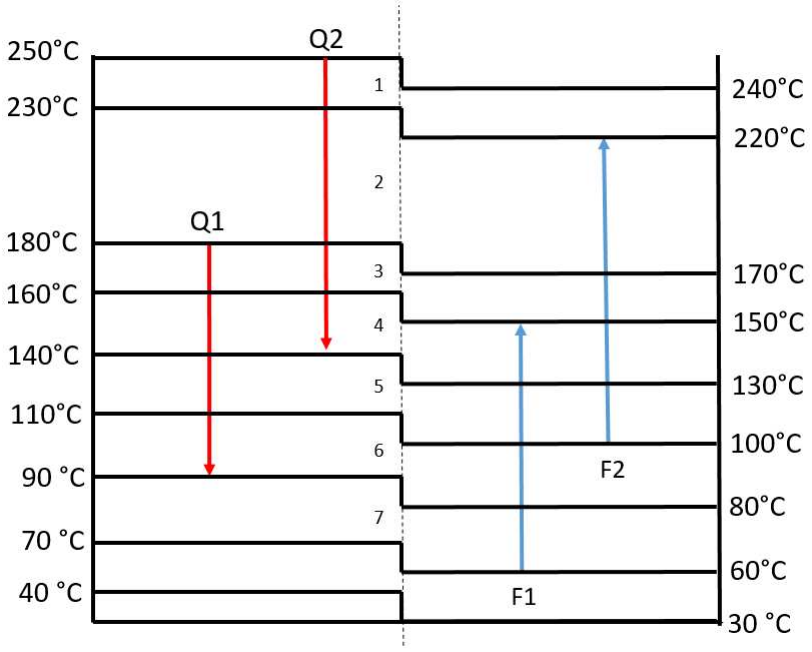

Source: adapted of (PERLINGEIRO, 2005)

From the first row on Table 3, the inlet temperature for stream Q2 is 250 ℃ and outlet of 140 ℃, which is represent by the red line Q2, on the left of Figure 15. An analog representation was done for Q1, F1, and F2 streams.The representation of Q1 is similar to the Q2. On the right side, one can see the representation of F1 and F2, the streams which demands heat, as well as the increase of temperature for each of stream, accordingly to the data table.

Each line in the diagram represents an interval of temperature, showing the inlet and outlet temperature, which the offer and demand of heat by the streams can be calculated. In Figure 15, the second interval, for example, includes only Q2 available as a hot stream and F2 as a cold stream for this interval.

The amount of heat offer by Q2 and demand by F2 is calculated by equation (51), where $\dot{m}$ (kg/s) is the mass flowrate, cp is the specific heat capacity in (W/kg.K) and ΔT is the delta temperature in (K), for a system without phase change.

$$Q_{i,k} = (\dot{m}C_p)_i(\Delta T_k) \tag{51}$$

Thus, for k_{th} interval is possible to calculate the residual heat rate by equation (52) where R_{k-1} is the amount of heat available from previous interval, $Q_{i,k}$ the offer of heat rate of ith hot stream (W), $Q_{j,k}$ the demand of heat rate of jth cold stream (W) and NF is the number of hot stream and NC number of cold streams. Therefore, the following scenarios are possible: a positive heat rate residual which should be transferred to in the next interval; a zero residual when all the heat available is used in demand, and a negative heat rate residual which requires the application of a hot utility to provide heat to system.

$$R_k = R_{k-1} + \sum_{i=1}^{NQ} Q_{i,k} - \sum_{j=1}^{NF} Q_{j,k} \tag{52}$$

4.4 MODEL IMPLEMENTATION

The model introduced in the previous sections was implemented using the Python language to represent the behavior of the solid oxide fuel cell (SOFC) integrated with a reformer. This implementation was made using the library Cantera and Numpy. Cantera is an open-source library capable of solving different problems related with chemical kinetics, thermodynamic and transport process (CANTERA, 2022). In this actual study, thermodynamic properties of all species were taken from the work of (MARINOV, 1999). Once the equilibrium state is calculated, the output of the equilibrium function shows the species quantities, allowing to calculate the partial pressures which integrated with the SOFC model permit the representation of the component.

To facilitate the comprehension of the available input parameters, Figure 16 present a general code flowchart including the user inputs and their respective propagation inside the code.

Figure 16 – Schematic of code flowchart including the user inputs.

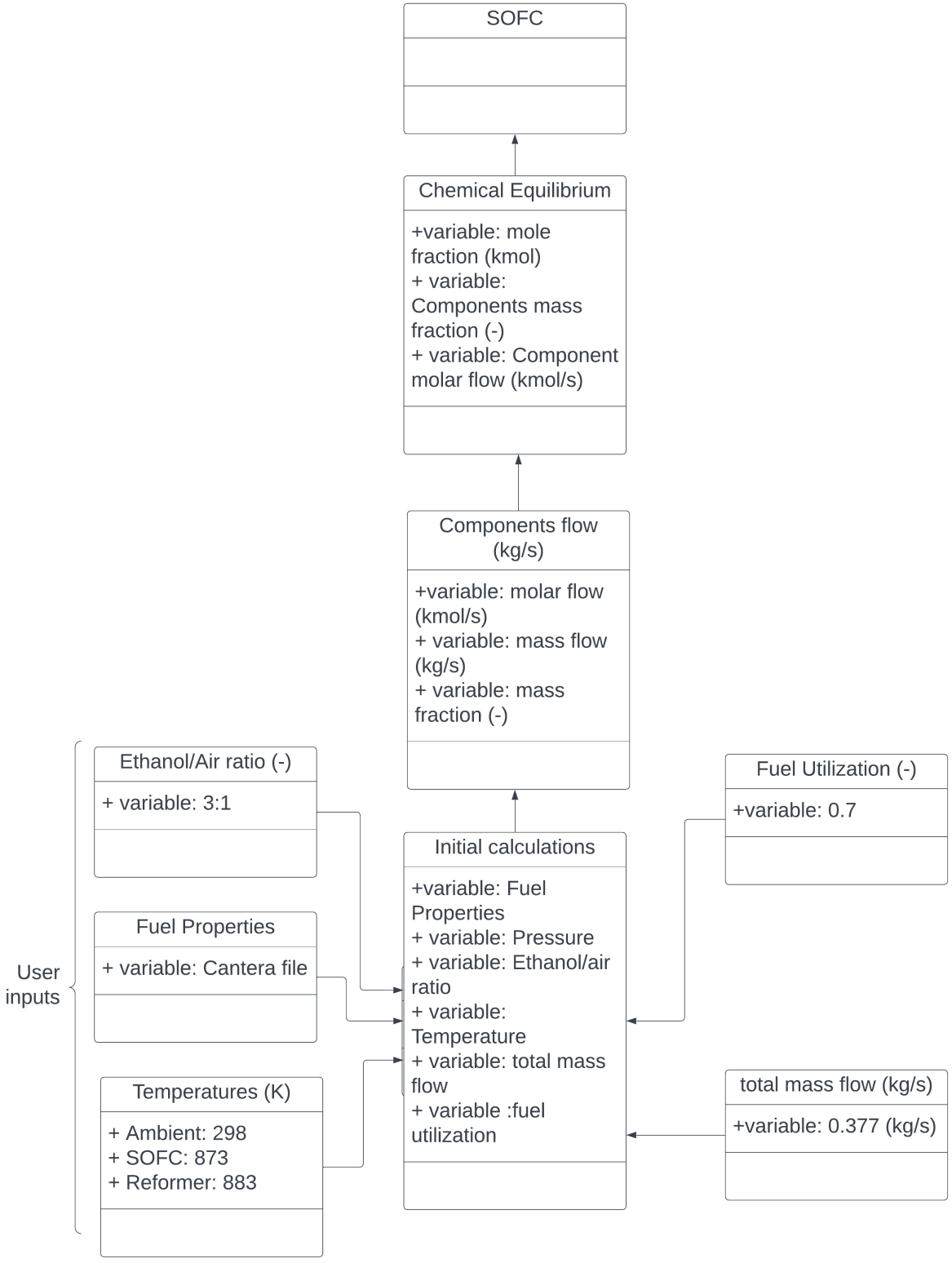

Source: (Author, 2023)

5 RESULTS AND DISCUSSIONS

Firstly, the results of a process flowsheet simulation are presented with the purpose of evaluating the efficiencies (as defined in Chapter 3) of the operation without heat integration. In particular, the effects of operational conditions, such as temperature, steam/ethanol ratio, and air/ethanol ratio on efficiencies, are discussed. In addition, the results of process flowsheet simulation with heat integration resulting from the pinch analysis are presented, and the efficiencies are also computed.

The model presented in Chapter 3 has some limitations. The diffusion coefficient for anode and cathode considered binary gas, (H_2 and H_2O) for anode, and (O_2 and N_2) for cathode. Although temperature can also affect the diffusion coefficient, the effect of temperature in diffusion coefficient for the range of temperature (considered in this work) can be neglected (SAEBEA; PATCHARAVORACHOT; ARPORNWICHANOP, 2012; THANOMJIT et al., 2015; ARPORNWICHANOP et al., 2009). Moreover, it is worth mentioning that all analysis were performed in steady state conditions. Therefore, the developed models for SOFC and reformer can not be used to evaluate the start-up of system. The developed models can not also be used to evaluate the lifetime of reforming catalyst and anode by carbon formation.

5.1 VALIDATION OF THE SOFC MODEL

5.1.1 Model parameters and inlet variables for validation

The simulation results from SOFC model were compared to the experimental results reported by (SAEBEA; PATCHARAVORACHOT; ARPORNWICHANOP, 2012; ZHANG et al., 2010). The SOFC model parameters utilized to represent the diffusion, conductivity and exchange of current density are presented in Table 4. In addition, the values used for inlet variables in simulated conditions are presented in Table 5. These information are the same data used in the literature reference (SAEBEA; PATCHARAVORACHOT; ARPORNWICHANOP, 2012), except for the E_{anode} and $E_{cathode}$, which were modified.

The modification of E_{anode} and $E_{cathode}$ was undertaken with the aim of enhancing the agreement between the model depicted and the empirical data employed for model validation. The values of 137 and 140 kJ/mol^{-1} were derived from the fitting by inspection of experimental data using Ceria and Sr- and Mg-doped LaGaO3 (LSGM) in cathode (AGUIAR; ADJIMAN; BRANDON, 2004; ZHAO; VIRKAR, 2005), and for anode material was selected nickel/zirconia cermet (AGUIAR; ADJIMAN; BRANDON, 2004). In particular, these changes are required due to the challenges associated with obtaining experimental data for the anode. The authors stated that the optimal range for anode activation is typically between 120 and 160 kJ/mol^{-1} as indicated by most studies, while

Table 4 – SOFC Model Parameters

Equations	Parameter	Description	Unit	Value	Reference
(22)	k_{anode}	Pre-exponential factor of anode exchange current density,	A m^{-2}	6.54×10^{11}	6.54×10^{11}
(23)	$k_{cathode}$	Pre-exponential factor of cathode exchange current density	A m^{-2}	2.35×10^{11}	2.35×10^{11}
(22)	E_{anode}	Activation energy of anode exchange current density	kJ mol^{-1}	140	166.72
(23)	$E_{cathode}$	Activation energy of cathode exchange current density	kJ mol^{-1}	137	154.88
(17), (18)	$D_{eff,anode}$	Anode diffusion coefficient	$m^2 s^{-1}$	3.66×10^{-5}	3.66×10^{-5}
(19)	$D_{eff,cathode}$	Cathode diffusion coefficient	$m^2 s^{-1}$	1.37×10^{-5}	1.37×10^{-5}
(37)	σ_{anode}	Anode electrical conductivity	$\Omega^{-1} m^{-1}$	$4.2\times10^7 exp(\frac{-1200}{T})$	$4.2\times10^7 exp(\frac{-1200}{T})$
(37)	$\sigma_{cathode}$	Cathode electrical conductivity	$\Omega^{-1} m^{-1}$	$9.5\times10^7 exp(\frac{-1200}{T})$	$9.5x10^7 exp(\frac{-1200}{T})$
(37)	$\sigma_{electrolyte}$	Electrolyte ionic conductivity	$\Omega^{-1} m^{-1}$	$33.4 \times 10^3 exp(\frac{-10300}{T})$	$33.4 \times 10^3 exp(\frac{-10300}{T})$
(37), (17)	τ_{anode}	Anode thickness	μm	500	500
(37), (19)	$\tau_{cathode}$	Cathode thickness	μm	50	50
(37)	$\tau_{electrolyte}$	Electrolyte thickness	μm	20	20

Source:(SAEBEA; PATCHARAVORACHOT; ARPORNWICHANOP, 2012)

the implementation was done for a internal direct reformer with a polymer-electrolyte membrane (PEM). The utilized values, therefore, fall within the range reported in the literature for these parameters.

Figure 17 presents the result of the voltage obtained from the model in comparison with the experimental results. The blue dots represent the experimental and simulated results at 873 K. When compared to the identity line, it shows a correlation between the model and the experimental results. At some degree, one can see a slight deviation from the identity line, indicating that simulated and experimental results presented some degree of deviation. However, considering possible measurements errors, which are not considered in this analysis, the model performance was satisfactory, and

Table 5 – SOFC and reformer parameters at nominal conditions

Equations	Parameter	Description	Unit	Value
-	U_f	Fuel utilization	-	0.7
-	T_R	Operating Temperature Reformer	K	973
(15),(16)	T_{SOFC}	Operating Temperature SOFC	K	1073
(22)	Ps	Operating Pressure SOFC	bar	1
-	P_R	Operating Pressure Reformer	bar	1
-	$n_{Ethanol}$	Molar flow of ethanol	mol s^{-1}	1
-	S/C	Steam Carbon ratio	-	1.5

Source:(SAEBEA; PATCHARAVORACHOT; ARPORNWICHANOP, 2012)

Figure 17 – Comparison between simulated and experimental results of cell voltage at 873 and 1073 K

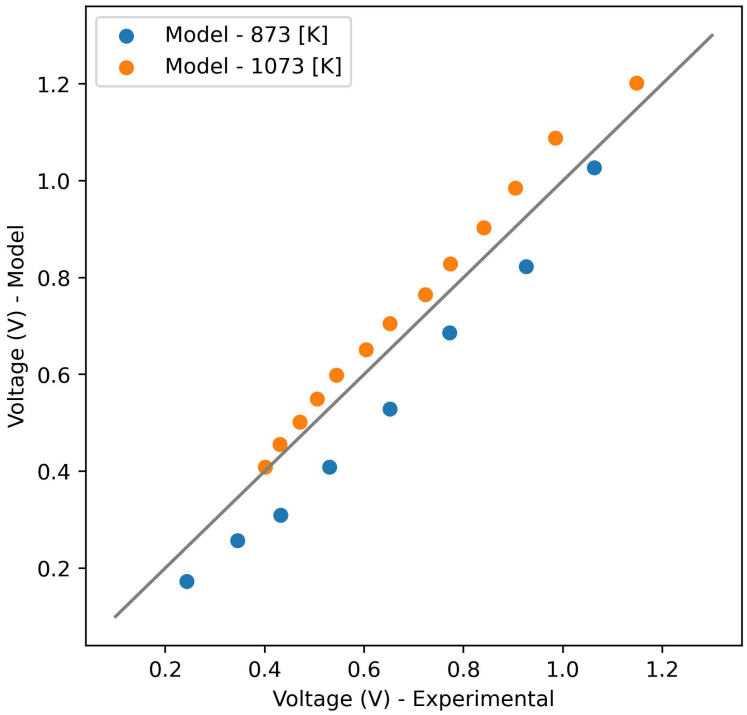

Source:(Author,2022)

parameters model can be considered proper. The orange dots represent the experimental and simulated results at 1073 K, which show a better correlation than 873 K, which can be seen by the lower deviation between the points and the identity line. When the voltage was higher than 0.9, the distance is farther from the identity line, indicating less correlation in comparison to using the range 0.4 to 0.8. The temperatures were specifically chosen as reference points for this validation, as they represent the highest

and lowest limits of the experiment and allow for a comparison within these boundaries. It worth to mention that, SOFC model was validated isolated in comparison with the experimental data in the temperatures of 873K and 1073K and the reformer was also validated in comparison with the data which will be discussed in the following section.

5.1.2 Ethanol reforming

The results of heat transfer rate of reformer, computed through the heat balance, were compared with experimental works published on the literature, with the purpose of validate the conditions of autothermal and steam reforming of ethanol. Regarding the condition of steam reforming, the simulation results were compared with the ones published by (SAEBEA; PATCHARAVORACHOT; ARPORNWICHANOP, 2012). These authors presented a result of 234.70 kW for a system without heat integration, considering the simulation conditions presented in Table 4. The result obtained with the model was 233.77 kW for the same configuration - a error variation of 0.39% for the point.

The simulated results of ethanol reforming model in autothermal condition were validated through a comparison with the data presented in the Table 6 which presents part of experimental results compared to the model results, considering the variation of S/E (steam/ethanol ratio), temperature and O/E (oxygen/ethanol ratio). The reference data is result of a comparative analysis of steam and autothermal reforming, and evaluation on the effect of different inlet variables in heat transfer rate of reformer (ROSHA; IBRAHIM, 2022).

In particular, the comparison between the experimental and simulated heat transfer rates presented deviations under 1% when compared with the reference work. Therefore, the simulated results of heat transfer rates of reformer can be considered satisfactory. Regarding the temperature effect in heat transfer rates, one can see the decrease of heat transfer rates released in ethanol reforming, when temperature is increased at the same oxygen/ethanol ratio. This behavior is associated to combination between the exothermic partial oxidation and endothermic steam reforming. With the increase of temperature, the heat rate of endothermic steam reforming also increases, leading to a decrease of heat released from combined reactions (partial oxidation and steam reforming). Moreover, the oxygen/ethanol ratio affected the heat transfer rates in ethanol reforming. For oxygen/ethanol ratio lower than 0.8, ethanol reforming presented endothermic behavior, while for ratio higher than 0.8, ethanol reformer presented exothermic behavior for isothermal operation. These results indicate that increasing oxygen amounts in ethanol reforming can be beneficial to improve the efficiencies of integrated system with SOFC, because heat can be recovered and used in heat integration strategies. The higher amounts of oxygen increase the partial oxidation rates and consequently the heat transfer rates released by reformer, allowing the reformer operates in exothermic condition.

Table 6 – Comparison between experimental and simulated results of heat transfer rates in ethanol reforming under different conditions of steam/ethanol ratio, oxygen/ethanol rate and temperature

S/E	Temperature [K]	O/E	Model [kW] (1)	Reference [kW] (2)	Error [%]
5	550	0.8	-40.61	-40.3	0.8
5	550	1	-64.48	-64.2	0.4
5	600	0	72.01	73.3	-1.8
5	600	0.2	49.07	49.4	-0.7
5	600	0.6	24.76	25	-0.9
5	600	0.8	-25.26	-25.1	0.6
5	600	1	-50.95	-50.8	0.3
5	650	0	90.24	90.4	-0.2
5	650	0.2	64.44	64.6	-0.2

Source:Adapted from (ROSHA; IBRAHIM, 2022)
Note (1): Outcomes achieved through the utilization of model.
Note (2): The reference paper conducted simulations in order to obtain the data presented.

5.2 SENSITIVITY ANALYSIS

The electrical power of the SOFC is affected directly by mass flowrates of ethanol and water in reformer. Preliminary simulations were performed to compute the inlet mass flowrates of reactants to reach 5 kW of power in SOFC, following the conditions of benchmark case (as illustrated in Table 5). The inlet variables of integrated simulation of reformer and SOFC were oxygen/ethanol ratio, water/ethanol ratio, reformer temperature, SOFC temperature and ethanol mass flowrate. Therefore, simulations were performed to evaluate the effect of inlet conditions on outlet variables such as: yields of hydrogen at outlet reformer, SOFC power and efficiency.

One of the objectives of this work is to obtain the design parameters for the cell power to reach approximately 5 kW. When the inlet flow rate is increased in a system, it is generally expected to result in an increase in power output. However, it is worth noting that in certain cases, particularly with solid oxide fuel cells (SOFC), increasing the flow rate can lead to a decrease in the SOFC voltage (O'HAYRE et al., 2016). This phenomenon can occur due to several reasons. Higher flow rates can provide a higher rate of reactant supplied to the SOFC, which can lead to an increase in the concentration overpotential. This overpotential arises from the limitations in the rate at which reactants can be consumed at the electrode surfaces. Additionally, increasing the flow rate can also result in a higher pressure drop across the fuel cell system,

decreasing the overall efficiency. These losses can contribute to a decrease in the SOFC voltage. This voltage decay is explained by the increase in current density, which consequently increases ohmic losses, due to activation and concentration, which is presented by the Equation (15) relating the SOFC voltage with the activation, ohmic and concentration losses (O'HAYRE et al., 2016; KUPECKI, 2018).

5.2.1 Temperature effect

Figure 18 presents the result of temperature effect in the yield of components in outlet ethanol reformer. It is possible to observe the effect of temperature in the H_2, CO and CO_2 yields. In these simulations, SOFC temperature was 10 ℃ higher than reformer temperature. The increase in temperature favors the partial oxidation and steam reforming of ethanol with growing amounts of hydrogen until 700 ℃, approximately. For temperatures higher than 700 ℃, one can see a slight decrease in hydrogen yields accomplished of decrease of carbon dioxide yield and increase of carbon monoxide and water yields. Therefore, the thermodynamic equilibrium is explained by water-gas shift reaction rates at high temperatures. As this reaction is exothermic, equilibrium constant decrease with temperature, and water-gas shift reaction is shifted toward to consumption of hydrogen and CO_2, with release of water and CO. The low yields of CH_4, an intermediary by-product produced in ethanol steam reforming, indicated its consumption by steam reforming reaction of this component.

Figure 18 – Effect of temperature on the H_2, CO, CO_2 and CH_4 yields from the reformer.

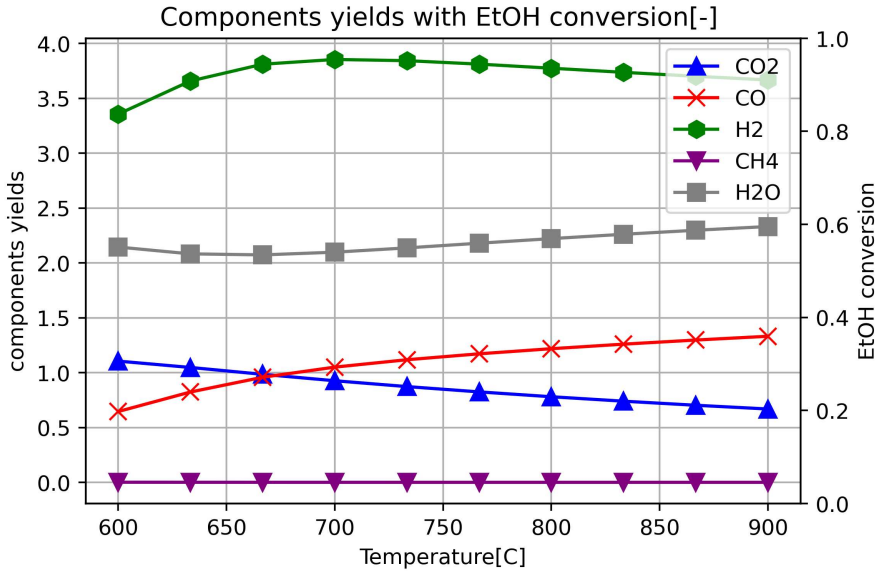

Source:(Author,2023)

Figure 19 illustrates the effect of temperature in efficiency of integrated system, electric power and nominal power. In particular, one can see the correspondence of

hydrogen yields in electric power. As higher the hydrogen yields, higher the electric power, as consequence of higher electrochemical reaction rates. Purple line show the results for nominal power, which is not affected by the temperature.This behavior is expected because nominal power is a function of the lower heat value (LHV) for and mass flow of the fuel.

Figure 19 – Effect of temperature in power and efficiency

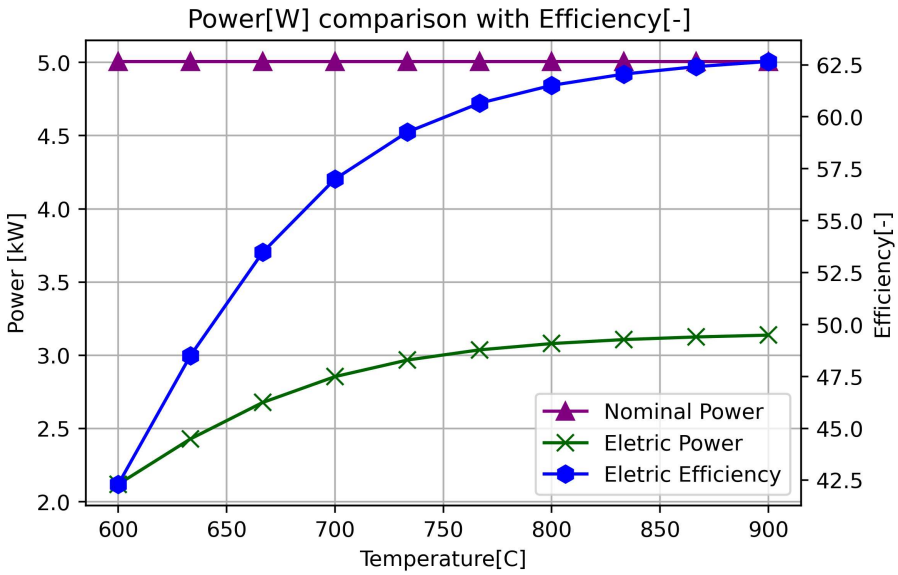

Source:(Author,2023)

The blue line represent the electric efficiency points for each temperature, followed by the green line with the electrical power results. The electric power increase, as the system has more H_2 available for the reaction, which is also observed in the efficiency. The equation (8), relate the electric power to the nominal power, which is observed in the chart. Although hydrogen yields presented a slight decrease from 750 ℃ the electric power and efficiency were not affected, because the increase of temperature allowed higher electrochemical reaction rates.

Temperature variations also affected directly the heat transfer rates of reformer and SOFC, as presented in Figure 20. The heat transfer rate of reformer for isothermal operation is represented by the red line. In particular, reformer requires higher heat transfer rates with the temperature increase. The operation changes from exothermic to endothermic between 600 and 650 ℃. With increase of temperature, reformer operation requires higher heat rates to kept the isothermal operation, as result of higher endothermic steam reforming and reverse water-gas shift reaction rates. These results motivate the evaluation of combined strategy in temperature and oxygen/ethanol ratio to increase the reaction rates of exothermic partial oxidation, decreasing the heat rates required by reformer. Regarding the heat rate released by SOFC, as higher the cell temperature, higher the heat rates, as result of higher electrochemical reaction rates.

Figure 20 – Effect of temperature in heat transfer rates of reformer and SOFC.

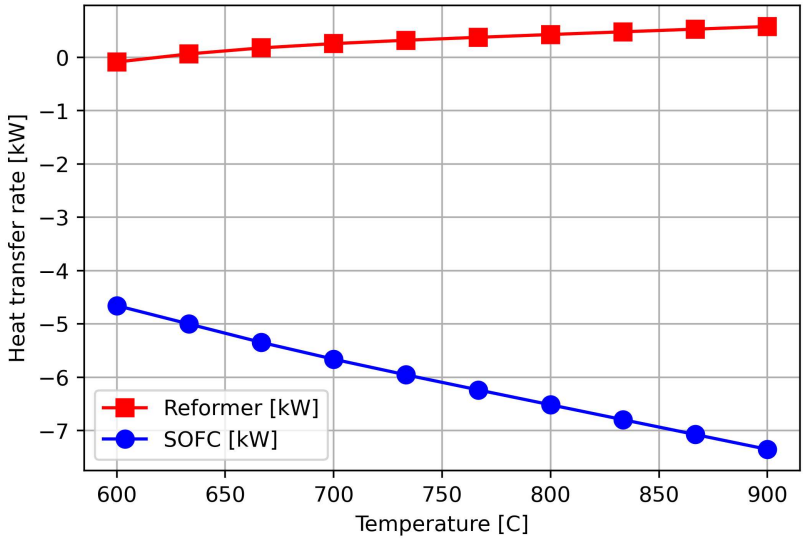

Source:(Author,2023)

Figure 21 – Effect of temperature in reformer heat rate and SOFC electrical power

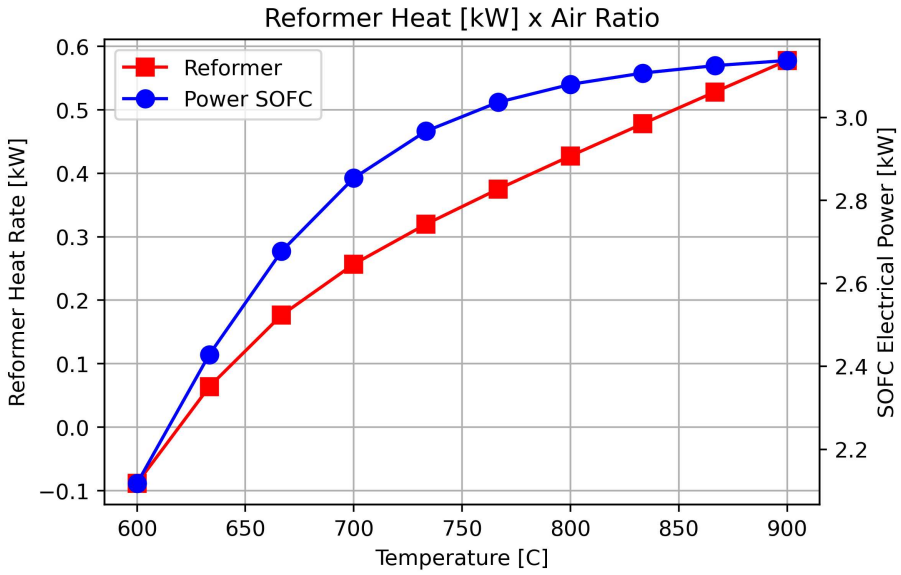

Source:(Author,2023)

Figure 21 presents the simultaneous effect of temperature in heat transfer rates of reformer and SOFC electrical power. Although higher temperatures allowed SOFC reaches higher electrical power, the heat rates required by reformer also increased, illustrating the trade-off between these variables. In this study, the target is defined, although this figure is helpful to understand possibilities of heat exchanger network synthesis accordingly the implementation.

5.2.2 Air/Ethanol effect

Air/ethanol ratio can have a significant effect on the power output of the system. Figure 22 illustrates the effect of oxygen/ethanol ratio in yield of components in ethanol reforming for a ethanol conversion of 100%. Therefore, with hydrogen yields decreased with oxygen/ethanol ratio. In particular, with higher amounts of O_2 and H_2O in reaction medium, CO is oxidized forming CO_2. For this reason, CO yields decreases while CO_2 yields increases. Moreover, ethanol also can reacts by complete oxidation in presence of oxygen in excess with formation of CO_2 and H_2O as by-products, explaining the decrease in H_2 yield. Since the generation of hydrogen is essential for power production in an SOFC, an increased air/ethanol ratio can lead to a lower H_2 yield (Figure 22), and consequently to a lower SOFC electrical power.

Figure 22 – Effect of oxygen/ethanol ratio in yields

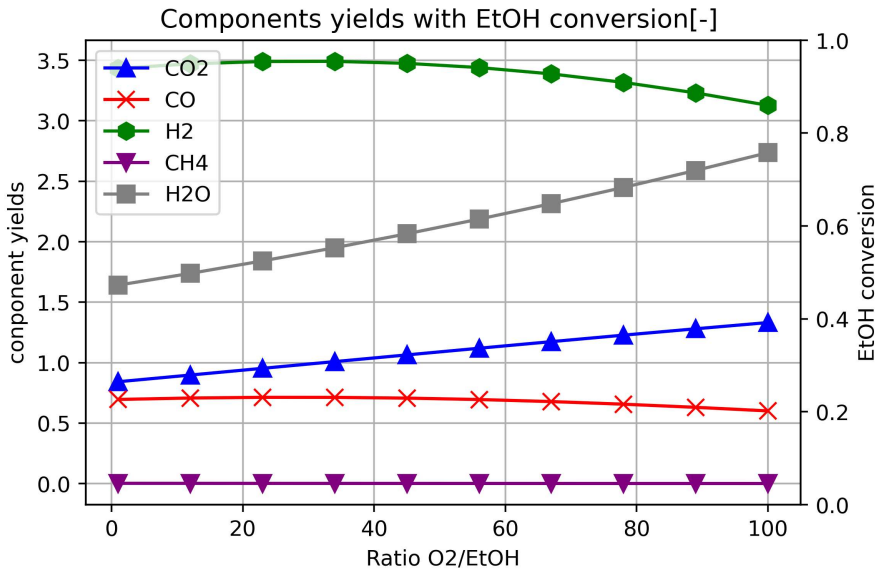

Source:(Author,2022)

In addition, the air/ethanol ratio increase not only affects the power output but also the heat transfer rates of reformer at isothermal operation. In particular, with the oxygen in excess, the exothermic oxidation reactions are favored in comparison with endothermic ethanol steam reforming. Therefore, the use of oxygen/ethanol ratio higher than approximately 40 allowed reformer operates at exothermic condition. The exothermic nature of the reforming reaction at higher air/ethanol ratios opens up the possibility of supplying heat to the system from heat integration strategies. Instead of relying solely on external heat sources, the excess heat generated from the exothermic reaction can be utilized within the system. However, the heat rate released by SOFC was lower for higher oxygen/ethanol ratios due to lower hydrogen yields. In this case, the electrochemical reaction rates in anode become lower and, consequently, the heat rate released by SOFC also decreases. This behavior is can be seen in Figure 23.

Figure 23 – Heat demand for SOFC and Reformer

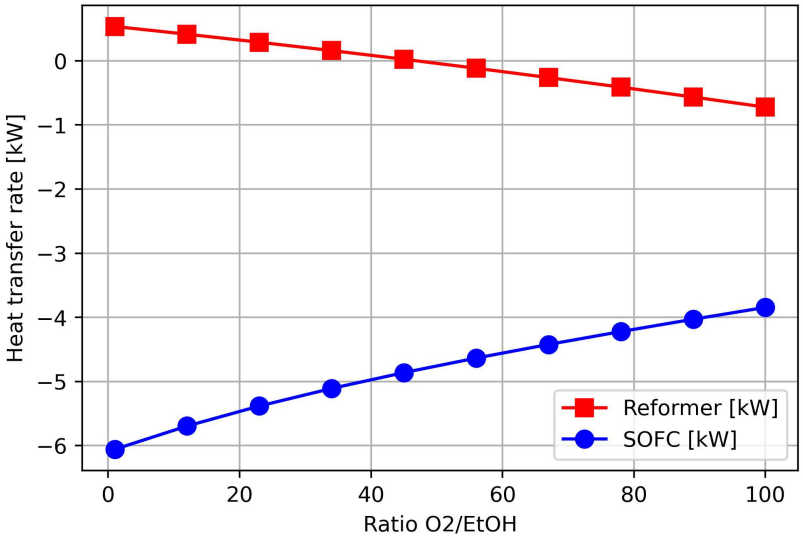

Source:(Author,2022)

The increase of air/ethanol ratio also decreases the efficiency of the system as presented in Figure 24. Conversely, although the heat rates released by reformer increase with oxygen/ethanol ratio, the electric power and efficiency of SOFC decreased due to lower hydrogen yields, illustrating the trade-off between these variables.

Figure 24 – Effect of oxygen/ethanol ratio in power and efficiency

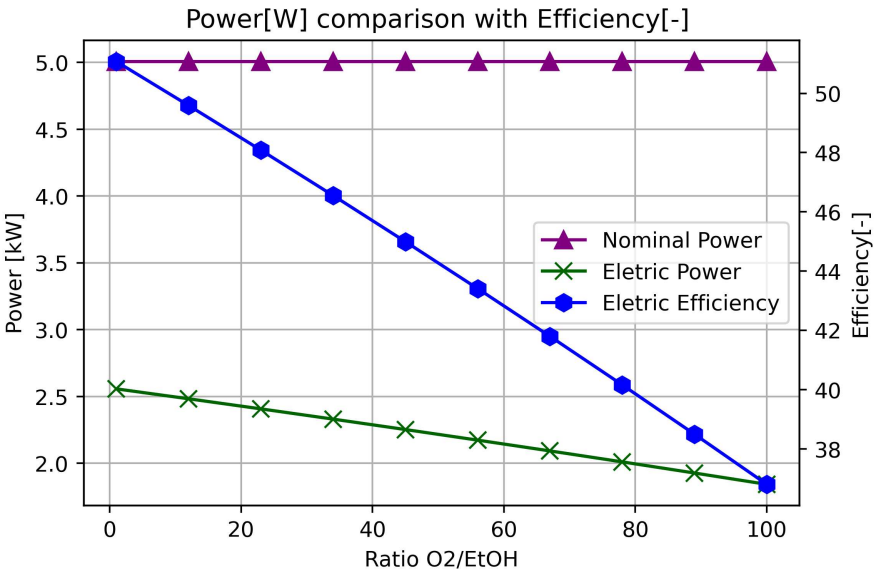

Source:(Author,2022)

The model properly predicts the behavior of SOFC cell and ethanol reformer, allowing further investigation of their thermal integration.

5.3 RESULTS OF MODEL WITHOUT HEAT INTEGRATION

In this section, the reference condition is presented for the analysis of the efficiency results of the SOFC system with and without heat recovery. To establish the benchmark condition, a set of variables listed in Table 7 was established with the objective of achieving a nominal power of 5 kW.

The diagram provided in Figure 14 illustrates the results of the heat transfer rates associated with each individual component that is presently accessible. The (SOFC) operated at 610 ℃, while the reformer was maintained at 600 ℃. This arrangement was implemented to ensure a minimum temperature difference of 10 ℃, as the hot stream at the outlet of the SOFC are utilized to heat the cold stream up to the reformer temperature. Consequently, the system achieved an electric power output of 2.23 kW, and a nominal power rating of 5 kW. As a result, the system efficiency was determined as 44.3% by the equation (8), which evaluate the electrical efficiency. This equation is the most observed in literature for expressing the system efficiency in cases where heat integration is not taken into account. Efficiencies obtained from this diagram can be compared to the literature presented in Table 1. It is evident that the calculated efficiency falls within the range of electric efficiency (40.5% to 51%) for systems using ethanol as a fuel. The lowest efficiency values reported were associated with SOFC temperatures close to 873 K.

Table 7 – SOFC parameters for system without heat integration

Description	Parameter	Value	Units
SOFC Temperature	T	883	(K)
Reformer Temperature	T	873	(K)
Pressure	P	1	(atm)
Input Flow	$\dot{m}$	0.377	(g/s)
Ratio Ethanol/Water	-	3:1	(mol/mol)
Ratio Air/Ethanol	-	0.5	(mol/mol)
Fuel Utilization	Uf	0.7	-

Source:(Author,2023)

5.4 PINCH ANALYSIS

Pinch analysis (as discussed in section 3.6) was applied to evaluate the thermal integration between a SOFC and an ethanol reformer by the reuse of available heat from hot streams at SOFC outlet. Moreover, the proper paring between the hot and cold

streams in heat exchangers, the corresponding number of equipments, the identification of pinch point (wherein hot utilities are used in the heat exchangers), as well as a preliminary proposal of heat exchanger network will also be presented in this section.

The first step of pinch analysis is the proper identification of hot and cold streams, their inlet and outlet temperatures, as well as the heat capacity of each stream, as presented in Table 8. Available data in Table 8 allow to build up the temperature-interval diagram (DIT), which includes all the streams, their respective temperatures, and provides a visualization of the system in graphic format. The first row in Table 8 corresponds to blue line F1 in Figure 25, represents water in a subcooling state (25 ℃) being heated to its saturation temperature (100 ℃). The second line is comprised by water at 100 ℃ which evaporates and the steam goes to superheating until 590 ℃ (blue line F2). The cold stream, represented by blue line F3, is comprised by mixture ethanol/water, which is heated from 492 ℃ until 600 ℃, the inlet reformer temperature. In this case, the temperature of 492 ℃ the one resulting from the mixture of ethanol at 25 ℃ with superheated water at 590 ℃, resulting in the stream F3. The hot streams are comprised by air and gas in SOFC outlet at 610 ℃. These streams, represented by red lines Q1 and Q2, are cooled to 25 ℃.

Table 8 – Inlet variables for heat integration using pinch analysis

Stream	Type	Description	$\dot{m}$ (g/s)	$\dot{m}$cp (W/℃)	Vaporization enthalpy (kJ/kg)	$T_{in}(C)$	$T_{out}(C)$
F1	Cold	Water inlet heating	0.204	0.85	-	25	100
F2	Cold	Water steam superheating and evaporation	0.204	0.41	2227	100	590
F3	Cold	Ethanol/water mixture heating	0.377	0.91	-	492	600
Q1	Hot	SOFC-air cooling	0.198	0.23	-	610	25
Q2	Hot	SOFC gas cooling	0.437	0.92	-	610	25

Source:(Author,2023)

The left side of Figure 25 shows all the hot streams available in the system, while the right side shows the cold streams. The inlet and outlet temperatures of each stream create intermediate lines that divide the diagram in different temperature intervals. One can see that between the first line on left and right, there is a step of 10℃, which was defined to avoid large heat exchanger area. There are 5 intervals in the temperature-interval diagram (from top to bottom), represented by the black lines:

- First interval - 610℃ to 600℃;
- Second interval - 600℃ to 590℃;

Figure 25 – Temperature-interval diagram for system

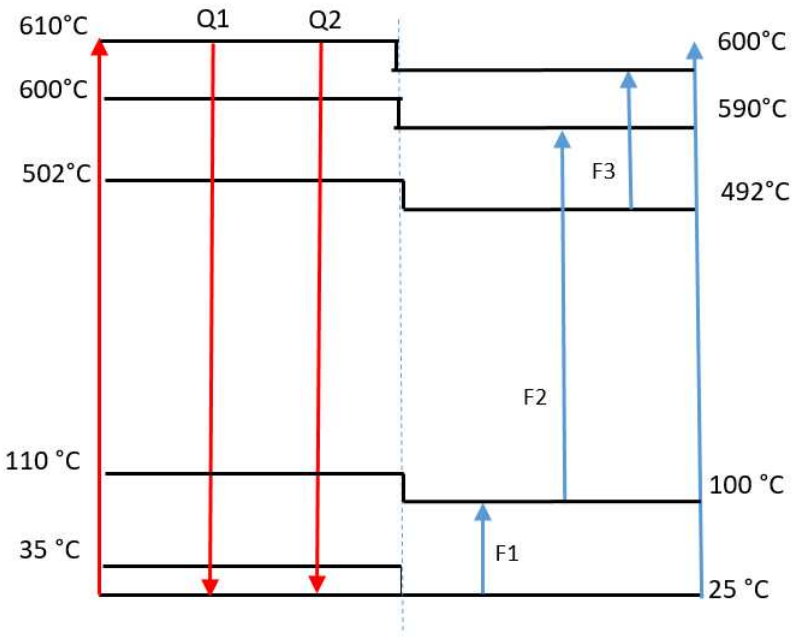

Source:(Author,2023)

- Third interval - 502℃ to 492℃;
- Forth interval - 110℃ to 100℃;
- Fifth interval - 35℃ to 25℃.

For each interval is possible to calculate the offer and demand of heat rate, which is share to the next interval if the offer is higher than demand. Table 9 provides the visualization of offer and demand heat rates, as well as the net balance for each temperature interval.

Table 9 – Residuals and heat rates for hot and cold streams in each interval-temperature

Interval	Residual (W)	Offer (W)		Demand (W)				Net Balance (W)
		Q1	Q2	F1	F2	F2v	F3	
1	0	2.3	9.2	0	0	0	9.1	2.4
2	2.4	22.54	90.16	0	40.18	0	89.18	-14.26
3	0	90.16	360.64	0	160.72	454.31	0	-164.23
4	0	17.25	69	63.75	0	0	0	22.5
5	22.5	2.3	9.2	0	0	0	0	34

Note: F2v - Phase transition heat (W)
Source:(Author,2023)

Heat offer and demand are calculated using equation (52) for each temperature interval. The second column shows the available heat rates from the previous interval, and the third column displays the heat rates offer and the fourth column represents the heat rates demand. The last column is the net heat balance for each interval.

5.4.1 First Interval

The intervals in Figure 25 are sequentially numbered from the top to the bottom. The first interval includes two heat sources, namely Q1 (SOFC-air cooling) and Q2 (SOFC gas cooling), which can be used to meet the heating need of F3 (Ethanol/water mixture heating). Within this defined range, the demand is 9.1 W in order to raise the temperature of the F3 stream by 10℃. This demand could be met by the source Q2 alone (9.3 W), as it possesses sufficient heat capacity to deliver the required heat rate for the F3 stream. Consequently, the supply of Q1 was not utilized to prevent the introduction of an additional heat exchanger into the system. Figure 26 displays the heat exchanger that is required, along with the corresponding temperatures.

Figure 26 – Flowsheet of heat exchanger network for 1st temperature interval

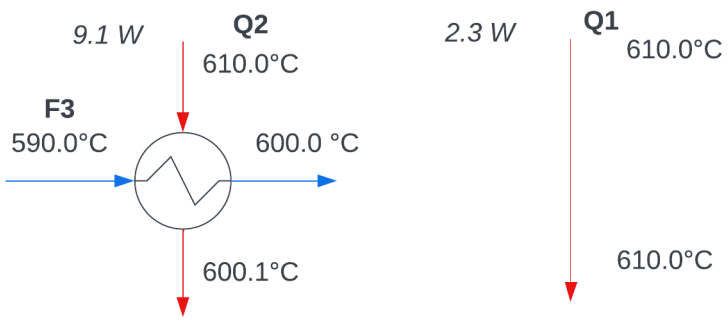

Source:(Author,2023)

5.4.2 Second Interval

In contrast to the previous interval, the second interval presents two additional demands, F2 (water steam superheating) and F3 (ethanol/water mixture heating), which need a temperature rise of 98℃. Upon examination of the last column in Table 9, it becomes evident that the net balance is negative in this range (the first pinch point), hence meaning a critical bottleneck inside the system. Therefore, in order to attain the specified temperature for the project, the system will require an external heat source.

Upon analyzing the hot streams Q1 and Q2, it can be determined that Q2 provides an offer that adequately fulfills the requirements of F3. This integration results in a residual heat rate availability of 0.98 W. Nevertheless, the remaining heat rate of

approximately 40 W required by the F2 stream cannot be sustained just by the left-over heat from Q2 and the residual contribution from Q1. Hence, an external source is necessary to meet this heat rate need. The distribution of residual heat is 0.1 W (from stream Q2) and 2.1 W (from stream Q1, which is not used in the previous interval).

Figure 27 presents the heat exchanger network that is necessary for this particular temperature interval. The first heat exchanger combines the stream F3 with the stream Q2, resulting in an exit temperature of 503 ℃ for stream Q2, while F3 is totally heated up to desired temperature (590 ℃). In order to optimize heat use, the output of stream Q2 is connected to the first heat exchanger of F2, therefore integrating Q2 into F2. This integration leads to a partial temperature of F2 at 495 ℃. This heat exchanger has a heat rate of 1.08 W (0.98 W plus 0.1 W, the residual heat rate of Q2 in first temperature interval). The resulting stream is introduced into a further heat exchanger, where it transfers heat of Q1 to steam water (F2). The heat rate of this device is 24.94 W (22.54 W plus 2.3 W, the residual heat rate of Q1 from first temperature interval). It can be observed that the output temperatures of Q1 and Q2 reach the outlet temperature in this interval of diagram, as the hot streams transfers all of the available heat to the respective cold streams. Lastly, a heat exchanger is incorporated in order to receive heat from a utility, which serves as an external source, and transfer heat to the cold stream F2.

The system has the capability to supply as external source by utilizing the heat generated from the solid oxide fuel cell (SOFC) and reformer. Nonetheless, it is possible to do this by employing a refrigerant fluid, either in gas or liquid form, depending on the specific application, to recover the available heat.

Figure 27 – Flowsheet of heat exchanger network for 2nd temperature interval

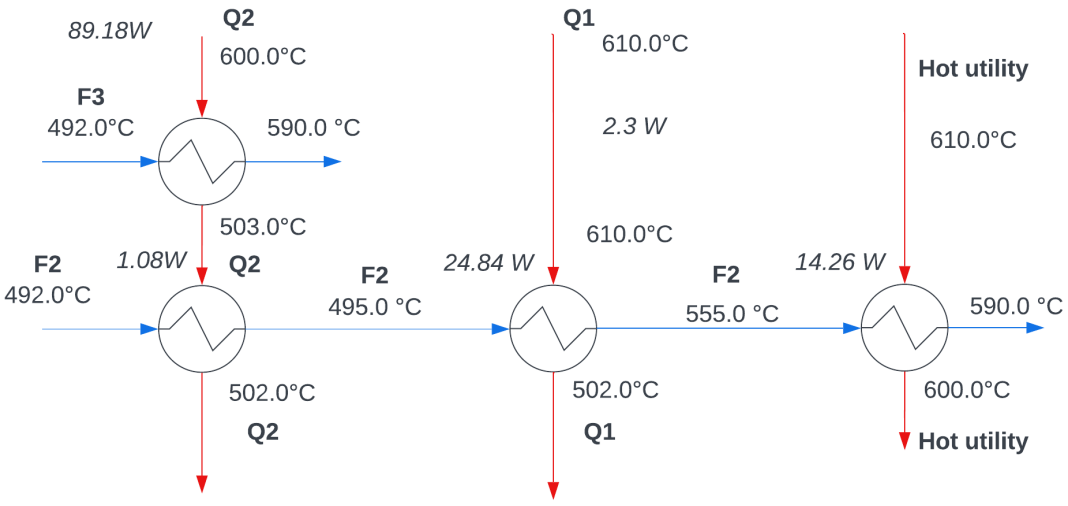

Source:(Author,2023)

5.4.3 Third Interval

The heat exchanger network in the third interval is depicted in Figure 28. The first heat exchanger is used to heat stream F2 from 100℃ (saturated steam) up 492℃ (superheated steam). The heat rate demand of F2 stream during the heating step is 160.72 W, which is supplied by stream Q2 (whose offer heat rate is 360.64 W) in this interval. Next, the second heat employs the remaining heat rate of stream Q2 (199.92 W) to evaporate the stream F2v. However, the complete evaporation of stream F2v requires 454.31 W, resulting in a steam fraction of 44% in this heat exchanger. The next heat exchanger employs the stream Q1 (with an offer heat rate of 90.16 W in this interval) to partially evaporate the stream F2v, resulting in a stream fraction of 64%. As illustrated in Table 9, the offer heat rates of Q1 and Q2 streams are not enough to supply the evaporation rate of F2v stream, as can be seen in negative heat rate residual value (-164.23 W) in this interval. Therefore, a hot utility should be used to complete the evaporation of F2v stream, as can be seen in the last heat exchanger.

Figure 28 – Flowsheet of heat exchanger network for 3rd temperature interval

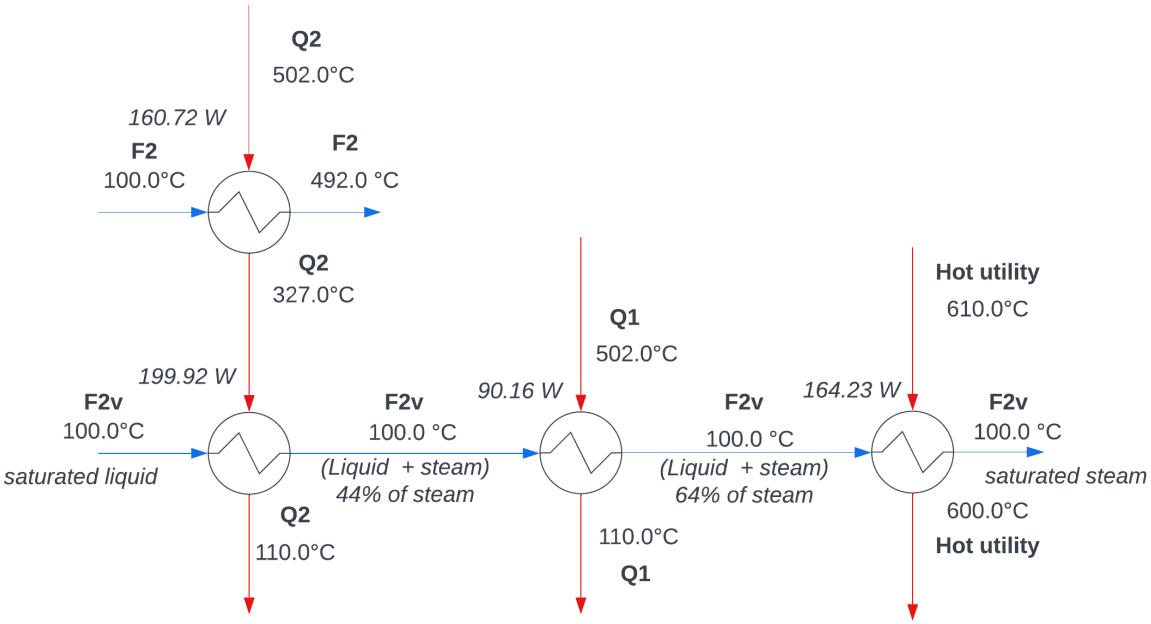

Source:(Author,2023)

5.4.4 Fourth Interval

The fourth interval has the same configuration of the first interval, in which Q1 and Q2 are available for a single demand from stream F2. In this temperature interval, as the heat offer of stream Q2 is enough to meet the heat demand of stream F1, the pairing between these streams was chosen to avoid an additional heat exchanger. In

this particular case, the option to choose Q2 was feasible. However, if Q1 is chosen in the streams pairing for this interval, an additional heat exchanger will be required, involving the heat exchange between Q2 and F1, because the heat rate offered by Q1 is not sufficient to meet the demand of F1. This addition subsequently leads to an increase in the overall implementation costs. As the Q1 stream was not utilized in this interval, a heat rate residual of 17.25 W is carried over to the next interval. Similarly, the Q2 stream has a heat rate residual of 5.25 W, which is also carried over to the next interval. The heat exchanger used in this interval is presented in Figure 29.

Figure 29 – Flowsheet of heat exchanger network for the 4th temperature interval

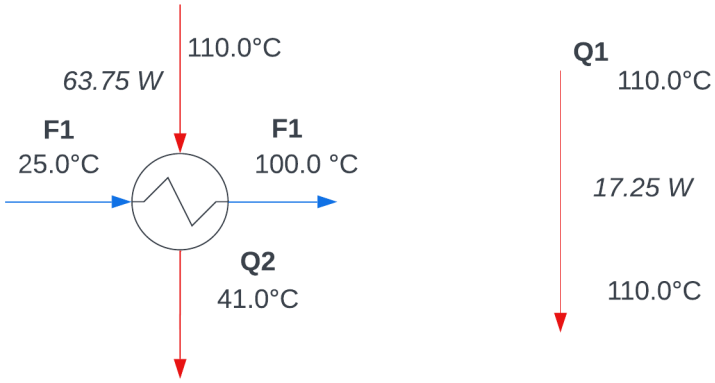

Source:(Author,2023)

5.4.5 Fifth Interval

Prior to being returned to the environment, both streams Q1 and Q2 are cooled to the ambient temperature, as depicted in Figure 30. In this interval, the first heat exchanger uses a cold utility to cool the Q2 stream to room temperature, with a heat rate of 14.45 W (5.25 W from the previous interval plus 9.2 W from this interval). The second heat exchanger is used to cooling the Q1 steam and employs a cold utility with a heat rate of 19.55 W (17.25 W from the previous interval plus 2.3 W from the current interval).

As one can see rather of provide heat with a cold utility for these two heat exchangers, the utilities are removing heat from the system. As a suggestion this could be provided by the water tank if the temperature is adequate to the required condition.

5.4.6 Heat exchanger network (HEN)

Figure 31 shows the integration of all heat exchangers required to the system reach the desired temperatures. The light green line represents the F2 stream, F3 is in yellow, while Q1 and Q2 are in orange and red, respectively. The diagram presents a

Figure 30 – Flowsheet of heat exchangers for 5th temperature interval

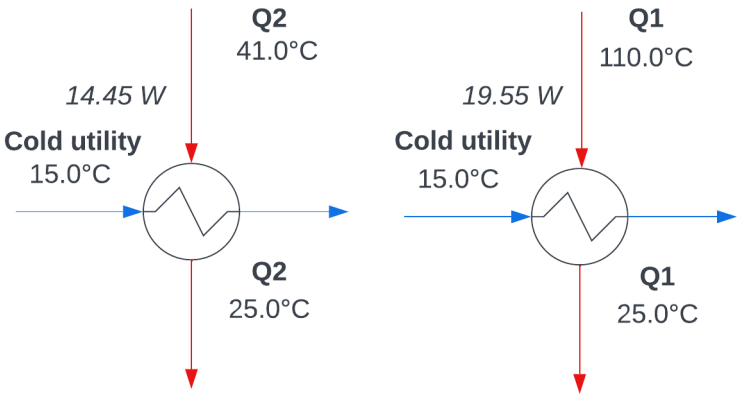

Source:(Author,2023)

feasible solution for the heat integration of the SOFC outlet streams at 610 ℃ with the heat exchangers required to the system.

The proposed heat exchanger network is not an optimal solution, which can be explored in future studies, however this proposal minimizes the use of hot utilities. It is possible to observe that only two heat exchangers in the system use hot utilities to increase the temperature, HX04 and HX08. To cool the outlet of Q1 and Q2 streams, cold utilities are used in HX09 and HX10.

The heat exchangers in this diagram were sized under the assumption of a temperature difference of 10℃ for hot and cold streams. The selected geometry for the heat exchangers was tube-shell. With the provided data on the heat exchangers, including their respective heat transfer rates and temperatures, it becomes feasible to estimate the required surface area for each heat exchanger.

This point allows for the verification of the validity of the 10℃ as the heuristic minimal temperature difference defined in pinch analysis to avoid large areas. This can be accomplished by the use of Equation (49) to estimate the area. The overall heat transfer coefficient was taken into account as 30 W/m^2K for a gas-gas heat exchanger, based on the literature reference and Equation (50) was utilized for the computation of the logarithmic mean temperature difference (ÇENGEL; GHAJAR, 2009; PERLINGEIRO, 2005).

Table 10 presents the area required for each heat exchanger, with the respective temperatures of inlet and outlet streams. The second column present the global heat transfer defined as 30 (W/m² K), a intermediate value in the literature for heat exchangers gas-gas (ÇENGEL; GHAJAR, 2009). These preliminary results show that the size of heat exchangers is not excessively high for these conditions, although further studies are required to define dimensional characteristics. These results shows that the heat exchangers have areas that are feasible for an embedded application,

which was expected and fulfilling the function of recovering 842 W heat for the system. Besides, further studies should be done in other to identify specific dimensional characteristics of the heat exchangers, heat transfer coefficients and materials to support the temperatures.

The combination of the heat exchange network proposed in this section with the studies done for the ethanol reforming allow to define a condition for the system in which the objective of project is reached. Further analysis could investigate impact of the variations in temperature to increase the electric efficiency, however, this impacts directly affect the benefits of SOFC, reformer and the heat exchangers. This leads the system to a trade-off of increasing temperatures to achieve higher efficiency, with the impacts it has on the heat exchangers. This may include considerations such as the number of heat exchangers.

Table 10 – Detailed list of heat exchangers used in the heat exchanger network

Heat Exchanger	Global heat transfer (W/m^2K)	Q (W)	$T_{in,cold}$(℃)	$T_{out,cold}$(℃)	$T_{in,hot}$(℃)	$T_{out,hot}$(℃)	$\Delta T_m(LMTD)$	Area (cm²)
HX01	30	63.75	25	100	110	41	12.77	1664.6
HX02	30	199.92	100	100	327	110	69.5	958.87
HX03	30	90.16	100	100	502	110	106.12	283.20
HX04	30	164.23	100	100	610	600	504.98	108.41
HX05	30	160.72	100	492	502	327	69.5	770.85
HX06	30	1.08	492	495	503	502	8.96	40.17
HX07	30	24.84	494.4	554.98	600	502	21.03	393.63
HX08	30	14.26	495	555	610	502	23.28	355.60
HX09	30	89.18	492	590	600	503	10.49	2833.25
HX10	30	14.45	15	25	41	30.5	15.75	305.85
HX11	30	19.55	15	25	110	85	77.26	84.35

Source:(Author, 2023)

In preliminary tests, the temperature of water/ethanol mixture at mixer outlet was fixed at 600℃ (the inlet reformer temperature). Next, the inlet temperature steam in mixer to allow heating, evaporation and superheating of ethanol stream was computed. However, it was observed that the temperature required for this condition was higher than the available hot streams. To mitigate this issue, a heat exchanger was include after the mixer, to provide the additional heat to the system.

Furthermore, the results of pinch analysis, which investigate the heat integration originating from SOFC as hot streams for the heat exchangers, provide the heat flowrate required in each temperature interval for the system reaches the desired temperature. The total heat flowrate of the heat exchangers within the network may be determined by summing the individual heat flowrates. This calculation reveals that the system needs to recover a total of 842 W from the heat sources, including the utilities.

The outcome of the pinch study yields the comprehensive measure of heat recovery achievable from the system, with the aim of enhancing system efficiency. In the system without heat integration, the efficiency obtained is 44.4% at a temperature of 883 K for a nominal power output of 5 kW, and the water/ethanol ratio of 3:1, considering the input variables specified in Table 7. By comparing the obtained findings with the efficiencies presented in Table 1, it can be demonstrated that the value falls within the given range (40.0% to 51.0%) for electrical efficiency. Focus in the studies with the same temperature range, one can observe a range of (40.5% to 44.0%), which demonstrate the agreement of the results obtained. On the other hand, the heat integration process yielded an overall efficiency of 61.2%, hence providing a system benefit of 16.8%, at the same conditions defined for the system without heat integration. This is within the observed range of 42% to 74.3% as indicated in Table 1.

The heat available from SOFC and reformer are enough for the heat exchanger network and the residual heat can be explored as an external source to any other part of the system. The available heat should to be recovery by a refrigerant fluid, which based in the literature could change accordingly the application and SOFC power. This particular issue can be explored in a future work.

Although some works of open literature suggest the use of an after-burner as a heat source, this research showed that it is possible operating the ethanol reforming in exothermic conditions (depending on operation conditions), which avoids the use of after-burner to produce the heat rate required by reformer (SAEBEA et al., 2013; HONG et al., 2011; TIPPAWAN; ARPORNWICHANOP, 2014a).

Figure 31 – HX Diagram

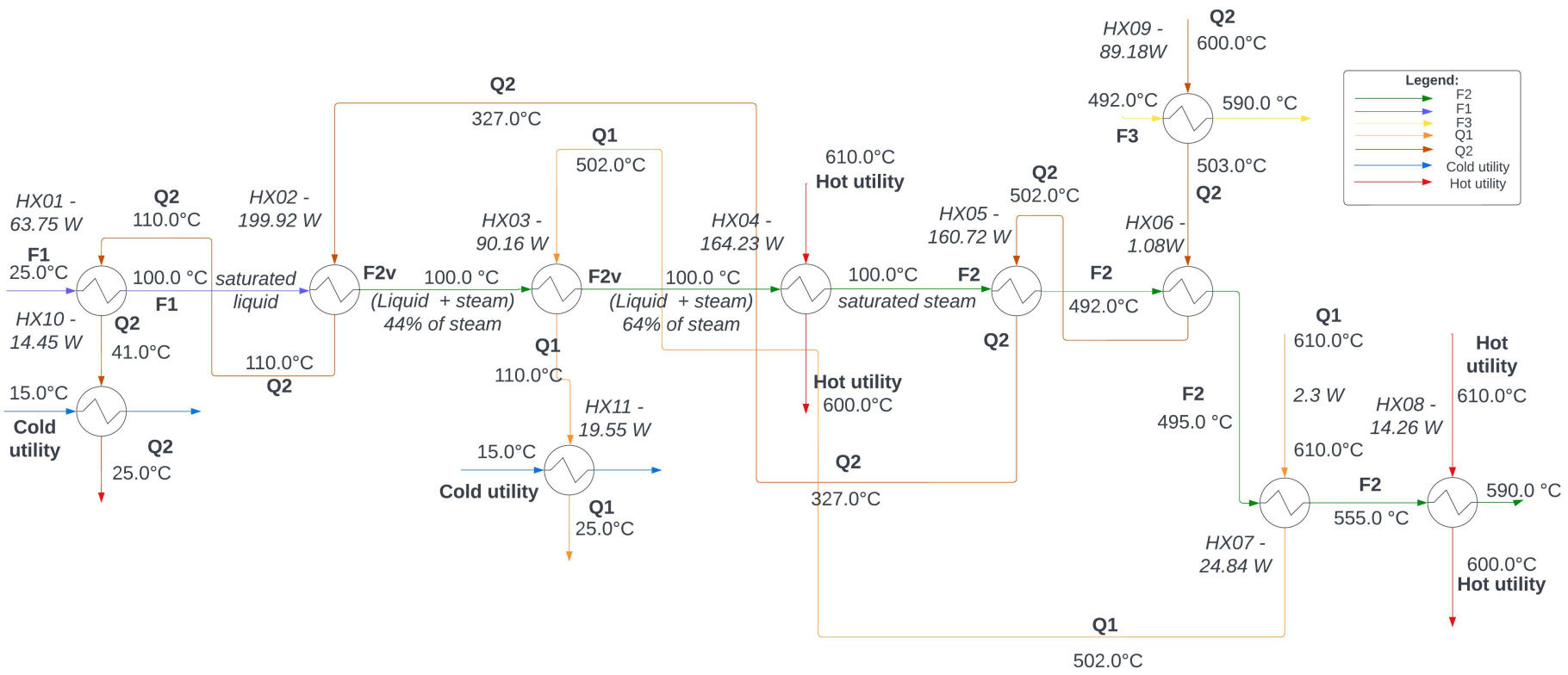

Source:(Author,2023)

6 CONCLUSIONS

Firstly in this work, a literature review was performed aiming at understanding possible diagrams and scenarios for energy efficiency in integrated SOFC systems. The analysis identified the three main types of integrated reformers in the literature, showing their advantages and disadvantages. Finally, a table was built with the main reference parameters of the study related to the use of ethanol in integrated SOFC systems, such as electrical, thermal, and overall efficiencies.

In order to study the improvement of the efficiency of the system, an SOFC model representation was chosen, integrated with a reformer in equilibrium state to simulate the set SOFC and reformer. Models to represent the heat exchangers and evaporators were implemented as part of the heat integration.

The study examined the effects of temperature fluctuations ranging from 600 to 900 ℃ on the SOFC. The findings indicate that an increase in temperature up to approximately 700 ℃ enhances the production of hydrogen. At temperatures exceeding 700 ℃, the production of hydrogen is reduced as a result of a decrease in carbon dioxide yield and an increase in carbon monoxide and water yields. The influence of temperature on hydrogen production has a beneficial effect on the electrical efficiency. While it is true that higher temperatures can enable SOFC to achieve higher electrical power outputs, it is important to note that this increase in temperature also leads to an increase in the heat rates required by the reformer.

A comparable study was conducted to examine the effects of the air/ethanol ratio on hydrogen yields and heat transfer in the reformer. The findings revealed that an increase in the oxygen/ethanol ratio leads to a decrease in hydrogen yields. Additionally, this change in ratio also influences the heat transfer in the reformer, thereby promoting exothermic oxidation reactions. Hence, employing an oxygen/ethanol ratio exceeding approximately 40 enables the reformer operating under exothermic conditions.

Given the findings derived from the examination of temperature variation and the air/ethanol ratio, a system without heat integration was suggested as a means to understand the influence of heat integration within the system. The system was designed to attain a nominal power of 5kW at a temperature of 883 K, resulting in an efficiency of 44.4%. This efficiency value falls within the studies reported efficiency range of 40.0% to 51.0% for electrical efficiency available in Table 1.

A pinch analysis was applied in the system aiming at proposing a possible heat exchange network. The heat exchanger network proposed was capable to recover 842 W of heat from the output streams from the SOFC with was an energy wasted in the scenario without heat integration. This amount of heat represents a benefit of 16.8% in efficiency, resulting an overall of 61.2%. The network is not optimized, although it fulfil the role of demonstrate that is possible to reuse the gas originating from SOFC as a

heat source for the system. Thus, the implementation of the system avoid the use of the external heat source for the system, and reuse available heat streams which will be discarded.

Thus, the system proposed in this work demonstrated that the heat recover from the hot streams of SOFC has a high impact in the system efficiency, as expect, and that exist a group of possible solutions for the aim of this project. Despite that steam reforming process allowed the higher hydrogen yields, there are feasible solutions with autothermal reforming process, which can provide benefits for the system in the heat integration. As demonstrated, there are trade-off between temperature operation, and the heat rates for the system with needs investigation.

Furthermore, this work proposed a system with heat integration which does not use the afterburner, with focus in the utilization of the heat available from SOFC operating at 883K temperature. This may offer an additional advantage in terms of cost implementation by eliminating a component, and operating within this intermediate temperature range decreases the need for thermal resistance materials.

6.1 SUGGESTION FOR FUTURE WORK

Lastly, some points that were not cover in this work and can be explore in the future works are listed bellow:

- Detail the heat exchangers in dimensions and technical characteristics which allow the build/implementation of vehicles;
- Understand if the amount of heat released by the system can be use in start-up of the system;
- Study the possibility of integration the SOFC model to the a reformer model with take in consideration all the aspects of the chemical reaction (plug-flow);
- Develop a multi objective study to identify the optimal configuration of heat exchanger network which provide enough heat to the system, minimizing the cost or number of heat exchangers;
- Validate the code with experiments developed for vehicles in stationary conditions;
- Examine the heat exchanger network from an exergy standpoint.

REFERENCES

AGUIAR, P.; ADJIMAN, C.S.; BRANDON, N.P. Anode-supported intermediate temperature direct internal reforming solid oxide fuel cell. I: model-based steady-state performance. **Journal of Power Sources**, v. 138, 1-2 Nov. 2004. ISSN 03787753.

ALHAZMI, N.; ALMUTAIRI, Ghzzai; ALENAZEY, Feraih; ALOTAIBI, Bandar. Three-dimensional computational fluid dynamics modeling of button solid oxide fuel cell. **Electrochimica Acta**, v. 390, Sept. 2021. ISSN 00134686.

AMBRÓS, W.M.; LANZANOVA, T.D.M.; FAGUNDEZ, J.L.S.; SARI, R.L.; PINHEIRO, D.K.; MARTINS, M.E.S.; SALAU, N.P.G. Experimental analysis and modeling of internal combustion engine operating with wet ethanol. **Fuel**, v. 158, p. 270–278, 2015. ISSN 0016-2361.

ARPORNWICHANOP, Amornchai; CHALERMPANCHAI, Nuttapong; PATCHARAVORACHOT, Yaneeporn; ASSABUMRUNGRAT, Suttichai; TADE, Moses. Performance of an anode-supported solid oxide fuel cell with direct-internal reforming of ethanol. **International Journal of Hydrogen Energy**, Elsevier BV, v. 34, n. 18, p. 7780–7788, Sept. 2009.

ARTEAGA, Luis E.; PERALTA, Luis M.; KAFAROV, Viatshelav; CASAS, Yannay; GONZALES, Erenio. Bioethanol steam reforming for ecological syngas and electricity production using a fuel cell SOFC system. **Chemical Engineering Journal**, v. 136, 2-3 Mar. 2008. ISSN 13858947.

ARTEAGA-PEREZ, Luis E.; CASAS, Yannay; PERALTA, Luis M.; KAFAROV, Viatshelav; DEWULF, Jo; GIUNTA, Pablo. An auto-sustainable solid oxide fuel cell system fueled by bio-ethanolProcess simulation and heat exchanger network synthesis. **Chemical Engineering Journal**, Elsevier BV, v. 150, n. 1, p. 242–251, July 2009.

ASSABUMRUNGRAT, Suttichai; ARPORNWICHANOP, Amornchai; SUKWATTANAJAROON, Vorachatra; SAEBEA, Dang. **Integrated Solid Oxide Fuel Cell Systems for Electrical Power Generation—A Review**. [S.l.]: Wiley, Apr. 2016. P. 526–546. Available from: https://doi.org/10.1002/9781119066354.ch51.

ASSABUMRUNGRAT, Suttichai; PAVARAJARN, Varong; CHAROJROCHKUL, Sumittra; LAOSIRIPOJANA, Navadol. Thermodynamic analysis

for a solid oxide fuel cell with direct internal reforming fueled by ethanol. **Chemical Engineering Science**, v. 59, 24 Dec. 2004. ISSN 00092509.

BADUR, Janusz; LEMAŃSKI, Marcin; KOWALCZYK, Tomasz; ZIÓŁKOWSKI, Paweł; KORNET, Sebastian. Zero-dimensional robust model of an SOFC with internal reforming for hybrid energy cycles. **Energy**, v. 158, Sept. 2018. ISSN 03605442.

BAO, Cheng; WANG, Ying; FENG, Daili; JIANG, Zeyi; ZHANG, Xinxin. Macroscopic modeling of solid oxide fuel cell (SOFC) and model-based control of SOFC and gas turbine hybrid system. **Progress in Energy and Combustion Science**, v. 66, May 2018. ISSN 03601285.

BARUAH, Renika; DIXIT, Marm; BASARKAR, Pratik; PARIKH, Dhrupad; BHARGAV, Atul. Advances in ethanol autothermal reforming. **Renewable and Sustainable Energy Reviews**, Elsevier BV, v. 51, p. 1345–1353, Nov. 2015.

BHATTACHARYYA, Debangsu; RENGASWAMY, Raghunathan. A Review of Solid Oxide Fuel Cell (SOFC) Dynamic Models. **Industrial Engineering Chemistry Research**, v. 48, 13 July 2009. ISSN 0888-5885.

BIANCHI, Fiammetta Rita; SPOTORNO, Roberto; PICCARDO, Paolo; BOSIO, Barbara. Solid Oxide Fuel Cell Performance Analysis through Local Modelling. **Catalysts**, MDPI, v. 10, n. 5, p. 519, 2020.

BIODIESELBR. **Próalcool - Programa brasileiro de álcool**. [S.l.: s.n.], 2006. Available from: https://www.biodieselbr.com/proalcool/pro-alcool/programa-etanol#:~:text.

BRAUN, B.; FISCHER, K.; RZEPKA, M.; STIMMING, U.; BIERMANN, J.W.; JOHANNABER, M.; WALLENTOWITZ, H. Simulation Code for Gasoline Driven Fuel Cell Cars. Wiley, v. 3, n. 3, p. 122–127, Nov. 2003.

BRITO, Marcos Lapa; JÚNIOR, José Mário Ferreira; SANTOS, Luiz Carlos Lobato dos; SIMONELLI, George. Advances in ethanol autothermal reform for hydrogen gas production: a review. **Research, Society and Development**, Research, Society and Development, v. 9, n. 5, e126953070, Mar. 2020.

CANTERA. **Cantera Properties**. 2022. Available from: https://cantera.org/documentation/docs-2.6/sphinx/html/cython/thermo.

html?highlight=equilibrate#cantera.Mixture.equilibrate. Visited on: 30 Mar. 2022.

ÇENGEL, Y.A.; GHAJAR, A.J. **Tranferência de Calor e Massa**. [S.l.]: McGraw Hill Brasil, 2009. ISBN 9788580551280.

CHAN, SH; KHOR, KA; XIA, ZT. A complete polarization model of a solid oxide fuel cell and its sensitivity to the change of cell component thickness. **Journal of power sources**, Elsevier, v. 93, n. 1-2, p. 130–140, 2001.

CHEDDIE, Denver F.; MUNROE, Norman D.H. A dynamic 1D model of a solid oxide fuel cell for real time simulation. **Journal of Power Sources**, v. 171, 2 Sept. 2007. ISSN 03787753.

CHEN, Bin; XU, Haoran; TAN, Peng; ZHANG, Yuan; XU, Xiaoming; CAI, Weizi; CHEN, Meina; NI, Meng. Thermal modelling of ethanol-fuelled Solid Oxide Fuel Cells. **Applied Energy**, v. 237, Mar. 2019. ISSN 03062619.

CHEN, X.; PAN, Y.; CHEN, J. Performance and Evaluation of a Fuel Cell-Thermoelectric Generator Hybrid System. **Fuel Cells**, v. 10, 6 Dec. 2010. ISSN 16156846.

CHOUDHURY, Arnab; CHANDRA, H.; ARORA, A. Application of solid oxide fuel cell technology for power generation—A review. **Renewable and Sustainable Energy Reviews**, Elsevier BV, v. 20, p. 430–442, Apr. 2013.

DOKMAINGAM, Pannipha; AREESINPITAK, Sureewan; LAOSIRIPOJANA, Navadol. Transient Modeling of Tubular-Designed IIR-SOFC Fueled by Methane, Methanol, and Ethanol. **Engineering Journal**, v. 21, 3 June 2017. ISSN 01258281.

DOUVARTZIDES, S.; TSIAKARAS, P. Ethanol and methane fueled solid oxide fuel cells: A comparative study. **Ionics**, v. 7, 3 May 2001. ISSN 0947-7047.

FAHEEM, Hafiz Hamza; ABBAS, Syed Zaheer; TABISH, Asif Nadeem; FAN, Liyuan; MAQBOOL, Fahad. A review on mathematical modelling of Direct Internal Reforming-Solid Oxide Fuel Cells. **Journal of Power Sources**, Elsevier BV, v. 520, p. 230857, Feb. 2022.

FAPESP, Agência. **Proálcool: Uma Das Maiores Realizações do Brasil baseadas em Ciência e Tecnologia**. [S.l.]: Agência FAPESP, Dec. 2016. Available from: https://agencia.fapesp.br/proalcool-uma-das-maiores-realizacoes-do-brasil-baseadas-em-ciencia-e-tecnologia/24432/.

HONG, Wen-Tang; YEN, Tzu-Hsiang; CHUNG, Tsang-Dong; HUANG, Cheng-Nan; CHEN, Bao-Dong. Efficiency analyses of ethanol-fueled solid oxide fuel cell power system. **Applied Energy**, v. 88, 11 Nov. 2011. ISSN 03062619.

KACZMARCZYK, Robert; GURGUL, Sebastian. A Thermodynamic Analysis of Heavy Hydrocarbons Reforming for Solid Oxide Fuel Cell Application as a Part of Hybrid Energy Systems. **Energies**, v. 14, 2 Jan. 2021. ISSN 1996-1073.

KELES, D; WIETSCHEL, M; MOST, D; RENTZ, O. Market penetration of fuel cell vehicles – Analysis based on agent behaviour. **International Journal of Hydrogen Energy**, Elsevier BV, v. 33, n. 16, p. 4444–4455, Aug. 2008.

KIM, Jai-Woh; VIRKAR, Anil V.; FUNG, Kuan-Zong; MEHTA, Karun; SINGHAL, Subhash C. Polarization Effects in Intermediate Temperature, Anode-Supported Solid Oxide Fuel Cells. **Journal of The Electrochemical Society**, The Electrochemical Society, Inc., v. 146, n. 1, p. 69, Jan. 1999.

KIM, Min Soo; KIM, Dong Kyu. Parametric study on dynamic heat and mass transfer response in polymer electrolyte membrane fuel cell for automotive applications. **Applied Thermal Engineering**, v. 167, Feb. 2020. ISSN 13594311.

KUPECKI, Jakub (Ed.). **Modeling, Design, Construction, and Operation of Power Generators with Solid Oxide Fuel Cells**. [S.l.]: Springer International Publishing, 2018. ISBN 978-3-319-75601-1.

LAOSIRIPOJANA, Navadol; WIYARATN, Wisitsree; KIATKITTIPONG, Worapon; ARPORNWICHANOP, Arnornchai; SOOTTITANTAWAT, Apinan; ASSABUMRUNGRAT, Suttichai. Reviews on Solid Oxide Fuel Cell Technology. **Engineering Journal**, Faculty of Engineering, Chulalongkorn University, v. 13, n. 1, p. 65–84, Feb. 2009.

MA, Shuai et al. Fuel cell-battery hybrid systems for mobility and off-grid applications: A review. **Renewable and Sustainable Energy Reviews**, v. 135, Jan. 2021. ISSN 13640321.

MARINOV, Nick M. A detailed chemical kinetic model for high temperature ethanol oxidation. **International Journal of Chemical Kinetics**, Wiley, v. 31, n. 3, p. 183–220, 1999.

NI, Meng. Modeling and parametric simulations of solid oxide fuel cells with methane carbon dioxide reforming. Elsevier BV, v. 70, p. 116–129, June 2013.

NISSAN. **Nissan unveils world's first Solid-Oxide Fuel Cell vehicle**. 2016. Available from: `https://global.nissannews.com/en/releases/nissan-unveils-worlds-first-solid-oxide-fuel-cell-vehicle`. Visited on: 30 July 2022.

O'HAYRE, Ryan; CHA, Suk-Won; COLELLA, Whitney; PRINZ, Fritz B. **Fuel Cell Fundamentals**. [S.l.]: John Wiley Sons, Inc, May 2016. ISBN 9781119191766.

OECHSLER, Bruno F.; DUTRA, Julio C. S.; BITTENCOURT, Roberto C.P.; PINTO, José C. Simulation and Control of Steam Reforming of Natural Gas—Reactor Temperature Control Using Residual Gas. **Industrial &amp Engineering Chemistry Research**, American Chemical Society (ACS), v. 56, n. 10, p. 2690–2710, Mar. 2017.

OLIVA, Diego G.; FRANCESCONI, Javier A.; MUSSATI, Miguel C.; AGUIRRE, Pio A. Ethanol and glycerin processor systems coupled to solid oxide fuel cells (SOFCs). Optimal operation and heat exchangers network synthesis. Elsevier BV, v. 38, n. 17, p. 7140–7158, June 2013.

PALUS, Mateusz; PIANKO-OPRYCH, Paulina. A mathematical model of two-stage Solid Oxide Fuel Cell, SOFC, stacks for dynamic simulation of Combined Heat and Power system fed by natural gas. **Polish Journal of Chemical Technology**, v. 0, 0 May 2021. ISSN 1899-4741.

PAZ FIUZA, Raigenis da; SILVA, Marcos Aurélio da; PONTES, Luiz Antônio Magalhães; TEIXEIRA, Leonardo Sena Gomes; BOAVENTURA, Jaime Soares. A utilização de etanol em célula a combustível de óxido sólido. **Química Nova**, v. 35, 8 2012. ISSN 0100-4042.

PERLINGEIRO, C.A.G. **Engenharia de processos: Análise, simulação, otimização e síntese de processos químicos**. [S.l.]: Editora Blucher, 2005. ISBN 9788521215004.

REVANKAR, Shripad T.; MAJUMDAR, Pradip. **Fuel Cells**. [S.l.]: CRC Press, Apr. 2016.

ROSHA, Pali; IBRAHIM, Hussameldin. Comparative analysis of ethanol-steam and -autothermal reforming for hydrogen production using Aspen Plus. **The Canadian Journal of Chemical Engineering**, Wiley, v. 101, n. 6, p. 3420–3430, Nov. 2022.

SAEBEA, Dang; AUTHAYANUN, Suthida; PATCHARAVORACHOT, Yaneeporn; PAENGJUNTUEK, Woranee; ARPORNWICHANOP, Amornchai. Use of different renewable fuels in a steam reformer integrated into a solid oxide fuel cell: Theoretical analysis and performance comparison. **Energy**, v. 51, Mar. 2013. ISSN 03605442.

SAEBEA, Dang; PATCHARAVORACHOT, Yaneeporn; ARPORNWICHANOP, Amornchai. Analysis of an ethanol-fuelled solid oxide fuel cell system using partial anode exhaust gas recirculation. **Journal of Power Sources**, v. 208, June 2012. ISSN 03787753.

SMITH, Joseph Mauk; VAN NESS, Hendrick C; ABBOTT, Michael M; QUEIROZ, Eduardo Mach. **Introdução à termodinâmica da engenharia química**. [S.l.]: LTC, 2000.

SRISIRIWAT, Anuchart. High temperature solid oxide fuel cell integrated with autothermal reformer. In: IEEE. 2008 IEEE 2nd International Power and Energy Conference. [S.l.: s.n.], 2008. P. 437–440.

SRISIRIWAT, Nawadee; WUTTHITHANYAWAT, Chananchai. Solid Oxide Fuel Cell and Steam Reformer System Steady State Modeling. Trans Tech Publications, Ltd., v. 446-447, p. 790–795, Nov. 2013.

TANIM, Tanvir; BAYLESS, David J.; TREMBLY, Jason P. Modeling a 5 kWe planar solid oxide fuel cell based system operating on JP-8 fuel and a comparison with tubular cell based system for auxiliary and mobile power applications. Elsevier BV, v. 245, p. 986–997, Jan. 2014.

THANOMJIT, Chollaphan; PATCHARAVORACHOT, Yaneeporn; PONPESH, Pimporn; ARPORNWICHANOP, Amornchai. Thermodynamic analysis of solid oxide fuel cell system using different ethanol reforming processes. **International Journal of Hydrogen Energy**, v. 40, 21 June 2015. ISSN 03603199.

TIPPAWAN, Phanicha; ARPORNWICHANOP, Amornchai. Energy and exergy analysis of an ethanol reforming process for solid oxide fuel cell applications. **Bioresource Technology**, v. 157, Apr. 2014. ISSN 09608524.

TIPPAWAN, Phanicha; ARPORNWICHANOP, Amornchai. Energy and exergy analysis of an ethanol reforming process for solid oxide fuel cell applications. **Bioresource Technology**, Elsevier BV, v. 157, p. 231–239, Apr. 2014.

TIPPAWAN, Phanicha; IM-ORB, Karittha; ARPORNWICHANOP, Amornchai. Efficient heat allocation in the two-step ethanol steam reforming and solid oxide fuel cell integrated process. **Energy**, v. 133, Aug. 2017. ISSN 03605442.

TSIAKARAS, P.; DEMIN, A.; DOUVARTZIDES, S.; GEORGAKAKIS, N. Ethanol utilization in solid oxide fuel cells: A thermodynamic approach. **Ionics**, v. 5, 3-4 May 1999. ISSN 0947-7047.

WANG, K. et al. A Review on solid oxide fuel cell models. **International Journal of Hydrogen Energy**, v. 36, 12 June 2011. ISSN 03603199.

WUTTHITHANYAWAT, Chananchai; SRISIRIWAT, Nawadee. Autothermal Reforming of Ethanol for Hydrogen Production: Modeling and Simulation. **Applied Mechanics and Materials**, Trans Tech Publications, Ltd., v. 541-542, p. 108–112, Mar. 2014.

YANG, Bo; WANG, Jingbo; ZHANG, Mengting; SHU, Hongchun; YU, Tao; ZHANG, Xiaoshun; YAO, Wei; SUN, Liming. A state-of-the-art survey of solid oxide fuel cell parameter identification: Modelling, methodology, and perspectives. **Energy Conversion and Management**, v. 213, June 2020. ISSN 01968904.

ZHANG, Xiongwen; CHAN, S.H.; LI, Guojun; HO, H.K.; LI, Jun; FENG, Zhenping. A review of integration strategies for solid oxide fuel cells. **Journal of Power Sources**, v. 195, 3 Feb. 2010. ISSN 03787753.

ZHAO, F; VIRKAR, A. Dependence of polarization in anode-supported solid oxide fuel cells on various cell parameters. **Journal of Power Sources**, Elsevier BV, v. 141, n. 1, p. 79–95, Feb. 2005.

ZHAO, Hengbing; BURKE, Andrew F. Optimization of fuel cell system operating conditions for fuel cell vehicles. **Journal of Power Sources**, v. 186, 2 Jan. 2009. ISSN 03787753.

ZHOU, Jieyang; WANG, Zhe; HAN, Minfang; SUN, Zaihong; SUN, Kaihua. Optimization of a 30 kW SOFC combined heat and power system with different cycles and hydrocarbon fuels. **International Journal of Hydrogen Energy**, Elsevier BV, v. 47, n. 6, p. 4109–4119, Jan. 2022.

APPENDIX A – PAPERS RESEARCH

The first stage of this work involved a systematic search for previous articles and works available in the literature of the time. The searches were made by combining a group of keywords, which resulted in a visualization of the number of papers per year and country. For reference, these charts are available in this section. In Figure 33 and Figure 34, the results for the SOFC and modeling words are present. In the first quarter on the left, the chart presents the countries with more papers published, in the same way, the chart in the bottom left presents the authors. On the right side, the charts present the number of publications per year in total and by Journal.

Figure 32 – Keyword:SOFC - Papers per Year, Countries and Journals

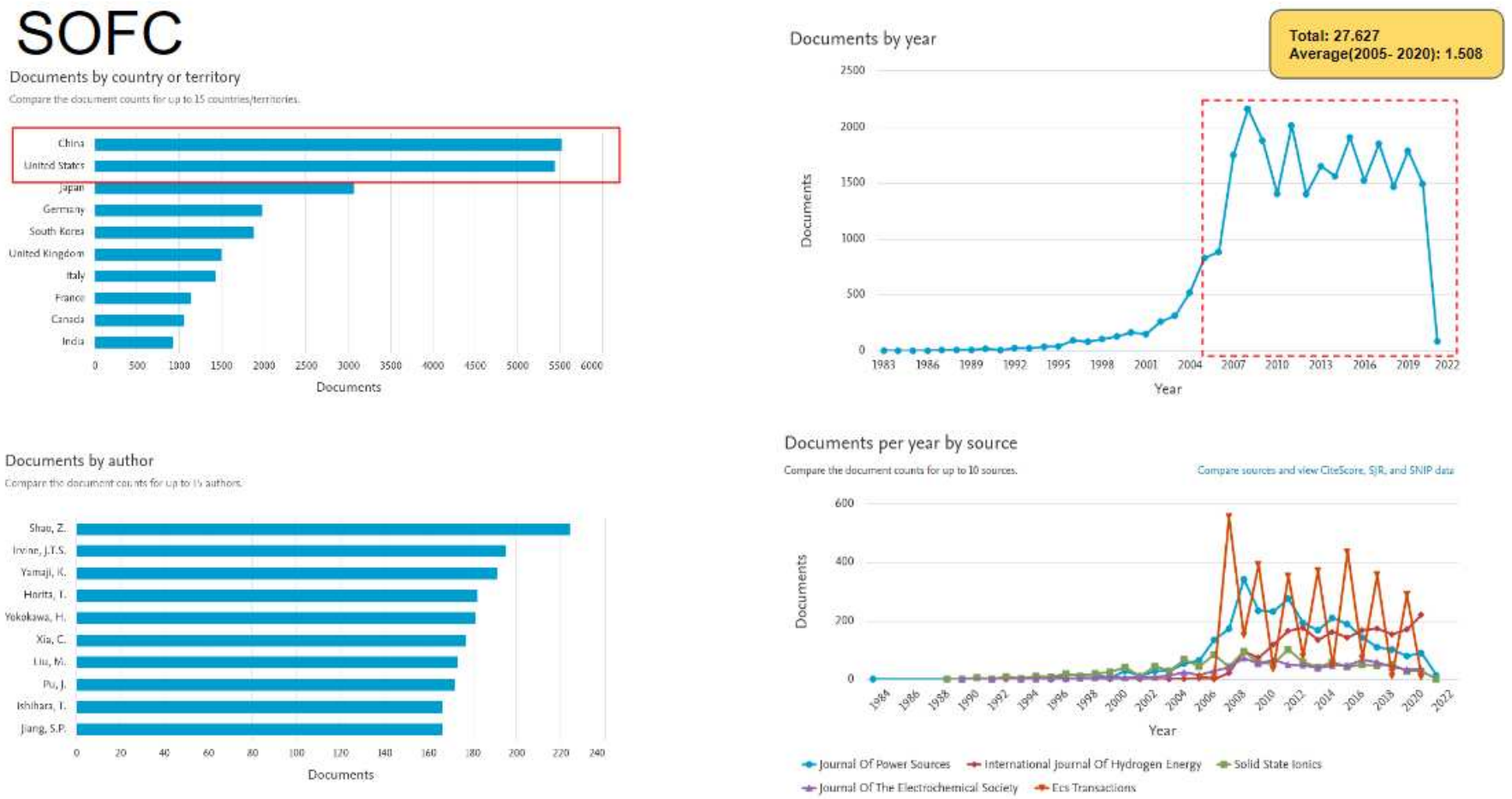

Source:(Author,2022)

Figure 33 – Keyword:SOFC + Modeling - Papers per Year, Countries and Journals

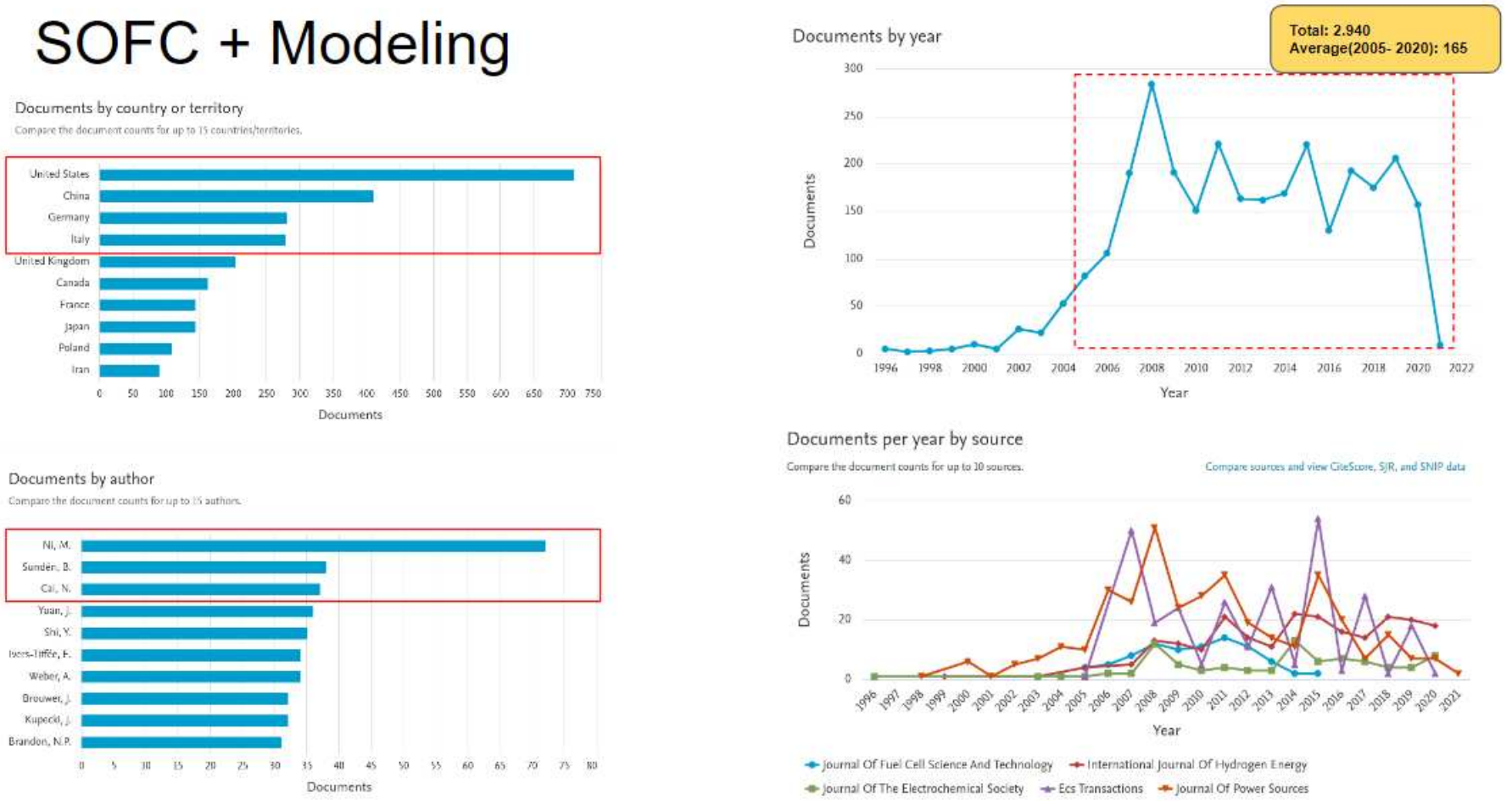

Source:(Author,2022)

APPENDIX B – EQUATION (22) AND EQUATION (23)

B.1 DEMONSTRATION OF EQUATION (22):

Considering that α is 0.5, the equation (22) can be rewritten to isolate η_{act}. Thus, the exponents remain the same with the sign changed.

$$j = j_{0,cathode}\left[exp\left(\frac{\alpha nF}{RT}\eta_{act,cathode}\right) - exp\left(-\frac{(1-\alpha)nF}{RT}\eta_{act,cathode}\right)\right] \quad (53)$$

Moving $j_{0,cathode}$ to the other side of equality,

$$\frac{j}{j_{0,cathode}} = \left[exp\left(\frac{\alpha nF}{RT}\eta_{act,cathode}\right) - exp\left(-\frac{(1-\alpha)nF}{RT}\eta_{act,cathode}\right)\right] \quad (54)$$

The equation (54) can be simplified , defining the group of variables as a single variable, as can be seen in Equations (56) and (57):

$$T = \frac{j}{j_{0,cathode}} \quad (55)$$

$$x = e^{\frac{0.5nF}{RT}\eta_{act,cathode}} \quad (56)$$

Thus, the Equation (55) can be rewritten as Equation (58):

$$T = x - \frac{1}{x} \quad (57)$$

which can be rearranged to:

$$x^2 - Tx = 1 \quad (58)$$

Adding $\frac{T^2}{4}$ for both sides:

$$x^2 - Tx + \frac{T^2}{4} = \frac{T^2}{4} + 1 \quad (59)$$

Reordering the left side, to combine similar terms, the following equation is obtained:

$$\left(x - \frac{T}{2}\right)^2 = \frac{T^2}{4} + 1 \quad (60)$$

Applying the square root for both sides, the result for left side is terms itself, thus:

$$\left(x - \frac{T}{2}\right) (= \sqrt{\frac{T^2}{4} + 1} \quad (61)$$

in which is possible to isolate x

$$x = \left(\frac{T}{2}\right) + \sqrt{\frac{T^2}{4} + 1} \tag{62}$$

replacing the value of x, by the Equation (62)

$$e^{\frac{0.5nF}{RT}\eta_{act,cathode}} = \left(\frac{T}{2}\right) + \sqrt{\frac{T^2}{4} + 1} \tag{63}$$

Applying the natural logarithm in both sides of equation (64)

$$\frac{0.5nF}{RT}\eta_{act,cathode} = ln\left[\frac{T}{2} + \sqrt{\left(\frac{T}{2}\right)^2 + 1}\right] \tag{64}$$

Moving the fraction to the right side of Equation (65), to isolate the η_{act},

$$\eta_{act,cathode} = \frac{RT}{0.5nF} ln\left[\frac{T}{2} + \sqrt{\left(\frac{T}{2}\right)^2 + 1}\right] \tag{65}$$

For n=2, Equation (66) is rewritten as:

$$\eta_{act,cathode} = \frac{RT}{F} ln\left[\frac{T}{2} + \sqrt{\left(\frac{T}{2}\right)^2 + 1}\right] \tag{66}$$

Replacing T in the Equation (67),

$$n_{act,cathode} = \frac{RT}{F} ln\left[\frac{j}{2j_{0\,cathode}} + \sqrt{\left(\frac{j}{2j_{0\,cathode}}\right)^2 + 1}\right] \tag{67}$$

B.2 DEMONSTRATION OF EQUATION (23):

In a similar way, the equation (29) can be rewritten as:

$$\frac{j}{j_{0,anode}} = \left[\frac{P_{H_2,TPB}}{P_{H_2,f}} exp\left(\frac{\alpha nF}{RT}\eta_{act,anode}\right) - \frac{P_{H_2O,TPB}}{P_{H_2O,f}} exp\left(-\frac{(1-\alpha)nF}{RT}\eta_{act,anode}\right)\right] \tag{68}$$

To simplify the rearrangement of variables, the following groups of variables were defined, as presented in Equations (70)-(74):

$$A = \frac{P_{H_2,TPB}}{P_{H_2,f}} \tag{69}$$

$$B = \frac{P_{H_2O,TPB}}{P_{H_2O,f}} \tag{70}$$

$$C = \frac{\alpha nF}{RT}\eta_{act,anode} \tag{71}$$

$$D = \frac{(1-\alpha)nF}{RT}\eta_{act,anode} \tag{72}$$

$$T = \frac{j}{j_{0,anode}} \tag{73}$$

Defining the value of alfa α as 0.5, them C = D, thus

$$T = Ae^{D} - Be^{-D} \tag{74}$$

To simplify the the rearrangement of variables, x is defined as presented in Equation (81):

$$x = e^{D} \tag{75}$$

Then, Equation (75) can be rewritten as:

$$Ax - \frac{B}{x} = T \tag{76}$$

Rearranging Equation (77), one can see:

$$Ax^2 - Tx - B = 0 \tag{77}$$

Dividing each term of Equation (78) by A, the following equation results:

$$x^2 - \frac{Tx}{A} = \frac{B}{A} \tag{78}$$

By adding $\frac{T^2}{4A^2}$ to both sides of Equation (79):

$$\frac{T^2}{4A^2} - \frac{Tx}{A} + x^2 = \frac{B}{A} + \frac{T^2}{4A^2} \tag{79}$$

Reordering the left side, to combine similar terms, one can see:

$$\left(x - \frac{T}{2A}\right)^2 = \frac{B}{A} + \frac{T^2}{4A^2} \tag{80}$$

$$x - \frac{T}{2A} = \sqrt{\frac{B}{A} + \frac{T^2}{4A^2}} \tag{81}$$

in which is possible to isolate x:

$$x = \frac{T}{2A} + \sqrt{\frac{B}{A} + \frac{T^2}{4A^2}} \tag{82}$$

Replacing the value of x, as defined in Equation (76), the following equation is given:

$$e^D = \frac{T}{2A} + \sqrt{\frac{B}{A} + \frac{T^2}{4A^2}} \tag{83}$$

Applying natural logarithm to both sides of Equation (84):

$$D = ln\left(\frac{T}{2A} + \sqrt{\frac{B}{A} + \frac{T^2}{4A^2}}\right) \tag{84}$$

Equation (85) can be rearranged, resulting in:

$$D = ln\left(\frac{T}{2A} + \frac{\sqrt{4AB + T^2}}{2A}\right) \tag{85}$$

Replacing A, B, D and T, Equation (86) is rewritten as:

$$n_{act,anode} = \frac{RT}{0.5nF} \log \frac{\left[\sqrt{4(\frac{P_{H_2,TPB}}{P_{H_2,f}})(\frac{P_{H2O,TPB}}{P_{H2O,f}}) + (\frac{j}{j_{0\,anode}})^2} + (\frac{j}{j_{0\,anode}})\right]}{(\frac{P_{H_2,TPB}}{P_{H_2,f}})} \tag{86}$$